E.J. Meester

# A Road to Improved Diagnostics

## Imaging Inflammatory Cells in Atherosclerosis

# A Road to Improved Diagnostics
# Imaging Inflammatory Cells in Atherosclerosis

Een pad naar verbeterde diagnostiek

Visualisatie van ontstekingscellen in aderverkalking

Eric Jan Meester

**A Road to Improved Diagnostics**
**Imaging Inflammatory Cells in Atherosclerosis**
Thesis, Erasmus MC, University Medical Centre, Rotterdam, The Netherlands

FSC
www.fsc.org
MIX
Paper from
responsible sources
FSC® C128610

# MILabs

Making Molecular Imaging Clear

altromin
International

Made in Germany

Hartstichting

# A Road to Improved Diagnostics
# Imaging Inflammatory Cells in Atherosclerosis

**Een pad naar verbeterde diagnostiek**
**Visualisatie van ontstekingscellen in aderverkalking**

**Proefschrift**

ter verkrijging van de graad van doctor aan de
Erasmus Universiteit Rotterdam
op gezag van de rector magnificus
Prof.dr. R.C.M.E. Engels
en volgens het besluit van het College voor Promoties.
De openbare verdediging zal plaatsvinden op
woensdag 7 oktober 2020 om 13:30 uur

door

**Eric Jan Meester**

geboren te Delft

**Erasmus University Rotterdam**

## promotor
Prof. dr. M. de Jong

## overige leden
Dr. M.R. Bernsen
Prof. dr. J.P. Norenberg
Prof. dr. C.W.G.M. Löwik

## copromotoren
Dr. K. van der Heiden
Dr. B.J. Krenning

# Contents

# Chapter 1

Introduction

Cardiovascular disease remains the major cause of death worldwide (1). Most acute cardio-vascular events, such as myocardial infarction and stroke, are a consequence of atherosclerosis in which plaques form due to chronic inflammation and lipid accumulation in the vessel wall. Cardiovascular events can be triggered by rupture of an atherosclerotic plaque, resulting in arterial thrombosis and concomitant occlusion of the vessel and a subsequent acute ischemic event (Figure 1). Plaques with a high risk of rupture are called vulnerable plaques, while plaques with a low risk of rupture are called stable plaques. These stable plaques may only cause symptoms when luminal obstruction is significant, limiting bloodflow. Traditionally, the burden of atherosclerotic disease is estimated from the percentage of stenosis detected by various imaging techniques, such as coronary angiography or Computed Tomography (CT). However, vulnerability depends on plaque composition. A vulnerable plaque usually exhibits characteristics such as a large necrotic core, infiltration of inflammatory cells, a thin fibrous cap, neovascularization, and intra-plaque haemorrhage (2). Although non-invasive imaging techniques, such as CT and MRI can assess certain aspects of plaque composition, such as calcification (Figure 2), these techniques fail to detect non-stenotic – possibly vulnerable – plaques. Patients without stenosis could therefore still present with vulnerable atherosclerosis and consequently be at risk of cardiovascular events.

Clot

Plaque

Blocked coronary artery

Damaged heart muscle
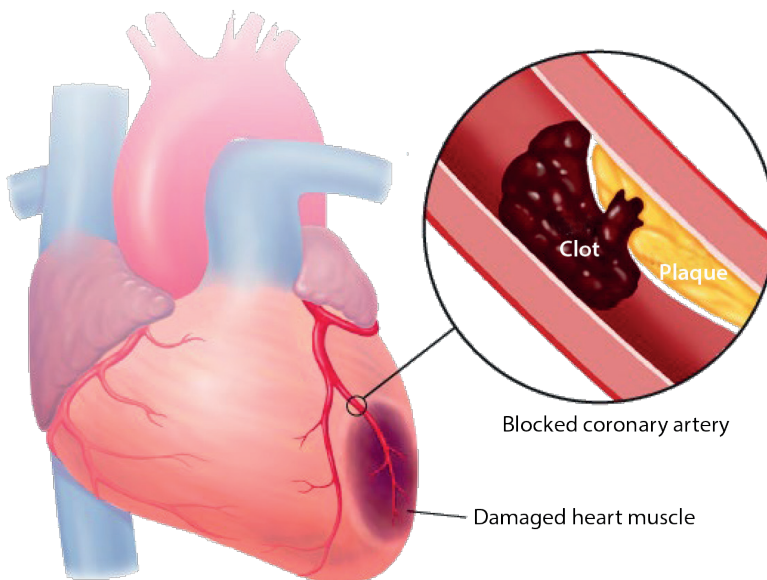
**Figure 1 | Cartoon of plaque rupture in a coronary artery followed by myocardial infarction.** Rupture of the plaque leads to arterial thrombosis, which prevents blood and therefore oxygen from flowing to downstream tissue. This leads to ischemia in these tissues, which results in death of the tissue if the artery is not unblocked in time. *From Patient Information: Atherosclerosis (The Basics). In: Basow DS, ed.* **UpToDate,** *Waltham, MA; 2013. with permission from the publisher. Copyright © 2013 UpToDate, Inc.*

Timely detection of plaque, and differentiation between stable and rupture-prone plaque would allow targeted treatment and prevention of potentially life-threatening cardiovascular events. Current imaging methods used for plaque detection are methods such as CT, ultrasound, or Magnetic Resonance Imaging (MRI) (Figure 2). CT and ultrasound give information on luminal narrowing or calcification, MR imaging can give information on stenosis and plaque composition. A luminal stenosis degree of 50–70% or higher is considered significant and may be an indication for revascularization, such as percutaneous coronary intervention. However, the majority of atherosclerotic lesions (68%) responsible for the initiation of acute myocardial infarction do not cause major obstruction of the coronary lumen with a stenosis degree below 50% (3-6). If the decision to treat is made only based on degree of stenosis, we therefore miss a large part of culprit plaques.

Visualisation of plaque components which are characteristic of vulnerable plaque should therefore be included. However, current techniques are either invasive, have limited resolution, or the identified features of vulnerability were not sufficient to predict an event. MRI can give additional information on plaque composition, most notably intra-plaque haemorrhage, but is due to its resolution mostly limited to the carotid arteries. CT and ultrasound have additional prognostic value by visualising features like plaque calcification. The prognostic value of imaging can be improved further by visualizing other features of vulnerable plaque.



CT: Stenosis, calcium     Ultrasound: Wall dimensions     MRI: Composition
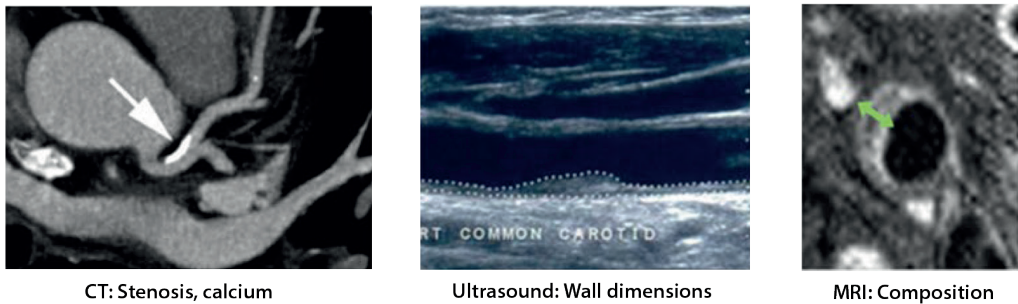
**Figure 2 | Shows traditional imaging methods used for plaque visualization.** CT angiography and ultrasound give information on luminal narrowing or calcification (calcification indicated by white arrow). MR imaging can give information on plaque composition, but often lacks the resolution required to give this information for small plaques, especially in the coronary arteries. From (7).

Inflammation is a major hallmark of atherosclerosis and a consistent predictor of cardiovascular risk. Moreover, inflammation plays a major role in all stages of the disease, and the degree of inflammation is linked to plaque vulnerability (8,9). Therefore, detection and assessment of the severity of plaque inflammation may help to identify patients at risk of future cardiac events. Currently, evaluation of blood biomarkers for inflammation such as high-sensitive C-Reactive Protein (hsCRP) (10) provides information on patient-wide inflammatory status. However, it

does not give an indication on the status of individual plaques. An imaging method which both detects plaque localization and provides information on the risk of rupture could result in significant advances in patient treatment.

Nuclear medicine has the potential to fulfil this need because it combines specifically targeted radiolabelled tracers (radioligands) with highly sensitive and accurate detection methods, like Single Photon Emission Computed Tomography (SPECT) or Positron Emission Tomography (PET) (11). Radiolabelled tracers directed towards certain targets are being developed for that purpose. After injection of such tracers or radioligands, SPECT or PET can be used to detect the location of the radioactivity, indicating the target's localization by which the cell type or process of interest can be followed (Figure 3 & Box 1). Because highly sensitive and quantitative data can be acquired with these techniques, an assessment of the abundance of the target molecule in a specific location can be made.
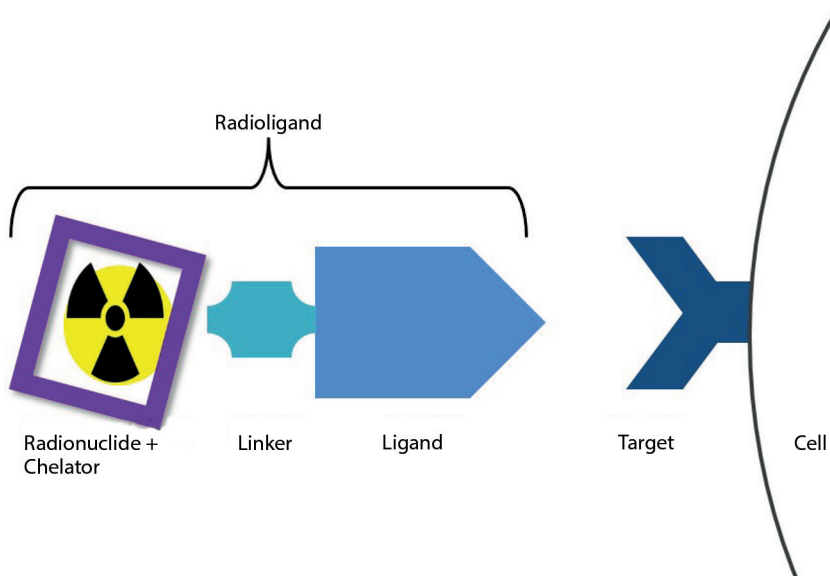


**Figure 3 | Schematic representation of a radioligand and its target.** SPECT and PET can be used to detect the radiation emitted by the radionuclide, which therefore indicates the location of the target, and therefore the location of the cells on which this target is expressed.

Nuclear imaging of inflammation was first explored with 2-deoxy-2-[$^{18}$F]fluoro-D-glucose ([$^{18}$F]FDG) (12). This molecule is taken up by metabolically active cells, including metabolically active macrophages in plaques. In this manner, $^{18}$F-FDG has successfully been used to visualize plaque and quantify the level of inflammation in plaques (13,14). However, uptake in the metabolically active myocardium severely hinders plaque detection in the coronary arteries

(15,16). Moreover, uptake in other metabolically active cells in the vasculature can complicate plaque visualization. Therefore, novel radioligands are required which more specifically target inflammatory cells, and which suffer less from interference from radioactivity uptake in surrounding tissues.

---

**Box 1 | A schematic representation of the imaging process of a radioligand.**



1
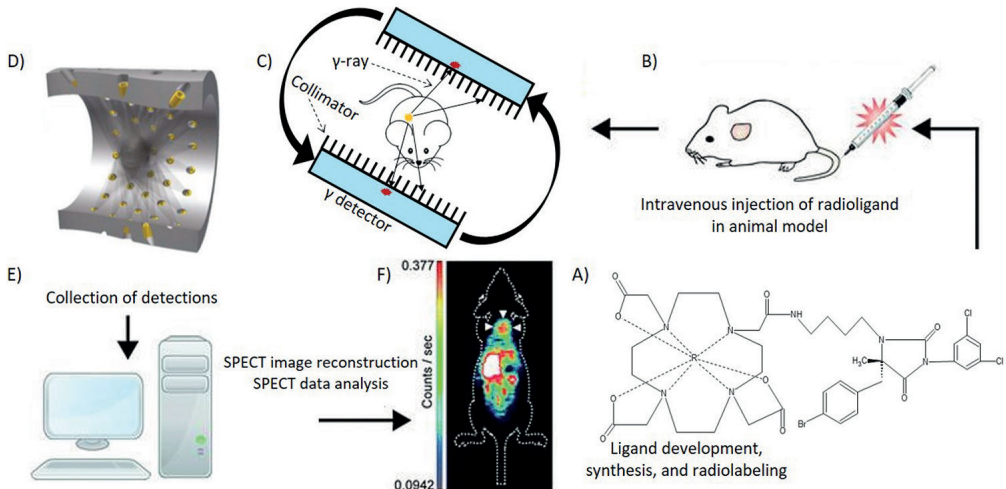
**A)** A tracer or ligand is radiolabelled with a radionuclide, for example [111]In (Location indicated by 'R'). This is the molecular formula of DANBIRT, one of the ligands evaluated in this thesis. **B)** The radioligand is intravenously injected into a subject like a patient or an animal model. The radioligand is distributed throughout the body and binds to its respective targets. Excess, unbound, radioligand is cleared by excretion via e.g. the kidneys and bladder or via the intestines. **C)** The radionuclide attached to the ligand emits radiation when it decays to a stable form, γ-rays are emitted by [111]In. The γ-rays are detectable with Single Photon Emission Computed Tomography (SPECT) imaging systems. SPECT relies on physical collimation, in which the γ-rays cannot penetrate the (usually) lead collimator in front of the detector. Only γ-rays travelling in the same direction as the collimator slits will reach the detector, therefore providing information on the source of the radiation. Here you see an image of a traditional parallel hole collimator. **D)** In this thesis we use a pinhole collimator, which greatly enhances the spatial resolution. **E)** By registering γ detections in detectors, the origin of the γ-rays can be estimated. If enough of these detections are registered, a single point of origin can be estimated. **F)** Based on these estimations, an image can be reconstructed indicating where the radiation originates from, which indicates where the radioligand and therefore the radioligand target is located. The location of the radioligand target in the body can be assessed by coupling SPECT to an anatomical imaging modality like Computed Tomography (CT) or Magnetic Resonance Imaging (MRI). Because PET and SPECT yield a quantifiable signal, the abundance of the radioligand target can estimated. Image adapted from (76).

# Thesis outline

This thesis work describes the assessment and evaluation of novel and existing radioligands for a new application: use in plaque detection and characterization. Moreover, novel imaging protocols, which might improve patient stratification, are discussed. Figure 4 provides a schematic visualisation of the research aims of this thesis.

In **Chapter 2** the considerations involved in nuclear imaging of plaques are discussed. We reflect on animal models applied, technical aspects, radioligand development, and provide a future outlook.

In **Chapter 3** we show the evaluation of a novel imaging ligand, [$^{111}$In]In-DANBIRT, targeted to the Leukocyte Function-associated Antigen-1 (LFA-1) for plaque detection. We tested the radioligand *in vitro* in human and mouse plaque tissue, and *in vivo* in a mouse model of atherosclerosis.

Somatostatin Subtype Receptor 2 (SST$_2$) is a promising target for atherosclerotic plaque visualization. In **Chapter 4** we describe the assessment of [$^{111}$In]In-DOTA-JR11, a receptor-antagonistic radioligand targeting SST$_2$. We evaluated the compound *in vivo* in a mouse model of atherosclerosis, and *in vitro* in both mouse and human plaque tissues.

A novel dual isotope imaging approach for plaque characterization is discussed in **Chapter 5**, in which we describe the evaluation of [$^{111}$In]In-DANBIRT and [$^{99m}$Tc]Tc-DEMOTATE 2, a radioligand targeting SST$_2$, in human plaque tissues. This approach could be used to simultaneously visualize all inflammatory cells as well as a subset of pro-inflammatory macrophages.

**Chapter 6** describes investigations *in vitro* in human plaque material to examine how the targets of a number of the most promising radioligands available are distributed throughout different plaque phenotypes, and how binding of these radioligands compare to each other in these tissues.

**Imaging inflammation in atherosclerosis**



1

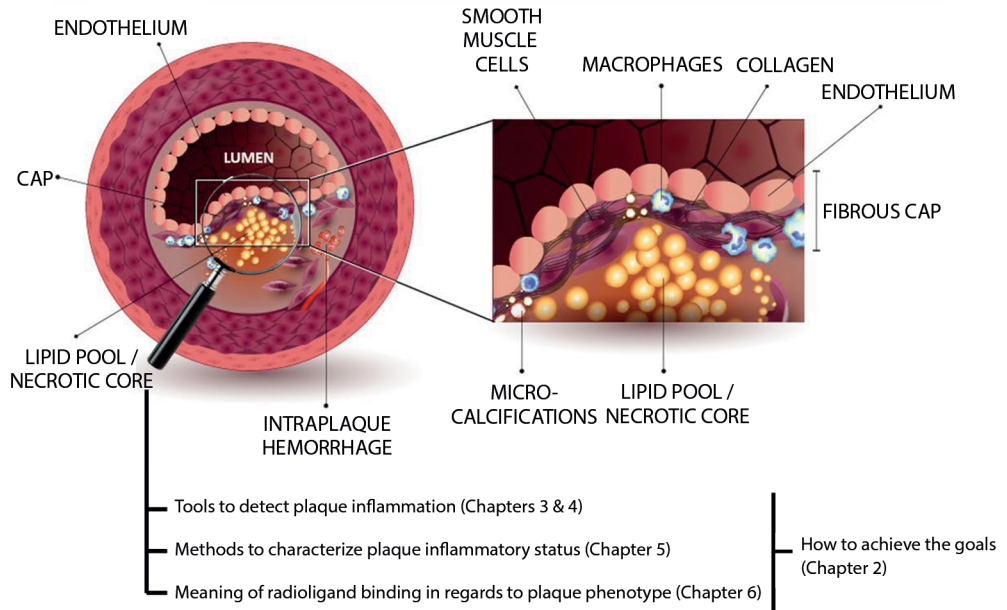**Figure 4 | A cartoon depicting the features of vulnerable plaque, and the research topics of this thesis:** detection of plaque based on imaging of inflammation, development of tools to assess the inflammatory status of plaque, and interpretation of radioligand binding in plaque. The aims can only be achieved with state-of-the-art equipment, and optimization of the experimental approach such as animal models and imaging protocols.

# References

1.  GBD 2015 Mortality and Causes of Death Collaborators I. Global, regional, and national life expectancy, all-cause mortality, and cause-specifi c mortality for 249 causes of death, 1980–2015: a systematic analysis for the Global Burden of Disease Study 2015. Lancet. 2016;380(9859):1459–544.

2.  Finn A V, Nakano M, Narula J, Kolodgie FD, Virmani R. Concept of vulnerable/unstable plaque. Arterioscler Thromb Vasc Biol [Internet]. 2010 Jul [cited 2014 Oct 31];30(7):1282–92. Available from: http://www.ncbi.nlm.nih.gov/pubmed/20554950

3.  Carità P, Guaricci AI, Muscogiuri G, Carrabba N, Pontone G. Prognostic value and therapeutic perspectives of coronary CT angiography: A literature review. Biomed Res Int. 2018;2018.

4.  Adamson PD, Newby DE. Noninvasive imaging of the coronary arteries. Eur Heart J. 2019;40:2444–54.

5.  Libby P, Buring JE, Badimon L, Hansson GK, Deanfield J, Bittencourt MS, et al. Atherosclerosis. Nat Rev. 2019;5(56):1–18.

6.  Newby DE. Acute coronary syndromes – Triggering of acute myocardial infarction: Beyond the vulnerable plaque. Heart. 2010;96(15):1247–51.

7.  Rudd JHF, Hyafil F, Fayad ZA. Inflammation imaging in atherosclerosis. Arterioscler Thromb Vasc Biol. 2009;29(7):1009–16.

8.  Moore KJ, Tabas I. Macrophages in the Pathogenesis of Atherosclerosis. Cell [Internet]. 2011;145(3):341–55. Available from: http://dx.doi.org/10.1016/j.cell.2011.04.005

9.  Hansson GK. Inflammation, Atherosclerosis, and Coronary Artery Disease. N Engl J Med [Internet]. 2005;352(16):1685–95. Available from: http://www.ncbi.nlm.nih.gov/pubmed/15843671%0Ahttp://www.nejm.org/doi/abs/10.1056/NEJMra043430

10. Ridker PM. Clinical Application of C-Reactive Protein for Cardiovascular Disease Detection and Prevention. Circulation. 2003;107:363–9.

11. Quillard T, Libby P. Molecular imaging of atherosclerosis for improving diagnostic and therapeutic development. Circ Res [Internet]. 2012 Jul 6 [cited 2015 Jun 26];111(2):231–44. Available from: http://circres.ahajournals.org/content/111/2/231.full

12. Rudd JHF, Warburton EA, Fryer TD, Jones HA, Clark JC, Antoun N, et al. Imaging atherosclerotic plaque inflammation with [18F]-fluorodeoxyglucose positron emission tomography. Circulation. 2002;105(23):2708–11.

13. Tawakol A, Fayad Z a, Mogg R, Alon A, Klimas MT, Dansky H, et al. Intensification of statin therapy results in a rapid reduction in atherosclerotic inflammation: results of a multicenter fluorodeoxyglucose-positron emission tomography/computed tomography feasibility study. J Am Coll Cardiol [Internet]. 2013 Sep 3 [cited 2015 Jun 12];62(10):909–17. Available from: http://www.ncbi.nlm.nih.gov/pubmed/23727083

14. Figueroa AL, Subramanian SS, Cury RC, Truong QA, Gardecki JA, Tearney GJ, et al. Distribution of Inflammation Within Carotid Atherosclerotic Plaques With High-Risk Morphological Features A Comparison Between Positron Emission Tomography Activity , Plaque Morphology , and Histopathology. Circ Cardiovasc Imaging. 2012;5:69–77.

15. Buettner C, Rudd JHF, Fayad ZA. Determinants of FDG Uptake in Atherosclerosis. JACC Cardiovasc Imaging [Internet]. 2011;4(12):1302–4. Available from: http://linkinghub.elsevier.com/retrieve/pii/S1936878X11006954

16. Tarkin JM, Joshi FR, Rudd JHF. PET imaging of inflammation in atherosclerosis. Nat Rev Cardiol [Internet]. 2014;11(8):443–57. Available from: http://www.ncbi.nlm.nih.gov/pubmed/24913061

17. Benjamin EJ, Virani SS, Callaway CW, Chamberlain AM, Chang AR, Cheng S, et al. Heart disease and stroke statistics – 2018 update: A report from the American Heart Association. Vol. 137, Circulation. 2018. 67–492 p.

18. Wong MCS, Zhang DX, Wang HHX. Rapid emergence of atherosclerosis in Asia: A systematic review of coronary atherosclerotic heart disease epidemiology and implications for prevention and control strategies. Curr Opin Lipidol. 2015;26(4):257–69.

19. Libby P. Inflammation in atherosclerosis. 2002;420(December).

20. Libby P, Ridker PM, Maseri A. Clinical Cardiology: New Frontiers Inflammation and Atherosclerosis The Scientific Basis of Inflammation. 2002;

21.   Ilhan F. Atherosclerosis and the role of immune cells. World J Clin Cases. 2015;3(4):345.

22.   Galkina E, Ley K. Immune and inflammatory mechanisms of atherosclerosis (*). Annu Rev Immunol. 2009;27:165–97.

23.   Tarkin JM, Joshi FR, Evans NR, Chowdhury MM, Figg NL, Shah AV, et al. Detection of Atherosclerotic Inflammation by 68Ga-DOTATATE PET Compared to [18F]FDG PET Imaging. J Am Coll Cardiol. 2017;69(14):1774–91.

24.   Wan MYS, Endozo R, Michopoulou S, Shortman R, Rodriguez-Justo M, Menezes L, et al. PET/CT Imaging of Unstable Carotid Plaque with 68Ga-Labeled Somatostatin Receptor Ligand. J Nucl Med [Internet]. 2017;58(5):774–80. Available from: http://jnm.snmjournals.org/lookup/doi/10.2967/jnumed.116.181438

25.   Fani M, Nicolas GP, Wild D. Somatostatin Receptor Antagonists for Imaging and Therapy. J Nucl Med [Internet]. 2017;58(Supplement 2):61S-66S. Available from: http://jnm.snmjournals.org/lookup/doi/10.2967/jnumed.116.186783

26.   Davies JR, Rudd JHF, Weissberg PL, Narula J. Radionuclide imaging for the detection of inflammation in vulnerable plaques. J Am Coll Cardiol [Internet]. 2006 Apr 18 [cited 2015 Jun 12];47(8 Suppl):C57-68. Available from: http://www.ncbi.nlm.nih.gov/pubmed/16631511

27.   Alie N, Eldib M, Fayad ZA, Mani V. Inflammation, Atherosclerosis, and Coronary Artery Disease: PET/CT for the Evaluation of Atherosclerosis and Inflammation. Clin Med Insights Cardiol [Internet]. 2014 Jan [cited 2015 May 12];8(Suppl 3):13–21. Available from: http://www.pubmedcentral.nih.gov/articlerender.fcgi?artid=4294600&tool=pmcentrez&rendertype=abstract

28.   Sadeghi MM. (18)F-FDG PET and vascular inflammation: time to refine the paradigm? J Nucl Cardiol [Internet]. 2015 Apr [cited 2015 Jun 12];22(2):319–24. Available from: http://www.ncbi.nlm.nih.gov/pubmed/24925623

29.   Hiari N, Rudd JHF. FDG PET imaging and cardiovascular inflammation. Curr Cardiol Rep. 2011;13(1):43–8.

30.   Tavakoli S, Vashist A, Sadeghi MM. Molecular imaging of plaque vulnerability. J Nucl Cardiol. 2014;21:1112–28.

31.   Langer HF, Haubner R, Pichler BJ, Gawaz M. Radionuclide imaging: a molecular key to the atherosclerotic plaque. J Am Coll Cardiol [Internet]. 2008 Jul 1 [cited 2015 Jun 18];52(1):1–12. Available from: http://www.pubmedcentral.nih.gov/articlerender.fcgi?artid=2683742&tool=pmcentrez&rendertype=abstract

32.   Magnoni M, Ammirati E, Camici PG. Non-invasive molecular imaging of vulnerable atherosclerotic plaques. J Cardiol [Internet]. 2015 Apr [cited 2015 Jun 12];65:261–9. Available from: http://www.ncbi.nlm.nih.gov/pubmed/25702846

33.   Joshi F, Rosenbaum D, Bordes S, Rudd JHF. Vascular imaging with positron emission tomography. J Intern Med [Internet]. 2011 Aug [cited 2015 Jun 12];270(2):99–109. Available from: http://www.ncbi.nlm.nih.gov/pubmed/21518037

34.   Weber C, Noels H. Atherosclerosis: current pathogenesis and therapeutic options. Nat Med [Internet]. 2011;17(11):1410–22. Available from: http://dx.doi.org/10.1038/nm.2538

35.   Sollini M, Berchiolli R, Kirienko M, Rossi A, Glaudemans AWJM, Slart R, et al. PET/MRI in Infection and Inflammation. Semin Nucl Med [Internet]. 2018;48(3):225–41. Available from: https://doi.org/10.1053/j.semnuclmed.2018.02.003

36.   Krishnan S, Otaki Y, Doris M, Slipczuk L, Arnson Y, Rubeaux M, et al. Molecular Imaging of Vulnerable Coronary Plaque : A Pathophysiologic Perspective. 2019;359–65.

37.   Quillard T, Libby P. Molecular imaging of atherosclerosis for improving diagnostic and therapeutic development. Circ Res [Internet]. 2012 Jul 6 [cited 2015 Jun 26];111(2):231–44. Available from: http://circres.ahajournals.org/content/111/2/231.full

38.   Libby P. History of Discovery : Inflammation in Atherosclerosis. Arterioscler Thromb Vasc Biol. 2012;32(9):2045–51.

39.   Mckenney-drake ML, Moghbel MC, Paydary K, Alloosh M, Houshmand S, Høilund-carlsen PF, et al. 18 F-NaF and 18 F-FDG as molecular probes in the evaluation of atherosclerosis. Eur J Nucl Med Mol Imaging [Internet]. 2018;2190–200. Available from: http://link.springer.com/10.1007/s00259-018-4078-0

40.   Marnane M, Merwick A, Sheehan OC, Hannon N, Foran P, Grant T, et al. Carotid plaque inflammation on 18F-fluorodeoxyglucose positron emission tomography predicts early stroke recurrence. Ann Neurol. 2012;71(5):709–18.

41. Kelly PJ, Camps-Renom P, Giannotti N, Martí-Fàbregas J, Murphy S, McNulty J, et al. Carotid Plaque Inflammation Imaged by 18 F-Fluorodeoxyglucose Positron Emission Tomography and Risk of Early Recurrent Stroke . Stroke. 2019;50(7):1766–73.

42. Figueroa AL, Abdelbaky A, Truong QA, Corsini E, MacNabb MH, Lavender ZR, et al. Measurement of arterial activity on routine FDG PET/CT images improves prediction of risk of future CV events. JACC Cardiovasc Imaging [Internet]. 2013;6(12):1250–9. Available from: http://dx.doi.org/10.1016/j.jcmg.2013.08.006

43. Moon SH, Cho YS, Noh TS, Choi JY, Kim BT, Lee KH. Carotid FDG uptake improves prediction of future cardiovascular events in asymptomatic individuals. JACC Cardiovasc Imaging. 2015;8(8):949–56.

44. Wenning C, Kloth C, Kuhlmann MT, Jacobs AH, Schober O, Hermann S, et al. Serial F-18-FDG PET / CT distinguishes inflamed from stable plaque phenotypes in shear-stress induced murine atherosclerosis. Atherosclerosis [Internet]. 2014;234(2):276–82. Available from: http://dx.doi.org/10.1016/j.atherosclerosis.2014.03.008

45. Weiberg D, Thackeray JT, Daum G, Sohns JM, Kropf S, Wester H-J, et al. Clinical Molecular Imaging of Chemokine Receptor CXCR4 Expression in Atherosclerotic Plaque using 68Ga-Pentixafor PET: Correlation with Cardiovascular Risk Factors and Calcified Plaque Burden. J Nucl Med [Internet]. 2018;59:266–72. Available from: http://jnm.snmjournals.org/lookup/doi/10.2967/jnumed.117.196485

46. Derlin T, Sedding DG, Dutzmann J, Haghikia A, König T, Napp LC, et al. Imaging of chemokine receptor CXCR4 expression in culprit and nonculprit coronary atherosclerotic plaque using motion-corrected [68Ga] pentixafor PET/CT. Eur J Nucl Med Mol Imaging. 2018;45(11):1934–44.

47. Li X, Yu W, Wollenweber T, Lu X, Wei Y, Beitzke D, et al. [68Ga]Pentixafor PET/MR imaging of chemokine receptor 4 expression in the human carotid artery. Eur J Nucl Med Mol Imaging. 2019;46:1616–25.

48. Reiter T, Kircher M, Schirbel A, Werner RA, Kropf S, Ertl G, et al. Imaging of C-X-C Motif Chemokine Receptor CXCR4 Expression After Myocardial Infarction With [68Ga]Pentixafor-PET/CT in Correlation With Cardiac MRI. JACC Cardiovasc Imaging [Internet]. 2018; Available from: https://doi.org/10.1016/j.jcmg.2018.01.001

49. Li X, Heber D, Leike T, Beitzke D, Lu X, Zhang X, et al. [68Ga]Pentixafor-PET/MRI for the detection of Chemokine receptor 4 expression in atherosclerotic plaques. Eur J Nucl Med Mol Imaging. 2018;45(4):558–66.

50. Magnoni M, Ammirati E, Camici PG. Non-invasive molecular imaging of vulnerable atherosclerotic plaques. J Cardiol [Internet]. 2015;1–9. Available from: http://linkinghub.elsevier.com/retrieve/pii/S0914508715000155

51. Meester EJ, Krenning BJ, Swart J De, Segbers M, Barrett HE. Perspectives on Small Animal Radionuclide Imaging ; Considerations and Advances in Atherosclerosis Animal Models of Atherosclerosis. 2019;6(March):1–11.

52. Andrews JPM, Fayad ZA, Dweck MR. New methods to image unstable atherosclerotic plaques. Atherosclerosis [Internet]. 2018;272:118–28. Available from: https://doi.org/10.1016/j.atherosclerosis.2018.03.021

53. Rominger A, Saam T, Vogl E, Ubleis C, la Fougère C, Förster S, et al. In vivo imaging of macrophage activity in the coronary arteries using 68Ga-DOTATATE PET/CT: correlation with coronary calcium burden and risk factors. J Nucl Med. 2010;51(2):193–7.

54. Li X, Bauer W, Kreissl MC, Weirather J, Bauer E, Israel I, et al. Specific somatostatin receptor II expression in arterial plaque: 68Ga-DOTATATE autoradiographic, immunohistochemical and flow cytometric studies in apoE-deficient mice. Atherosclerosis. 2013;230(1):33–9.

55. Rinne P, Hellberg S, Kiugel M, Virta J, Li X, Käkelä M, et al. Comparison of Somatostatin Receptor 2-Targeting PET Tracers in the Detection of Mouse Atherosclerotic Plaques. Mol Imaging Biol. 2015;18(1):99–108.

56. Mojtahedi A, Alavi A, Thamake S, Amerinia R, Ranganathan D, Tworowska I, et al. Assessment of vulnerable atherosclerotic and fibrotic plaques in coronary arteries using 68 Ga-DOTATATE PET/CT. Am J Nucl Med Mol Imaging. 2015;5(1):65–71.

57. Malmberg C, Ripa RS, Johnbeck CB, Knigge U, Langer SW, Mortensen J, et al. 64Cu-DOTATATE for non-invasive assessment of atherosclerosis in large arteries and its correlation with risk factors: head-to-head comparison with 68Ga-DOTATOC in 60 patients. J Nucl Med [Internet]. 2015;1–33. Available from: http://jnm.snmjournals.org/cgi/doi/10.2967/jnumed.115.161216

58. Pedersen SF, Sandholt BV, Keller SH, Hansen AE, Clemmensen AE, Sillesen H, et al. 64Cu-DOTATATE PET/MRI for Detection of Activated Macrophages in Carotid Atherosclerotic PlaquesSignificance. Arterioscler Thromb Vasc Biol [Internet]. 2015;35(7):1696–703. Available from: http://atvb.ahajournals.org/lookup/doi/10.1161/ATVBAHA.114.305067

59.  Thackeray JT, Bankstahl JP, Wang Y, Korf-klingebiel M, Walte A, Wittneben A, et al. Targeting post-infarct inflammation by PET imaging: comparison of 68Ga-citrate and 68Ga-DOTATATE with 18F-FDG in a mouse model. Eur J Nucl Med Mol Imaging. 2015;42(2):317–27.

60.  Li X, Samnick S, Lapa C, Israel I, Buck AK, Kreissl MC, et al. 68Ga-DOTATATE PET/CT for the detection of inflammation of large arteries: correlation with18F-FDG, calcium burden and risk factors. EJNMMI Res [Internet]. 2012;2:52. Available from: EJNMMI Research

61.  Poria RB, Norenberg JP, Anderson TL, Erion J, Wagner CR, Arterburn JB, et al. Characterization of a radiolabeled small molecule targeting leukocyte function-associated antigen-1 expression in lymphoma and leukemia. Cancer Biother Radiopharm [Internet]. 2006 Oct;21(5):418–26. Available from: http://www.ncbi.nlm.nih.gov/pubmed/17105416

62.  Mota R, Campen MJ, Cuellar ME, Garver WS, Hesterman J, Qutaish M, et al. In-DANBIRT In Vivo Molecular Imaging of Inflammatory Cells in Atherosclerosis. 2018;2018.

63.  Mumaw CL, Levesque S, Mcgraw C, Robertson S, Lucas S, Staf JE, et al. Microglial priming through the lung – brain axis : the role of air pollution – induced circulating factors. FASEB J. 2016;30(5):1880–91.

64.  Verma NK, Kelleher D. Adaptor regulation of LFA-1 signaling in T lymphocyte migration: Potential druggable targets for immunotherapies? Eur J Immunol. 2014;44(12):3484–99.

65.  Phongpradist R, Chittasupho C, Okonogi S, Siahaan T, Anuchapreeda S, Ampasavate C, et al. LFA-1 on Leukemic Cells as a Target for Therapy or Drug Delivery. Curr Pharm Des. 2010;16(21):2321–30.

66.  Nicolls MR, Gill RG. LFA-1 (CD11a) as a therapeutic target. Am J Transplant. 2006;6(1):27–36.

67.  Walling BL, Kim M. LFA-1 in T cell migration and differentiation. Front Immunol. 2018;9(MAY).

68.  Reina M, Espel E. Role of LFA-1 and ICAM-1 in cancer. Cancers (Basel). 2017;9(11):1–14.

69.  Pflugfelder SC, Stern M, Zhang S, Shojaei A. LFA-1/ICAM-1 Interaction as a Therapeutic Target in Dry Eye Disease. J Ocul Pharmacol Ther. 2017;33(1):5–12.

70.  Badell IR, Russell MC, Thompson PW, Turner AP, Weaver TA, Robertson JM, et al. LFA-1 – Specific therapy prolongs allograft survival in rhesus macaques. J Clin Invest. 2010;120(12):4520–31.

71.  Laudanna C. Integrin activation under flow: A local affair. Nat Immunol. 2005;6(5):429–30.

72.  Borchert T, Beitar L, Langer LBN, Polyak A, Wester HJ, Ross TL, et al. Dissecting the target leukocyte subpopulations of clinically relevant inflammation radiopharmaceuticals. J Nucl Cardiol. 2019;https://doi.org/10.1007/s12350-019-01929-z

73.  Hung JC. Bringing new PET drugs to clinical practice – A regulatory perspective. Theranostics. 2013;3(11):885–93.

74.  Mosessian S, Duarte-Vogel SM, Stout DB, Roos KP, Lawson GW, Jordan MC, et al. INDs for PET molecular imaging probes – Approach by an academic institution. Mol Imaging Biol. 2014;16(4):441–8.

75.  Walrand S, Hesse M, Jamar F. Update on novel trends in PET / CT technology and its clinical applications. Br J Radiol. 2018;89.

76.  Nguyen QD, Challapalli A, Smith G, Fortt R, Aboagye EO. Imaging apoptosis with positron emission tomography: "Bench to bedside" development of the caspase-3/7 specific radiotracer [18F]ICMT-11. Eur J Cancer [Internet]. 2012;48(4):432–40. Available from: http://dx.doi.org/10.1016/j.ejca.2011.11.033

1

# Chapter 2

## Perspectives on Small Animal Radionuclide Imaging; Considerations and Advances in Atherosclerosis

Authors: **E.J. Meester Msc**[1,2]; B.J. Krenning MD, PhD[3]; J. de Swart[1]; M. Segbers Msc[1]; HE Barrett PhD[2];

M.R. Bernsen PhD[1]; K. Van der Heiden PhD[2]; M. de Jong PhD[1*]

Author affiliations:

[1] Department of Radiology & Nuclear Medicine, Erasmus MC, Rotterdam, The Netherlands

[2] Department of Biomedical Engineering, Thorax Center, Erasmus MC, Rotterdam, The Netherlands

[3] Department of Cardiology, Thorax Center, Erasmus MC, Rotterdam, The Netherlands

# Abstract

This review addresses nuclear SPECT and PET imaging in small animals in relation to the atherosclerotic disease process, one of our research topics of interest. Imaging of atherosclerosis in small animal models is challenging, as it operates at the limits of current imaging possibilities regarding sensitivity and spatial resolution. Several topics are discussed, including technical considerations that apply to image acquisition, reconstruction, and analysis. Moreover, molecules developed for or applied in these small animal nuclear imaging studies are listed, including target-directed molecules, useful for imaging organs or tissues that have elevated expression of the target compared to other tissues, and molecules that serve as substrates for metabolic processes. Differences between animal models and human pathophysiology that should be taken into account during translation from animal to patient as well as differences in tracer behaviour in animal versus man are also described. Finally, we give a future outlook on small animal radionuclide imaging in atherosclerosis, followed by recommendations. The challenges and solutions described might be applicable to other research fields of health and disease as well.

# Introduction

**Small animal radionuclide imaging:** nuclear imaging using Single Photon Emission Computed Tomography (SPECT) or Positron Emission Tomography (PET) allows high-sensitivity and (semi-) quantitative imaging of physiological processes or molecular targets *in vivo*. Before clinical application, preclinical evaluation of novel radiotracers is a requisite to assess tracer characteristics such as *in vivo* tracer kinetics, target specificity, stability, and biodistribution. This is greatly facilitated by the wide-spread use of small animal models of disease as well as the development of state of the art small animal SPECT and PET systems, which allow tracer examination up to sub-mm resolution (1-6). However, preclinical nuclear imaging of small animals comes with a particular set of challenges and opportunities different from clinical nuclear imaging.

**Atherosclerosis:** The challenges and opportunities of small animal imaging become apparent in e.g. atherosclerosis imaging. Atherosclerosis is an inflammatory disease in which fatty plaques might occlude an artery through continued lipid deposition or sudden rupture of vulnerable plaques. Occlusion of an artery can lead to myocardial infarction, stroke, or limb ischemia. Early detection and characterization of atherosclerosis is therefore important, but remains problematic. Many imaging techniques such as contrast enhanced Computed Tomography (CT) focus on degree of stenosis, but fail to identify vulnerable plaques. Functional imaging of biological processes involved in plaque development or progression may identify and localize plaques at risk of rupture. Moreover, the characteristics of a vulnerable plaque, such as the presence of intraplaque haemorrhage, a large influx of inflammatory cells, neovessel formation, or a thin fibrous cap (7), provides ample possibilities for nuclear imaging. Yet, when studying novel tracers that might fulfil this need, research teams are faced with challenges. Differences between animal models of atherosclerosis and the human pathophysiology can make imaging results difficult to interpret. Furthermore, the small size of the plaques in small animal models, as well as the low and diffuse density of targets in a plaque, can severely complicate the evaluation process including quantification options *in vivo*.

**Nuclear imaging of atherosclerosis:** 2-deoxy-2-[$^{18}$F]fluoro-D-glucose ($^{18}$F-FDG) has been extensively studied for the detection and quantification of inflammatory cells in atherosclerosis (8,9), and has been shown an independent predictor of recurrent events after stroke (10-12). Moreover, differentiation between different plaque phenotypes in the carotid arteries was successfully investigated using this tracer (13). However, unspecific uptake of $^{18}$F-FDG, especially in the metabolically active myocardium, limits its use to detect plaques in coronary arteries. As such more specific tracers are urgently needed.

In this review, we describe small animal radionuclide imaging with a strong focus on applications in atherosclerosis. We discuss differences between the pathophysiology of human and mouse

atherosclerosis, related technical aspects and challenges of small animal radionuclide imaging, as well as atherosclerosis tracer development and evaluation. Moreover, we discuss the future outlook and give recommendations.

# Considerations on models of atherosclerosis

**Animal models of atherosclerosis:** A number of atherosclerotic animal models have been developed, as reviewed in (14). In short, porcine and primate models resemble human atherosclerosis best, yet are costly to maintain and are less established with regard to genetic modification. The plaques in rabbit models resemble human plaque less, as rabbit plaques mainly contain lipids. Rabbit models have certain advantages over mouse models, including the diameter of the abdominal aorta being similar to human coronary arteries and less subjected to movement. However, rabbit models are less frequently used since the introduction of the Apolipoprotein E deficient (ApoE$^{-/-}$) and low density lipoprotein receptor knock-out (LDLR$^{-/-}$) (KO) mouse models (15). Most atherosclerosis studies therefore use murine models, as mouse plaques develop faster than rabbit plaques, the mouse models are well characterized, have low costs, and are widely available. Recent developments like clustered regularly interspaced short palindromic repeats/Cas9 (CRISPR/Cas9) targeted genome editing to create KOs (16), and pro-protein convertase subtilisin/kexin type 9 (PCSK9) injection to rapidly induce atherosclerosis (17), have created new opportunities in modelling human-like atherosclerotic disease in mice. We refer to (18) for a more extensive review of mouse models of atherosclerosis. Besides advantages in using atherosclerotic mice, there are several considerations to be taken into account when choosing a mouse model and interpreting imaging results.

**Plaque location and composition:** Like in humans, atherosclerosis in mice is multifocal and locates in specific regions of the vasculature, determined by the hemodynamic environment (19). Pre-clinical imaging studies generally study plaques located in the inner curve of the aorta, the carotid arteries, and brachiocephalic artery, while translating their results to human coronary disease. Plaque composition as well as plaque stability or vulnerability differ between mice and men; differences in lipid metabolism lead to different lipid profiles related to the ratio between high, very low, and low density lipoprotein (HDL, VLDL, and LDL) (14,20). Moreover, thin caps or intraplaque haemorrhage are rare in traditional mouse models, whereas they are characteristic of human vulnerable atherosclerosis (21), and plaque rupture is rarely seen in commonly used mouse models (22). To create a mouse model with plaque rupture, double knock outs (23,24) or invasive experimental interventions are required, which arguably do not mimic human plaque rupture mechanisms (25).

**Immune subsets:** Inflammatory cells are often used as imaging targets, because of the important role they have in plaque formation and progression. Yet, it is reported that human

and mouse macrophage subsets differ (26,27), which therefore makes validation in human tissue necessary.

Despite these differences between human and murine atherosclerosis, mice are valuable in testing radiotracers, as processes like angiogenesis and inflammation are present in mouse plaques. Therefore, mice can be used for proof of concept studies, or to assess tracer behaviour *in vivo*. Moreover, *ex vivo* validation by gamma-counting, autoradiography, and immunohistochemistry allows better quantification of radiotracers. However, for reasons discussed above, translating results obtained in mouse models to expected human results should be done with caution.

# Technical developments and applications in small animal radionuclide imaging

**Nuclear imaging of mouse and human plaques:** SPECT and PET can both provide very high sensitivity, even suitable for imaging of very small quantities of radiotracers (nM-pM range), enabling investigation of specific cells or pathophysiological processes. Developments in these systems for small animal imaging and in processing of imaging data allow better examination of novel radiotracers. Moreover, preclinical systems allow high resolution and sensitive examination of human tissues (28,29). When imaging mouse atherosclerosis challenges become apparent: high spatial resolution is crucial in small murine plaques. The largest murine plaques are located in the aorta, which has a diameter of ~1mm. High sensitivity is however also very important, as these small plaques contain relatively few target cells, on which receptor expression can be low compared to other disease models such as tumour models. Here we highlight a number of developments in imaging and image processing, see (30-36) for more extensive reviews on nuclear imaging methods.

**Preclinical SPECT:** SPECT systems require a collimator to obtain directional information on gamma rays emitted from within the animal or patient sample to be imaged. Traditional clinical SPECT systems generally use a parallel hole collimator, which limits resolution and sensitivity in comparison to clinical PET systems that do not require a collimator (Table 1) (37). The choice of collimator heavily depends on the imaging task at hand because of the classic trade-off between resolution and sensitivity in collimator design. Regarding spatial resolution, major improvements have been made in preclinical SPECT by the introduction of pinhole cameras, in which magnified projection data can be acquired by choosing the right positions of the pinholes between the scintillation crystal and the animal (38), enabling sub-mm resolutions (Table 1 and Figure 1). Such high spatial resolutions can be achieved by decreasing the diameter of the pinhole, but come with the obvious trade-off of lower sensitivity. Multipinhole cameras combat the very low sensitivity of a single pinhole (39), and can reduce or even eliminate the

**Table 1** | Shows a tabulated overview of properties of clinical and preclinical PET and SPECT.

| | Small Animal Scanners | | Standard Clinical Scanners | |
|---|---|---|---|---|
| | Resolution [mm] | Sensitivity ** [%] | Resolution [mm] | Sensitivity [%] |
| SPECT Tc-99m | 0.38–0.76 (83) | 0.07–0.39 (83) | ~10 | ~0.01 |
| SPECT In-111 | 0.71–0.85 (83) | – | – | ~0.01 |
| Pinhole PET F-18 | <0.85* (84) | 0.37 (84) | – | – |
| Coincidence PET F-18 | 1.61–2.34 (39) | 1.19–6.72 (39) | 6.4 (46) | 1.33–2.29 (85) |
| Coincidence PET Ga-68 | 2.19 (86), 2.2 (87) | – | 7 (46) | – |

* Resolution was determined by visual assessment of a Jaszczak phantom instead of measuring the FWHM of a line source.
** Values for sensitivity should be interpreted with care, as no standard method exists to directly compare SPECT and coincidence PET sensitivity quantitatively. When covering a FOV the size of a PET FOV, the effective sensitivity of SPECT could well be several factors lower.
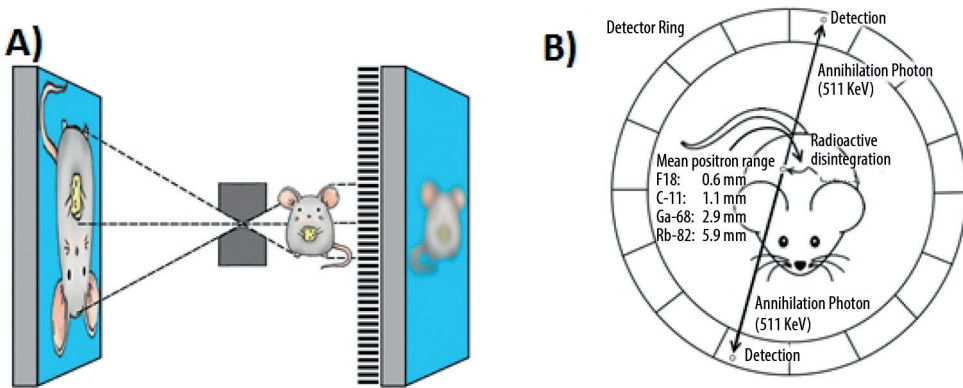


**Figure 1** | **A)** illustrates the principle of pinhole imaging. The collimator can be placed close to the source of radiation in preclinical imaging, resulting in a magnifying effect on the detector. The limited sensitivity is improved by using multiple pinholes and different pinhole geometries. Clinical SPECT mostly uses parallel hole collimators, which directly limits spatial resolution. Pinhole magnification can also achieve a higher spatial resolution for positron emitting isotopes In comparison to traditional coincidence PET *(Image reproduced from thesis O. Ivashchenko, LUMC, ISBN 978-94-92516-35-0)*. **B)** shows the principle of PET coincidence detection. Two opposing detectors simultaneously measure a gamma photon providing the line along which the positron annihilated with an electron. This line does not coincide with the location the positron was emitted, because the positron travels a finite range before it annihilates. Especially for high energy positrons, e.g. [68]Ga (mean positron range of 2.9 mm (52)), the positron range may limit spatial resolution in both pinhole PET and coincidence PET. Image adapted with permission from (131).

need of rotating detectors or movement of the bed if only a small field of view (FOV) is required to answer the research question (40,41). This greatly improves temporal resolution, offers the possibility of 3D gated imaging of the heart, and enables imaging of fast tracer kinetics (42). High sensitivity collimators have been developed (43), but the sensitivity of SPECT systems remains limited in comparison to that of PET because of the relatively low fraction of photons transmitted through the collimators.

**Preclinical PET:** The sensitivity of PET scanners is at least an order of magnitude higher than SPECT cameras (>10 times (44), see Table 1), since no physical collimator is needed. In preclinical PET (ring diameter <20 cm), the resolution is mostly limited by the positron range and the size of the detector elements. For low energy positron emitters ($^{18}$F) both factors limit spatial resolution, for high energy positron emitters ($^{68}$Ga) the positron range is the main limiting factor (44-46).

Positron emitting radionuclides can be imaged with a traditional coincidence based PET system and also with special pinhole collimation (47,48). Traditional ring PET systems can achieve a better image quality in very low count rate studies, for higher count rate studies a multi-pinhole system may yield higher quality images due to the higher spatial resolution that can be achieved by pinhole magnification.

**Hybrid Imaging:** Use of hybrid systems, providing an anatomical reference by (contrast-enhanced) CT or MRI (1,2,39,49), are crucial in atherosclerotic mouse studies because the small plaques are located close to other tissues. MRI has the major advantage of providing soft tissue contrast, which is crucial to distinguish arteries from surrounding tissue. However, the better resolution and faster scanning time of CT make this method preferable in many instances, especially if contrast agents can be used. Moreover, CT provides direct means for attenuation correction (50), whereas an MR image is usually segmented into different tissue classes to obtain an estimate of the amount of attenuating material. New opportunities are opened by the combination of more modalities, such as optical tomography, or integrating PET and SPECT to allow dual-tracer imaging. Moreover, dual tracer imaging is also explored in PET (reviewed in 51), allowing further possibilities in tracer imaging.

**Preclinical versus clinical imaging:** Preclinical SPECT can achieve a higher spatial resolution than preclinical PET platforms, whereas this is the other way round in clinical imaging (see Table 1). The higher resolution of preclinical SPECT often makes it the imaging method of choice for imaging of atherosclerotic mice because of the small sized plaques. Preclinical visualisation of plaques with PET isotopes can further be complicated by positron range, as this can exceed the size of a plaque (e.g. $^{68}$Ga has a mean positron range of 2.9 mm (52)). Image quality of clinical PET can be improved by Time of Flight (ToF), which reduces image noise by incorporating the time difference of the detected annihilation photon pair in the reconstruction. Clinical systems

obtain a timing resolution of ~300 ps (53). In a preclinical system image quality did not improve for a timing resolution of 260 ps (54). Another difference comprises the small deviation from 180° between the annihilating photon pair (noncollinearity) that reduces the spatial resolution for systems with a larger PET ring diameter. This becomes a major limiting factor in clinical PET (44), whilst this effect is negligible in small animal PET. Also, in clinical practice gated imaging is used to improve image quality of moving structures like the heart and its coronary arteries (55,56). A trade-off has to be made between scan time and image quality to obtain sufficient count statistics in each gate. Using image registration techniques, motion-free static images can be obtained without affecting count statistics (57). This application is thus not commonly applied in preclinical imaging. Finally, the high sensitivity and simultaneous acquisition of all projection angles in whole body PET makes it superior over SPECT with regard to temporal resolution, as the time needed to obtain sufficient counts directly determines scanning time.

**Image reconstruction:** Virtually all preclinical and clinical images are reconstructed by an iterative reconstruction algorithm. These algorithms rely on a model of the physics in the imaging process, where improvement of the model improves the quality of the reconstructed images. For example, spatial resolution can be improved by including the point spread function in the model (58). Monte Carlo based methods can improve scatter estimation and can include depth of interaction effects for PET in the iterative reconstruction (59,60). Efficient algorithms can reduce reconstruction time while preserving image quality even in low count studies (61).

**Quantification:** Besides visualizing the radiotracer distribution, most atherosclerosis imaging studies perform (semi-) quantitative Volume Of Interest (VOI) or voxel based measurements. This is expressed in percentage injected dose per gram, standardized uptake value, or target to background ratio (%ID/g, SUV, or TBR). It is important to consider against which background a target tissue is visualized. Plaque to blood ratio is usually a useful TBR in atherosclerosis imaging, as blood signal can interfere with plaque signal. The myocardium would be a suitable background when using a radiotracer such as ^{18}F-FDG in the coronary arteries. Images can be quantified when applying a suitable predetermined calibration factor to convert counts per volume to activity per volume (Bq/ml). Attenuation and scatter correction is less important in preclinical imaging due to the smaller amount of attenuating material, but their application still improves quantification accuracy (50,62-64). When imaging structures with sizes around or below the resolution of the camera, like plaques in mice, it is important to realize that partial volume effects can cause a substantial underestimation of the true value (65,66). This makes absolute quantification accuracy dependent on the imaging task. Numerous compensation techniques for partial volume effects have been described (67), but none have been validated or used in preclinical arthrosclerosis imaging yet.

# Radiotracers and their targets

**Radiotracers and radionuclides:** Radiotracers should target processes relevant to disease, which in atherosclerosis are e.g. inflammation, endothelial dysfunction, neovascularization, hypoxia, cell death, or microcalcification. Moreover, the target should ideally be abundantly expressed and specifically localized in plaques and not in surrounding tissues. Also, blocking studies should be performed, as non-specific uptake in the arterial wall could complicate plaque visualization. Radiotracers need to be stable *in vivo* without pharmacological or toxic effects, and should be labelled with an appropriate radionuclide, matching the pharmacokinetics of the tracer. Radiotracers labelled with short-lived PET radionuclides should have a fast clearance to prevent blood signal from interfering with plaque visualization. Moreover, it is advantageous if radiotracers show rapid diffusion into tissues. If a radiopharmaceutical is being developed with the objective of use in humans, then the radionuclide intended for human use should be used in the animal studies if at all possible as this will simplify translation of preclinical data. In some cases, however, the use of a different radionuclide for some of the preclinical studies is unavoidable or even preferable, as it can be preferred to label radiotracers with SPECT radionuclides for high-resolution preclinical evaluation versus PET radionuclides for clinical use.

**Beyond ^{18}F-FDG:** ^{18}F-FDG PET has shown major promise in atherosclerosis imaging (8). ^{18}F-FDG, being a glucose analogue, is taken up by metabolically active cells such as macrophages in plaque, and can therefore be used for PET imaging of atherosclerosis. Plaque inflammation can be quantified using ^{18}F-FDG, plaques can be monitored over time, and the effect of treatment can be visualized (68). However, unspecific myocardial uptake of ^{18}F-FDG limits the applicability of imaging in coronary artery disease. Therefore, novel radiotracers targeting different disease processes with a higher specificity are being developed and evaluated. Table 2 lists a number of radiotracers and their targets tested in preclinical *in vivo imaging* studies in the past 10 years, and potential clinical follow up studies. Figure 2 includes 2 cases in which the possibilities and challenges of small radionuclide imaging of atherosclerosis are exemplified. Reference (69) reviews older studies performed with PET.

Currently, Pentixafor (70,71), DOTATATE (72,73), and NaF (reviewed in 9) show very promising results in patients. Recent successful mouse studies have been performed on other tracers such as DANBIRT (74), Tilmanocept (75), or Maraciclatide (76). Direct comparisons between radiotracers as performed in (72), are lacking however, which makes it difficult to see where radiotracers can complement each other, or which radiotracer is most suitable for different aspects of plaque visualization.

**Table 2** | shows radiotracers applied in a selection of preclinical *in vivo* atherosclerosis imaging studies from 2008–2018, and mentions potential clinical follow-up studies.

| Disease characteristic | Target | Radiotracer | Radio-nuclide | Animal studies | Clinical studies |
|---|---|---|---|---|---|
| **Inflammation** | Macrophages | FDG | [18]F | (13) | (11) Retrospective, n=513 |
| | Macrophages, SST2 | DOTATATE | [68]Ga | (72) | (88) Retrospective, n=70 (89) Prospective, n=20 (73) Prospective, n=42 |
| | Macrophages, MR | FDM Tilmanocept | [18]F [111]In | (90) (75) | |
| | Macrophages, FR | EC20 ECO800 FOL | [99m]Tc [111]In [18]F | (91) (92) (93) | |
| | Macrophages, CXCR4 | Pentixafor | [68]Ga | (70) | (71) Retrospective, n=38 (94) Retrospective, n=51 |
| | Leukocytes, LFA-1 | DANBIRT | [111]In | (74) | |
| | Macrophage proliferation | FLT | [18]F | (95) | |
| | Chemokine receptors | DOTA-vMIP-II | [64]Cu | (96,97) | |
| | | DOTA-DAPTA | [64]Cu | (98) | |
| | LOX-1 | Liposome-LOX-1 | [111]In | (99) | |
| | | Camelid antibody fragment | [99m]Tc | (100) | |
| | TSPO | PK11195 | [11]C | | (101) Prospective, n=15 (102) Prospective, n=32 (103) |
| | | Ge-180 | [18]F | | |
| | Macrophage phagocytosis | TNP Macroflor | [64]Cu [18]F | (104) (105) | |
| **Apoptosis** | Apoptosis &Necrosis | AnxAF568 Hypericin | [99m]Tc, [124]I | (106) | |
| | Apoptosis | Duramycin | [99m]Tc | (107) | |
| | Apoptosis | Duramycin & Annexin V | [99m]Tc | (108) | |

| Disease characteristic | Target | Radiotracer | Radio-nuclide | Animal studies | Clinical studies |
|---|---|---|---|---|---|
| **Angiogenesis** | $\alpha_v\beta_3$ integrin | NC100692 | $^{99m}$Tc | (109) | |
| | | NOTA-RGD | $^{68}$Ga | (110) | (110) Prospective, n=4 |
| | | Flotegatide | $^{18}$F | (111) | |
| | | Galacto-RGD | $^{18}$F | (112) | (113) Prospective, n=10 |
| | | NOTA-3-4A | $^{64}$Cu | (114) | |
| | | Maraciclatide | $^{99m}$Tc | (76) | |
| | | IDA-D-[c(RGDfK)]$_2$ | $^{99m}$Tc | (115) | |
| | VEGF 1 & 2 | scV/Tc | $^{99m}$Tc | (112, 113) | |
| **Proteolysis** | MMP activation | RP805 | $^{99m}$Tc | (114, 115) | |
| | | RP782 | $^{111}$In | (116, 117) | |
| | GPVI | GPVI-fragment crystallized | $^{64}$Cu | (122) | |
| **Endothelial activation** | P-selectin | P-selectin antibody | $^{64}$Cu | (123) | |
| | | Fucoidan | $^{68}$Ga | (124) | |
| | VCAM-1 | cAbVCAM1-5 | $^{99m}$Tc $^{18}$F | (125–127) (128) | |
| | | 4V | $^{18}$F | (129) | |
| **Hypoxia** | Redox | FMISO | $^{18}$F | (130) | |

*Abbreviations:* SST2, somatostatin receptor subtype 2; MR, Mannose Receptor; FR, Folate Receptor; CXCR4, C-X-C Chemokine Receptor type 4; LFA-1, Leukocyte Function associated Antigen-1; LOX-1, oxidized LDL receptor 1; TSPO, Translocatio Protein; VEGF, Vascular Endothelial Growth Factor; MMP, Matrix Metalloprotease; GPVI, Platelet Glycoprotein VI; VCAM-1, Vascular Cell Adhesion Molecule-1.
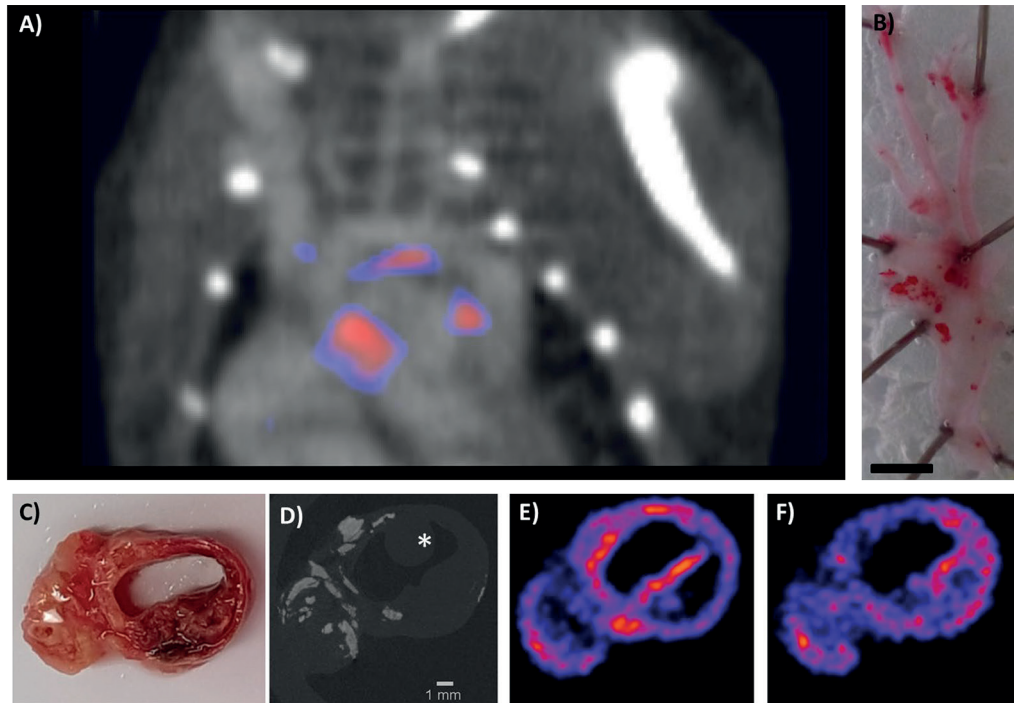
2

**Figure 2 | Shows 2 cases which exemplify the opportunities and challenges in preclinical imaging using multi-pinhole collimators. Image A)** shows a contrast enhanced SPECT/CT scan of the thoracic region of an ApoE^{-/-} mouse (on 20 weeks high fat diet), imaged with ^{111}In-DANBIRT, which targets leukocytes via Leukocyte Function associated Antigen 1 (LFA-1). LFA-1 is expressed in a high-affinity state on leukocytes near regions of inflammation, and can therefore be used to visualize inflamed plaque. The image shows uptake in plaque regions in the inner curve of the aortic arch and near the aortic leaflets. These common sites of plaque formation in this mouse model are visible in the excised, opened Oil Red O stained artery of an ApoE^{-/-} mouse on the right **B). Image A** shows the high resolution which can be achieved with preclinical SPECT, considering the mouse aorta is approximately 1 mm in diameter. This case also illustrates some of the challenges in preclinical imaging as the small size of the plaque and the presence of few target cells require a state of the art imaging system with high resolution and sensitivity. Moreover, the recommended injection dose of 20 uL contrast agent per 5 g bodyweight (Exitron nano 12000) can be challenging, as the combined injection volume of contrast agent and radiotracer injection can easily exceed the recommended injection volume for mice, which can have adverse effects on the animal health and experimental outcome. Reduction of the injection volume of the radiopharmaceuticals can be achieved by using smaller tubing during radiolabelling. The timing of injection is also important, as blood signal of radiotracers can be high after injection, yet the amount of activity reduces with radionuclide half-life. Moreover, many contrast agents circulate a limited period in the vasculature. Optimization before an experiment, considering the dose and timing of injection, is therefore crucial. In this example, we injected 50 MBq (200 pmol) ^{111}In-DANBIRT 2 hrs before SPECT imaging, and the contrast agent directly at the start of CT imaging. Scale bar=2 mm. (reproduced from (74), no permissions required).

**Images C-F** depict an example of a high resolution dual-isotope preclinical SPECT/CT scanning protocol applied to diseased human arterial tissue. Examination of the local differences in dual-radiotracer uptake with respect to the atherosclerotic pathophysiology was performed on **C)** a human carotid endarterectomy slice of 2 mm thickness, which was incubated for 60 min with ^{111}In-DANBIRT (targeting leukocytes) and ^{99m}Tc-DEMOTATE (targeting activated macrophages) (both 1 nmol, 100 MBq/nmol). DEMOTATE targets somatostatin receptor subtype 2, which is expressed on activated macrophages. **D)** Functional plaque morphology was resolved with high resolution µCT (15 min scan, full scan angle, 0.24 mA, 50 kV, 75 ms, 500 µm reconstructed resolution), where calcifications are denoted by the bright white regions. The asterisk (*) marks the sample holder. µCT was co-registered to SPECT (90min scan) reconstructions of **E)** ^{111}In-DANBIRT and **F)** ^{99m}Tc-DEMOTATE. The two radioisotopes can be separated by selecting the correct energy windows for the photon peaks of ^{111}In and [99m]Tc (^{111}In photopeaks 171 and 245 keV, energy windows 158–187 keV and 219–267 keV. [99m]Tc photopeak 140 keV, energy window 125–152 keV). This hybrid functional imaging approach can be used to gain greater insights into radiotracer uptake in diseased tissues. Plaque status can be assessed via the presence of calcifications, whereas DANBIRT and DEMOTATE ascertain inflammatory status by visualizing total inflammation and activated macrophages, respectively. Such scans could lead to a better risk stratification of atherosclerotic patients. It is interesting to see the different distribution patterns of these inflammation-targeted tracers within the plaque, which indicates that plaque detection alone gives only limited information when making a risk stratification of atherosclerotic patients. The timing of imaging is important as the radionuclides have different half-lives, and correct separation of the photon peaks requires sufficient counts to be acquired. Another challenge is to examine which incubation time allows the radiotracers to diffuse into the tissue, while keeping tissue degradation at a minimum *(Courtesy H.E.B, Erasmus MC)*.

# Perspectives and recommendations

**Risk stratification in atherosclerosis:** The development of non-invasive imaging techniques visualizing atherosclerosis and particularly vulnerable plaque is a major aim in cardiovascular imaging (77). The individual and societal impact of such imaging tools can be substantial. They could contribute to current risk stratification, which is based on conventional cardiovascular risk factors and non-traditional risk factors such as biomarkers and coronary artery calcium score. Recent clinical trials focus on the importance of anti-inflammatory strategies for treatment of cardiovascular disease (78,79). Biomarkers (e.g. hsCRP, IL-6) are mostly used for assessment of inflammation, and might be complemented by non-invasive molecular imaging of arterial inflammation in guiding treatment with these new anti-inflammatory drugs. Novel tracers therefore could provide extra prognostic value, and aid in further risk-stratification by identifying plaques at risk and patients in need of treatment.

**Crossing borders:** Diagnostic imaging tools developed for other (non-cardiac) diseases such as oncology have been shown to be of significance in atherosclerosis research (80). Somatostatin receptor imaging using ^{68}Ga-DOTATATE, developed for diagnosis of neuro-endocrine tumours, has been validated as a novel marker of atherosclerotic inflammation via overexpression of the somatostatin receptor subtype 2 (SST2) on activated macrophages.

This has led to better discriminating power of high risk coronary lesions compared to ^{18}F-FDG (72,73). Similarly, imaging of macrophages with ^{68}Ga-Pentixafor also originates from oncology (70,71). Furthermore, technical challenges in image post-processing in atherosclerosis might be improved by developments from other research fields (81,82). Vice versa, research on other diseases can benefit from our increased knowledge, as diagnosis of other inflammatory diseases such as arthritis can be difficult and hampered by similar challenges encountered in atherosclerosis.

# Conclusion

Developments in animal models and imaging systems have facilitated and enhanced the opportunities for small radionuclide imaging and will likely continue to do so in the foreseeable future. These advances have been essential in preclinical imaging of atherosclerosis, which requires high resolution and sensitivity, and has resulted in a large number of novel radiotracers being evaluated. This allows ample opportunity for clinical translation, where more insight into atherosclerosis, as well as relevant imaging targets, are highly required.

## Author contributions statement
All authors listed have made a substantial, direct, and intellectual contribution to the work and approved it for publication.

## Conflict of interest statement

# References

1.  Wehrl HF, Wiehr S, Divine MR, Gatidis S, Gullberg GT, Maier FC, et al. Preclinical and Translational PET/MR Imaging. J Nucl Med. 2014;55:11S–18S.

2.  Gaitanis A, Kastis GA, Vlastou E, Bouziotis P, Verginis P, Anagnostopoulos CD. Investigation of Image Reconstruction Parameters of the Mediso nanoScan PC Small-Animal PET/CT Scanner for Two Different Positron Emitters Under NEMA NU 4-2008 Standards. Mol Imaging Biol. 2017;19(4):550–9.

3.  Lauber DT, Fülöp A, Kovács T, Szigeti K, Máthé D, Szijártó A. State of the art in vivo imaging techniques for laboratory animals. Lab Anim. 2017;1(14).

4.  España S, Marcinkowski R, Keereman V, Vandenberghe S, van Holen R. DigiPET : Sub-millimeter spatial resolution small-animal PET imaging using thin monolithic scintillators. Phys Med Biol. 2014;59(13).

5.  Nekolla SG, Rischpler C, Paschali A, Anagnostopoulos C. Cardiovascular preclinical imaging. Q J Nucl Med Mol imaging. 2017;61(1):48–59.

6.  Ivashchenko O, Have F Van Der, Goorden MC, Ramakers RM, Beekman FJ. Ultra-High-Sensitivity Submillimeter Mouse SPECT. J Nucl Med. 2015;56(3):470–6.

7.  Virmani R, Kolodgie FD, Burke AP, Farb A, Schwartz SM. Lessons From Sudden Coronary Death A Comprehensive Morphological Classification Scheme for Atherosclerotic Lesions. Arter Thromb Biol. 2000;20:1262–75.

8.  Rudd JHF, Warburton EA, Fryer TD, Jones HA, Clark JC, Antoun N, et al. Imaging atherosclerotic plaque inflammation with [18F]-fluorodeoxyglucose positron emission tomography. Circulation. 2002;105(23):2708–11.

9.  Mckenney-drake ML, Moghbel MC, Paydary K, Alloosh M, Houshmand S, Høilund-carlsen PF, et al. 18 F-NaF and 18 F-FDG as molecular probes in the evaluation of atherosclerosis. Eur J Nucl Med Mol Imaging. 2018;2190–200.

10. Marnane M, Merwick A, Sheehan OC, Hannon N, Foran P, Grant T, et al. Carotid plaque inflammation on 18F-fluorodeoxyglucose positron emission tomography predicts early stroke recurrence. Ann Neurol. 2012;71(5):709–18.

11. Figueroa AL, Abdelbaky A, Truong QA, Corsini E, MacNabb MH, Lavender ZR, et al. Measurement of arterial activity on routine FDG PET/CT images improves prediction of risk of future CV events. JACC Cardiovasc Imaging. 2013;6(12):1250–9.

12. Moon SH, Cho YS, Noh TS, Choi JY, Kim BT, Lee KH. Carotid FDG uptake improves prediction of future cardiovascular events in asymptomatic individuals. JACC Cardiovasc Imaging. 2015;8(8):949–56.

13. Wenning C, Kloth C, Kuhlmann MT, Jacobs AH, Schober O, Hermann S, et al. Serial F-18-FDG PET / CT distinguishes in fl amed from stable plaque phenotypes in shear-stress induced murine atherosclerosis. Atherosclerosis. 2014;234(2):276–82.

14. Getz GS, Reardon CA. Animal Models of Atherosclerosis Animal Models of Atherosclerosis. Arterioscler Thromb Vasc Biol. 2012;32:1104–15.

15. Fan J, Kitajima S, Watanabe T, Xu J, Zhang J, Liu E, et al. Rabbit models for the study of human atherosclerosis: from pathophysiological mechanisms to translational medicine. Pharmacol Ther. 2015;(0):104–19.

16. Jarrett KE, Lee C, De Giorgi M, Hurley A, Gillard BK, Doerfler AM, et al. Somatic Editing of *Ldlr* With Adeno-Associated Viral-CRISPR Is an Efficient Tool for Atherosclerosis Research. Arterioscler Thromb Vasc Biol. 2018;28:1997-2006.

17. Kumar S, Kang DW, Rezvan A, Jo H. Accelerated atherosclerosis development in C57Bl6 mice by overexpressing AAV-mediated PCSK9 and partial carotid ligation. Lab Investig.2017;97(8):935–45.

18. Veseli BE, Perrotta P, De Meyer GRA, Roth L, Van der Donckt C, Martinet W, et al. Animal Models of Atherosclerosis. Eur J Pharmacol. 2017;816:3–13.

19. Suo J, Ferrara DE, Sorescu D, Guldberg RE, Taylor WR, Giddens DP. Hemodynamic shear stresses in mouse aortas: Implications for atherogenesis. Arterioscler Thromb Vasc Biol. 2007;27(2):346–51.

20. Li X, Liu Y, Zhang H, Ren L, Li Q, Li N. Animal models for the atherosclerosis research: A review. Protein Cell. 2011;2(3):189–201.

2

21.    Falk E. Pathogenesis of Atherosclerosis. J Am Coll Cardiol. 2006;47(8):C7-12.

22.    Daeichin V, Sluimer JC, van der Heiden K, Skachkov I, Kooiman K, Janssen A, et al. Live Observation of Atherosclerotic Plaque Disruption in Apolipoprotein E-Deficient Mouse. Ultrasound Int Open. 2015;01(02):E67–71.

23.    Zhang S, Picard MH, Vasile E, Zhu Y, Raffai RL, Weisgraber KH, et al. Diet-induced occlusive coronary atherosclerosis, myocardial infarction, cardiac dysfunction, and premature death in scavenger receptor class B type I-deficient, hypomorphic apolipoprotein ER61 mice. Circulation. 2005;111(25):3457–64.

24.    Van Herck JL, De Meyer GRY, Martinet W, Van Hove CE, Foubert K, Theunis MH, et al. Impaired fibrillin-1 function promotes features of plaque instability in apolipoprotein E-deficient mice. Circulation. 2009;120(24):2478–87.

25.    Heiden K Van Der, Hoogendoorn A, Daemen MJ, Gijsen FJH. Animal models for plaque rupture: a biomechanical assessment. Thrombosis and Haemostasis 2016;115(3):501–8.

26.    Mestas J, Hughes CCW. Of Mice and Not Men: Differences between Mouse and Human Immunology. J Immunol. 2004;172(5):2731–8.

27.    Martinez FO, Helming L, Milde R, Varin A, Melgert BN, Draijer C, et al. Genetic programs expressed in resting and IL-4 alternatively activated mouse and human macrophages: Similarities and differences. Blood. 2013;121(9):57–70.

28.    Jager NA, Westra J, Golestani R, van Dam GM, Low PS, Tio RA, et al. Folate receptor-β imaging using 99mTc-folate to explore distribution of polarized macrophage populations in human atherosclerotic plaque. J Nucl Med. 2014;55(12):1945–51.

29.    Irkle A, Vesey AT, Lewis DY, Skepper JN, Bird JLE, Dweck MR, et al. Identifying active vascular microcalcification by 18F-sodium fluoride positron emission tomography. Nat Commun. 2015;6:7495.

30.    de Kemp RA, Epstein FH, Catana C, Tsui BMW, Ritman EL. Small-Animal Molecular Imaging Methods. J Nucl Med. 2010;51:18S–32S.

31.    Van Audenhaege K, Van Holen R, Vandenberghe S, Vanhove C, Metzler SD, Moore SC. Review of SPECT collimator selection, optimization, and fabrication for clinical and preclinical imaging. Med Phys. 2015;42(8):4796–813.

32.    Yao R, Lecomte R, Crawford ES. Small-Animal PET: What Is It, and Why Do We Need It? J Nucl Med Technol. 2012;40(3):157–65.

33.    Wells RG. Instrumentation in molecular imaging.J Nucl Cardiol 2016;6:1343–7.

34.    Clark DP, Badea CT. Micro-CT of rodents: State-of-the-art and future perspectives. Phys Medica. 2014;30(6):619–34.

35.    Weissleder R, Ross BD, Rehemtulla A, Gabmhir SS. Molecular Imaging: Principles and Practice. 2011, PMPH, USA.

36.    Zaidi H. Molecular imaging of small animals: instrumentation and applications. 2014, Springer-Verlag, NY.

37.    Anger HO. Scintillation Camera With Multichannel Collimators. J Nucl Med. 1964;5:515–31.

38.    Beekman F, van Der Have F. The pinhole: Gateway to ultra-high-resolution three-dimensional radionuclide imaging. Eur J Nucl Med Mol Imaging. 2007;34(2):151–61.

39.    Goertzen AL, Bao Q, Bergeron M, Blankemeyer E, Blinder S, Cañadas M, et al. Comparison of preclinical PET imaging systems. J Nucl Med. 2012;53(8):1300–9.

40.    Branderhorst W, Vastenhouw B, Van Der Have F, Blezer ELA, Bleeker WK, Beekman FJ. Targeted multi-pinhole SPECT. Eur J Nucl Med Mol Imaging. 2011;38(3):552–61.

41.    Lange C, Apostolova I, Lukas M, Huang KP, Hofheinz F, Gregor-Mamoudou B, et al. Performance evaluation of stationary and semi-stationary acquisition with a non-stationary small animal multi-pinhole SPECT system. Mol Imaging Biol. 2014;16(3):311–6.

42.    Vaissier PEB, Goorden MC, Vastenhouw B, van der Have F, Ramakers RM, Beekman FJ. Fast Spiral SPECT with Stationary -Cameras and Focusing Pinholes. J Nucl Med. 2012;53(8):1292–9.

43.    Mahani H, Raisali G, Kamali-Asl A, Ay MR. Spinning slithole collimation for high-sensitivity small animal SPECT: Design and assessment using GATE simulation. Phys Medica. 2017;40:42–50.

44.    Rahmim A, Zaidi H. PET versus SPECT: strengths, limitations and challenges. Nucl Med Commun. 2008;29(3):193–207.

45. Levin CS, Hoffman EJ. Calculation of positron range and its effect on the fundamental limit of positron emission tomography system spatial resolution. Phys Med Biol. 1999;44:781–99.

46. Sanchez-Crespo A. Comparison of Gallium-68 and Fluorine-18 imaging characteristics in positron emission tomography. Appl Radiat Isot. 2013;76:55–62.

47. Goorden MC, van der Have F, Kreuger R, Ramakers RM, Vastenhouw B, Burbach JPH, et al. VECTor: A Preclinical Imaging System for Simultaneous Submillimeter SPECT and PET. J Nucl Med. 2013;54(2):306–12.

48. DiFilippo FP. Design of a Tri-PET collimator for high-resolution whole-body mouse imaging: Med Phys. 2017;44(8):4230–8.

49. Hamamura MJ, Ha S, Roeck WW, Wagenaar DJ, Meier D, Patt BE, et al. Initial investigation of preclinical integrated SPECT and MR imaging. Technol Cancer Res Treat. 2010;9(1):21–7.

50. Vanhove C, Defrise M, Bossuyt A, Lahoutte T. Improved quantification in multiple-pinhole SPECT by anatomy-based reconstruction using microCT information. Eur J Nucl Med Mol Imaging. 2009;38(1):153–65.

51. Walrand S, Hesse M, Jamar F. Update on novel trends in PET / CT technology and its clinical applications. Br J Radiol. 2018;89.

52. Partridge M, Spinelli A, Ryder W, Hindorf C. The effect of β+energy on performance of a small animal PET camera. Nucl Inst Methods Phys Res. 2006;568(2):933–6.

53. Surti S, Karp JS. Advances in time-of-flight PET. Phys Medica. 2016;32(1):12–22.

54. Schug D, Lerche C, Weissler B, Gebhardt P, Goldschmidt B, Wehner J, et al. Initial PET performance evaluation of a preclinical insert for PET/MRI with digital SiPM technology. Phys Med Biol. 2016;61(7):2851–78.

55. Buther F, Dawood M, Stegger L, Wubbeling F, Schafers M, Schober O, et al. List Mode-Driven Cardiac and Respiratory Gating in PET. J Nucl Med. 2009;50(5):674–81.

56. Rubeaux M, Joshi N V., Dweck MR, Fletcher A, Motwani M, Thomson LE, et al. Motion Correction of 18F-NaF PET for Imaging Coronary Atherosclerotic Plaques. J Nucl Med. 2016;57(1):54–9.

57. Wu C, Vaissier PE, Vastenhouw B, de Jong JR, Slart RH, Beekman FJ. Influence of respiratory gating, image filtering, and animal positioning on high-resolution electrocardiography-gated murine cardiac single-photon emission computed tomography. Mol Imaging. 2014;13:1–11.

58. Peterson TE, Shokouhi S. Advances in Preclinical SPECT Instrumentation. J Nucl Med. 2012;53(6):841–4.

59. Magdics M, Szirmay-Kalos L, Toth B, Legrady D, Cserkaszky A, Balkay L, et al. Performance evaluation of scatter modeling of the GPU-based "Tera-Tomo" 3D PET reconstruction.IEEE Nuclear Science Symposium Conference Record. IEEE; 4086–8.

60. Nagy K, Toth M, Major P, Patay G, Egri G, Haggkvist J, et al. Performance Evaluation of the Small-Animal nanoScan PET/MRI System. J Nucl Med. 2013;54(10):1825–32.

61. Vaissier PEB, Beekman FJ, Goorden MC. Similarity-regulation of OS-EM for accelerated SPECT reconstruction. Phys Med Biol.2016;61(11):4300–15.

62. Chen CL, Wang Y, Lee JJS, Tsui BMW. Toward quantitative small animal pinhole SPECT: Assessment of quantitation accuracy prior to image compensations. Mol Imaging Biol. 2009;11(3):195–203.

63. Wu C, de Jong JR, Gratama van Andel HA, van der Have F, Vastenhouw B, Laverman P, et al. Quantitative multi-pinhole small-animal SPECT: uniform versus non-uniform Chang attenuation correction. Phys Med Biol. 2011;56(18):N183-93.

64. Vandeghinste B, Van Holen R, Vanhove C, De Vos F, Vandenberghe S, Staelens S. Use of a ray-based reconstruction algorithm to accurately quantify preclinical microspect images. Mol Imaging. 2014;13(4):1–13.

65. Bettinardi V, Castiglioni I, De Bernardi E, Gilardi MC. PET quantification: Strategies for partial volume correction. Clin Transl Imaging. 2014;2(3):199–218.

66. Mannheim JG, Judenhofer MS, Schmid A, Tillmanns J, Stiller D, Sossi V, et al. Quantification accuracy and partial volume effect in dependence of the attenuation correction of a state-of-the-art small animal PET scanner. Phys Med Biol. 2012;57(12):3981–93.

67. Erlandsson K, Buvat I, Pretorius PH, Thomas BA, Hutton BF. A review of partial volume correction techniques for emission tomography and their applications in neurology, cardiology and oncology. Phys Med Biol. 2012;57(21).

2

68. Tawakol A, Fayad Z a, Mogg R, Alon A, Klimas MT, Dansky H, et al. Intensification of statin therapy results in a rapid reduction in atherosclerotic inflammation: results of a multicenter fluorodeoxyglucose-positron emission tomography/computed tomography feasibility study. J Am Coll Cardiol. 2013 Sep 3;62(10):909–17.

69. Hag AMF, Ripa RS, Pedersen SF, Bodholdt RP, Kjaer A. Small animal positron emission tomography imaging and in vivo studies of atherosclerosis. Clin Physiol Funct Imaging. 2013;33(3):173–85.

70. Hyafil F, Pelisek J, Laitinen I, Schottelius M, Mohring M, Yvonne D, et al. Imaging the Cytokine Receptor CXCR4 in Atherosclerotic Plaques with the Radiotracer 68 Ga-Pentixafor for PET. J Nucl Med. 2017;58:499–506.

71. Li X, Heber D, Leike T, Beitzke D, Lu X, Zhang X, et al. [68Ga]Pentixafor-PET/MRI for the detection of Chemokine receptor 4 expression in atherosclerotic plaques. Eur J Nucl Med Mol Imaging. 2018;45(4):558–66.

72. Rinne P, Hellberg S, Kiugel M, Virta J, Li X-G, Käkelä M, et al. Comparison of Somatostatin Receptor 2-Targeting PET Tracers in the Detection of Mouse Atherosclerotic Plaques. Mol Imaging Biol. 2015;18(1):99–108.

73. Tarkin JM, Joshi FR, Evans NR, Chowdhury MM, Figg NL, Shah AV, et al. Detection of Atherosclerotic Inflammation by 68Ga-DOTATATE PET Compared to [18F]FDG PET Imaging. J Am Coll Cardiol. 2017;69(14):1774–91.

74. Meester EJ, Krenning BJ, de Blois RH, Norenberg JP, de Jong M, Bernsen MR, et al. Imaging of atherosclerosis, targeting LFA-1 on inflammatory cells with 111In-DANBIRT. J Nucl Cardiol. 2018;1–8.

75. Varasteh Z, Hyafil F, Anizan N, Diallo D, Aid-launais R, Mohanta S, et al. Targeting mannose receptor expression on macrophages in atherosclerotic plaques of apolipoprotein E-knockout mice using In-tilmanocept. EJNMMI Res. 2017;7(1):40.

76. Vancraeynest D, Roelants V, Bouzin C, Hanin F, Walrand S, Bol V, et al. αVβ3 integrin-targeted microSPECT / CT imaging of inflamed atherosclerotic plaques in mice. EJNMMI Res. 2016;6(29).

77. Quillard T, Libby P. Molecular imaging of atherosclerosis for improving diagnostic and therapeutic development. Circ Res 2012;111(2):231–44.

78. Ridker PM, Everett BM, Thuren T, MacFadyen JG, Chang WH, Ballantyne C, et al. Antiinflammatory Therapy with Canakinumab for Atherosclerotic Disease. N Engl J Med. 2017;377(12):1119-1131.

79. Kottoor SJ, Arora RR. The Utility of Anti-Inflammatory Agents in Cardiovascular Disease. J Cardiovasc Pharmacol Ther. 2018;23(6):483-493.

80. Sarikaya I, Larson SM, Freiman A, Strauss HW. What nuclear cardiology can learn from nuclear oncology. J Nucl Cardiol. 2003;10(3):324–8.

81. Carlier T, Bailly C. State-Of-The-Art and Recent Advances in Quantification for Therapeutic Follow-Up in Oncology Using PET. Front Med. 2015;2:1–12.

82. van der Vos CS, Koopman D, Rijnsdorp S, Arends AJ, Boellaard R, van Dalen JA, et al. Quantification, improvement, and harmonization of small lesion detection with state-of-the-art PET. Eur J Nucl Med Mol Imaging. 2017;44:4–16.

83. Deleye S, Van Holen R, Verhaeghe J, Vandenberghe S, Stroobants S, Staelens S. Performance evaluation of small-animal multipinhole μSPECT scanners for mouse imaging. Eur J Nucl Med Mol Imaging. 2013;40(5):744–58.

84. Walker MD, Goorden MC, Dinelle K, Ramakers RM, Blinder S, Shirmohammad M, et al. Performance Assessment of a Preclinical PET Scanner with Pinhole Collimation by Comparison to a Coincidence-Based Small-Animal PET Scanner. J Nucl Med. 2014;55(8):1368–74.

85. Ilan E, Deller T, Kjellberg F, Peterson W, Lubberink M. Performance comparison of three commercially available PET systems: SIGNA PET/MR, Discovery IQ and Discovery MI. J Nucl Med, 2017;58(S1):1353.

86. Liu X, Laforest R. Quantitative small animal PET imaging with nonconventional nuclides. Nucl Med Biol.2009 Jul 1;36(5):551–9.

87. Canadas M, Sanz ER, Vives MO, Vaquero JJ, Desco M, Vicente E, et al. Performance evaluation for 68Ga and 18F of the ARGUS small-animal PET scanner based on the NEMA NU-4 standard. IEEE Nuclear Science Symposuim & Medical Imaging Conference. IEEE; 2010. p. 3454–7.

88. Rominger A, Saam T, Vogl E, Ubleis C, la Fougère C, Förster S, et al. In vivo imaging of macrophage activity in the coronary arteries using 68Ga-DOTATATE PET/CT: correlation with coronary calcium burden and risk factors. J Nucl Med. 2010;51(2):193–7.

89.   Wan MYS, Endozo R, Michopoulou S, Shortman R, Rodriguez-Justo M, Menezes L, et al. PET/CT Imaging of Unstable Carotid Plaque with Ga-68 labelled Somatostatin Receptor Ligand. J Nucl Med. 2017;58(5):774-780.

90.   Tahara N, Mukherjee J, de Haas HJ, Petrov AD, Tawakol A, Haider N, et al. 2-deoxy-2-[18F]fluoro-D-mannose positron emission tomography imaging in atherosclerosis. Nat Med. 2014;20(2):215–9.

91.   Ayala-lopez W, Xia W, Varghese B, Low PS. Imaging of Atherosclerosis in Apoliprotein E Knockout Mice: Targeting of a Folate-Conjugated Radiopharmaceutical to Activated Macrophages. J Nucl Med. 2010;51(5):768–74.

92.   Winkel LCJ, Groen HC, van Thiel BS, Müller C, van der Steen AFW, Wentzel JJ, et al. Folate receptor–targeted single-photon emission computed tomography/computed tomography to detect activated macrophages in atherosclerosis: can it distinguish vulnerable from stable atherosclerotic plaques? Mol Imaging. 2013;13:1–5.

93.   Silvola JMU, Li X-G, Virta J, Marjamäki P, Liljenbäck H, Hytönen JP, et al. Aluminum fluoride-18 labeled folate enables in vivo detection of atherosclerotic plaque inflammation by positron emission tomography. Sci Rep. 2018;8(1):9720.

94.   Weiberg D, Thackeray JT, Daum G, Sohns JM, Kropf S, Wester H-J, et al. Clinical Molecular Imaging of Chemokine Receptor CXCR4 Expression in Atherosclerotic Plaque using 68 Ga-Pentixafor PET: Correlation with Cardiovascular Risk Factors and Calcified Plaque Burden. J Nucl Med. 2018;59(2):266-272.

95.   Ye Y, Calcagno C, Binderup T, Courties G, Keliher EJ, Wojtkiewicz GR, et al. Imaging Macrophage and Hematopoietic Progenitor Proliferation in Atherosclerosis. Circ Res. 2015;117:835–45.

96.   Liu Y, Pierce R, Luehmann HP, Sharp TL, Welch MJ. PET Imaging of Chemokine Receptors in Vascular Injury-Accelerated Atherosclerosis. J Nucl Med. 2013;54(7):1135–41.

97.   Luehmann HP, Detering L, Fors BP, Pressly ED, Woodard PK, Randolph GJ, et al. PET/CT Imaging of Chemokine Receptors in Inflammatory Atherosclerosis Using Targeted Nanoparticles. J Nucl Med. 2016;57(7):1124–9.

98.   Luehmann HP, Pressly ED, Detering L, Wang C, Pierce R, Woodard PK, et al. PET/CT Imaging of Chemokine Receptor CCR5 in Vascular Injury Model Using Targeted Nanoparticle. J Nucl Med. 2014;55(4):629–34.

99.   Li D, Patel AR, Klibanov AL, Kramer CM, Ruiz M, Kang BY, et al. Molecular imaging of atherosclerotic plaques targeted to oxidized LDL receptor LOX-1 by SPECT/CT and magnetic resonance. Circ Cardiovasc Imaging. 2010;3(4):464–72.

100.  De Vos J, Mathijs I, Xavier C, Massa S, Wernery U, Bouwens L, et al. Specific Targeting of Atherosclerotic Plaques in ApoE-/- Mice Using a New Camelid sdAb Binding the Vulnerable Plaque Marker LOX-1. Mol Imaging Biol. 2014;16:690–698.

101.  Pugliese F, Gaemperli O, Kinderlerer AR, Lamare F, Shalhoub J, Davies AH, et al. Imaging of vascular inflammation with [11C]-PK11195 and positron emission tomography/computed tomography angiography. J Am Coll Cardiol. 2010;56(8):653–61.

102.  Gaemperli O, Shalhoub J, Owen DRJ, Lamare F, Johansson S, Fouladi N, et al. Imaging intraplaque inflammation in carotid atherosclerosis with 11C-PK11195 positron emission tomography/computed tomography. Eur Heart J. 2012;33(15):1902–10.

103.  Hellberg S, Liljenbäck H, Eskola O, Morisson-Iveson V, Morrison M, Trigg W, et al. Positron Emission Tomography Imaging of Macrophages in Atherosclerosis with 18 F-GE-180, a Radiotracer for Translocator Protein (TSPO). Contrast Media Mol Imaging. 2018;2018:1–11.

104.  Nahrendorf M, Zhang H, Hembrador S, Panizzi P, Sosnovik DE, Aikawa E, et al. Nanoparticle PET-CT imaging of macrophages in inflammatory atherosclerosis. Circulation. 2008;117(3):379–87.

105.  Keliher EJ, Ye YX, Wojtkiewicz GR, Aguirre AD, Tricot B, Senders ML, et al. Polyglucose nanoparticles with renal elimination and macrophage avidity facilitate PET imaging in ischaemic heart disease. Nat Commun. 2017;8:1–12.

106.  De Saint-Hubert M, Bauwens M, Deckers N, Drummen M, Douma K, Granton P, et al. In vivo molecular imaging of apoptosisand necrosis in atherosclerotic plaques using MicroSPECT-CT and MicroPET-CT Imaging. Mol Imaging Biol. 2014;16(2):246–54.

107.  Liu Z, Larsen BT, Lerman LO, Gray BD, Barber C, Hedayat AF, et al. Detection of atherosclerotic plaques in ApoE-deficient mice using 99m Tc-duramycin. Nucl Med Biol. 2016;43(8):496–505.

108.  Hu Y, Liu G, Zhang H, Li Y, Gray BD, Pak KY, et al. A Comparison of [99mTc]Duramycin and [99mTc]Annexin V in SPECT/CT Imaging Atherosclerotic Plaques. Mol Imaging Biol; 2018;20(2):249–59.

2

109. Razavian M, Marfatia R, Mongue-Din H, Tavakoli S, Sinusas AJ, Zhang J, et al. Integrin-targeted imaging of inflammation in vascular remodeling. Arterioscler Thromb Vasc Biol. 2011;31(12):2820–6.

110. Paeng JC, Lee YS, Lee JS, Jeong JM, Kim KB, Chung JK, et al. Feasibility and kinetic characteristics of 68Ga-NOTA-RGD PET for in vivo atherosclerosis imaging. Ann Nucl Med. 2013;27(9):847–54.

111. Su H, Gorodny N, Gomez LF, Gangadharmath UB, Mu F, Chen G, et al. Atherosclerotic plaque uptake of a novel integrin tracer 18 F-Flotegatide in a mouse model of atherosclerosis. J Nucl Cardiol. 2015;21(3):553–62.

112. Laitinen I, Saraste A, Weidl E, Poethko T, Weber AW, Nekolla SG, et al. Evaluation of αvβ3 integrin-targeted positron emission tomography tracer 18F-galacto-RGD for imaging of vascular inflammation in atherosclerotic mice. Circ Cardiovasc Imaging. 2009;2(4):331–8.

113. Beer AJ, Pelisek J, Heider P, Saraste A, Reeps C, Metz S, et al. PET/CT imaging of integrin αvβ3 expression in human carotid atherosclerosis. JACC Cardiovasc Imaging. 2014;7(2):178–87.

114. Jiang L, Tu Y, Kimura RH, Habte F, Chen H, Cheng K, et al. 64Cu-Labeled Divalent Cystine Knot Peptide for Imaging Carotid Atherosclerotic Plaques. J Nucl Med. 2015;56(6):939–44.

115. Sun Yoo J, Lee J, Ho Jung J, Seok Moon B, Kim S, Chul Lee B, et al. SPECT/CT Imaging of High-Risk Atherosclerotic Plaques using Integrin-Binding RGD Dimer Peptides. Sci Rep. 2015;5:11752.

116. Tekabe Y, Kollaros M, Zhang G, Backer M V, Backer JM, Johnson LL. Imaging VEGF receptor expression to identify accelerated atherosclerosis. EJNMMI Res. 2014;4(41).

117. Tekabe Y, Johnson LL, Rodriquez K, Li Q, Backer M, Backer JM. Selective Imaging of Vascular Endothelial Growth Factor Receptor-1 and Receptor-2 in Atherosclerotic Lesions in Diabetic and Non-diabetic ApoE⁻/⁻ Mice. Mol Imaging Biol; 2018;20(1):85-93.

118. Tavakoli S, Razavian M, Zhang J, Nie L, Marfatia R, Dobrucki LW, et al. Matrix metalloproteinase activation predicts amelioration of remodeling after dietary modification in injured arteries. Arterioscler Thromb Vasc Biol. 2011;31(1):102–9.

119. Razavian M, Nie L, Challa A, Zhang J, Golestani R, Jung JJ, et al. Lipid lowering and imaging protease activation in atherosclerosis. J Nucl Cardiol. 2014;21(2):319–28.

120. Zhang J, Nie L, Razavian M, Ahmed M, Dobrucki LW, Asadi A, et al. Molecular imaging of activated matrix metalloproteinases in vascular remodeling. Circulation. 2008;118(19):1953–60.

121. Razavian M, Tavakoli S, Zhang J, Nie L, Dobrucki LW, Sinusas a. J, et al. Atherosclerosis Plaque Heterogeneity and Response to Therapy Detected by In Vivo Molecular Imaging of Matrix Metalloproteinase Activation. J Nucl Med. 2011;52(11):1795–802.

122. Bigalke B, Phinikaridou A, Andia ME, Cooper MS, Schuster A, Schönberger T, et al. Positron emission tomography/computed tomographic and magnetic resonance imaging in a murine model of progressive atherosclerosis using 64Cu-labeled glycoprotein VI-Fc. Circ Cardiovasc Imaging. 2013;6(6):957–64.

123. Nakamura I, Hasegawa K, Wada Y, Hirase T, Node K, Watanabe Y. Detection of early stage atherosclerotic plaques using PET and CT fusion imaging targeting P-selectin in low density lipoprotein receptor-deficient mice. Biochem Biophys Res Commun. 2013;433(1):47–51.

124. Li X, Bauer W, Israel I, Kreissl MC, Weirather J, Richter D, et al. Targeting P-selectin by gallium-68-labeled fucoidan positron emission tomography for noninvasive characterization of vulnerable plaques: correlation with in vivo 17.6T MRI. Arterioscler Thromb Vasc Biol. 2014;34(8):1661–7.

125. Broisat A, Hernot S, Toczek J, De Vos J, Riou LM, Martin S, et al. Nanobodies targeting mouse/human VCAM1 for the nuclear imaging of atherosclerotic lesions. Circ Res. 2012;110(7):927–37.

126. Broisat A, Toczek J, Dumas LS, Ahmadi M, Bacot S, Perret P, et al. 99mTc-cAbVCAM1-5 Imaging Is a Sensitive and Reproducible Tool for the Detection of Inflamed Atherosclerotic Lesions in Mice. J Nucl Med. 2014;55(10):1678–84.

127. Dumas LS, Briand F, Clerc R, Brousseau E, Montemagno C, Ahmadi M, et al. Evaluation of Antiatherogenic Properties of Ezetimibe Using ³H-Labeled Low-Density-Lipoprotein Cholesterol and ⁹⁹ᵐTc-cAbVCAM1–5 SPECT in ApoE ⁻/⁻ Mice Fed the Paigen Diet. J Nucl Med. 2017;58(7):1088–93.

128. Bala G, Blykers A, Xavier C, Descamps B, Broisat A, Ghezzi C, et al. Targeting of vascular cell adhesion molecule-1 by ¹⁸F-labelled nanobodies for PET/CT imaging of inflamed atherosclerotic plaques. Eur Hear J – Cardiovasc Imaging. 2016;17(9):1001–8.

129.  Nahrendorf M, Keliher E, Panizzi P, Zhang H, Hembrador S, Figueiredo J-L, et al. 18F-4V for PET-CT imaging of VCAM-1 expression in atherosclerosis. JACC Cardiovasc Imaging. 2009;2(10):1213–22.

130.  Mateo J, Izquierdo-Garcia D, Badimon JJ, Fayad ZA, Fuster V. Noninvasive assessment of hypoxia in rabbit advanced atherosclerosis using 18f-fluoromisonidazole positron emission tomographic imaging. Circ Cardiovasc Imaging. 2014;7(2):312–20.

131.  Fontaine R, Bélanger F, Cadorette J, Leroux JD, Martin JP, Michaud JB, et al. Architecture of a dual-modality, high-resolution, fully digital positron emission tomography/computed tomography (PET/CT) scanner for small animal imaging. IEEE Trans Nucl Sci. 2005;52(3 I):691–6.

2

# Chapter 3

## Imaging of atherosclerosis, Targeting LFA-1 on Inflammatory Cells with ^{111}In-DANBIRT

Authors: **E.J. Meester** Msc[1,2]; B.J. Krenning MD, PhD[3]; R.H. de Blois PhD[2]; J.P. Norenberg PhD; PharmD,[4];
M. de Jong PhD[2]; M.R. Bernsen PhD[2]; K Van der Heiden PhD[1*]

Author affiliations:

[1] Department of Biomedical Engineering, Thorax Center, Erasmus MC, Rotterdam, The Netherlands

[2] Department of Radiology & Nuclear Medicine, Erasmus MC, Rotterdam, The Netherlands

[3] Department of Cardiology, Thorax Center, Erasmus MC, Rotterdam, The Netherlands

[4] Radiopharmaceutical Sciences, University of New Mexico, Albuquerque, NM, USA

*Corresponding author

# Abstract

**Background |** ^{111}In-DOTA-butylamino-NorBIRT (DANBIRT) is a novel radioligand which binds to Leukocyte Function associated-Antigen-1 (LFA-1), expressed on inflammatory cells. This study evaluated ^{111}In-DANBIRT for the visualization of atherosclerotic plaque inflammation in mice.

**Methods and Results |** ApoE^{-/-} mice fed an atherogenic diet up to 20 weeks (n=10), were imaged by SPECT/CT 3 hours post injection of ^{111}In-DANBIRT (~200pmol, ~40MBq). Focal spots of ^{111}In-DANBIRT were visible in the aortic arch of all animals, with an average Target to Background Ratio (TBR) of 1.7 ± 0.5. *In vivo* imaging results were validated by *ex vivo* SPECT/CT imaging, with a TBR up to 11.5 (range: 2.6–11.5). Plaques, identified by Oil Red O lipid-staining on excised arteries, co-localised with ^{111}In-DANBIRT uptake as determined by *ex vivo* autoradiography. Subsequent histological processing and *in vitro* autoradiography confirmed ^{111}In-DANBIRT uptake at plaque areas containing CD68 expressing macrophages and LFA-1 expressing inflammatory cells. *Ex vivo* incubation of a human carotid endarterectomy specimen with ^{111}In-DANBIRT (~950nmol, ~190MBq) for 2 hours showed heterogeneous plaque uptake on SPECT/CT, after which immunohistochemical analysis demonstrated co-localization of ^{111}In-DANBIRT uptake and CD68 and LFA-1 expressing cells.

**Conclusions |** Our results indicate the potential of radiolabelled DANBIRT as a relevant imaging radioligand for non-invasive evaluation of atherosclerotic inflammation.

## Abbreviations

| | |
|---|---|
| LFA-1 | Leukocyte Function-associated Antigen-1 |
| SPECT | Single Photon Emission Computed Tomography |
| CT | Computed Tomography |
| PET | Positron Emission Tomography |
| ^{18}F-FDG | 2-deoxy-2-^{18}F-fluoro-D-glucose |
| DANBIRT | ^{111}In-DOTA-butylamino-NorBIRT |
| ApoE | Apolipoprotein E |
| CEA | Carotid Endarterectomy |
| ROI | Region of Interest |
| TBR | Target to Background Ratio |

Key words: Atherosclerosis, Inflammation, SPECT, Molecular imaging

# Introduction

Cardiovascular disease remains the major cause of death worldwide[1]. Most cardiovascular events are a consequence of atherosclerosis, in which plaques form due to chronic inflammation and lipid accumulation in the vessel wall. Plaque progression can result in plaque rupture and subsequent thrombus formation, potentially leading to myocardial infarction or stroke. Timely detection of plaque, before rupture, would allow targeted treatment and prevention of a potentially life-threatening cardiovascular event.

Inflammation is a major hallmark of atherosclerosis and a consistent predictor of cardiovascular risk (2,3). The recent CANTOS (Canakinumab Anti-inflammatory Thrombosis Outcomes Study) trial showed that reduction of inflammation in patients after myocardial infarction could reduce the risk of new adverse cardiovascular events in the future (4). Assessment of the severity of inflammation in atherosclerosis using biomarkers is cumbersome however. High sensitive C-reactive protein (hsCRP) is a prototypic marker of inflammation and a strong independent predictor for future cardiovascular events, yet is influenced by risk factors such as hypertension, smoking, and periodontal disease (5). Non-invasive visualization of arterial inflammation may complement biomarkers such as hsCRP in guiding treatment with new anti-inflammatory drugs.

2-deoxy-2-^{18}F-fluoro-D-glucose Positron Emission Tomography (^{18}F-FDG PET) imaging is an established method to non-invasively detect and quantify inflammation within atherosclerotic plaques (6-8). FDG is a glucose analogue, which accumulates in metabolically active cells, including plaque-associated macrophages. However, due to the high metabolic activity of myocardial cells, ^{18}F-FDG uptake by the myocardium might hinder detection of coronary atherosclerotic plaques. Furthermore, a necessary fasting period before imaging and non-specific uptake limit the applicability of ^{18}F-FDG (9,10). These limitations warrant the search for additional radiotracers which might complement ^{18}F-FDG.

Development of atherosclerosis is initiated by adhesion of monocytes as well as T lymphocytes to the arterial endothelial surface, followed by their migration into the subendothelial space (11). Leukocyte Function-associated Antigen-1 (LFA-1), consisting of CD11a and CD18 subunits, is an integrin cell-surface receptor expressed on leukocytes. LFA-1 binds to endothelial cells via interaction with Intercellular Adhesion Molecule 1 (ICAM-1), and is involved in transmigration of inflammatory cells to sites of inflammation (12). LFA-1 was first identified as one of several adhesion molecules playing a role in leukocyte trafficking, antigen presentation and cell activation. Immunohistochemical studies on animal models of atherosclerosis have demonstrated the presence of LFA-1 positive cells in atherosclerotic lesions (13,14). Therefore, LFA-1 may be a promising imaging target for atherosclerotic plaque detection. Recently, an allosteric inhibitor of LFA-1 (15) was chemically adapted for nuclear diagnostic

3

and therapeutic purposes ((R)-1-(4-aminobutyl)-5-(4-bromobenzyl)-3-(3,5-dichlorophenyl)-5-methylimidazolidine-2,4-dione; butylamino-NorBIRT) (16). Butyl-amino-NorBIRT can be labelled with various radionuclides for Single Photon Emission Computed Tomography (SPECT) and PET imaging via a chelator (e.g. 1,4,7,10-tetraazacyclododecane-1,4,7,10-tetraacetic acid (DOTA)), depicted in Figure 1. Indium-111-DOTA-butylamino-NorBIRT (^{111}In-DANBIRT) is used for SPECT imaging and has been shown to specifically bind LFA-1 on cultured human leukemic and mouse lymphoma cells (16,17).

The aim of this study was to examine the feasibility of plaque detection using ^{111}In-DANBIRT. To this end, we studied *in vivo* uptake in ApoE^{-/-} mice via SPECT/Computed Tomography (CT) scanning, and established its binding to human plaque material.
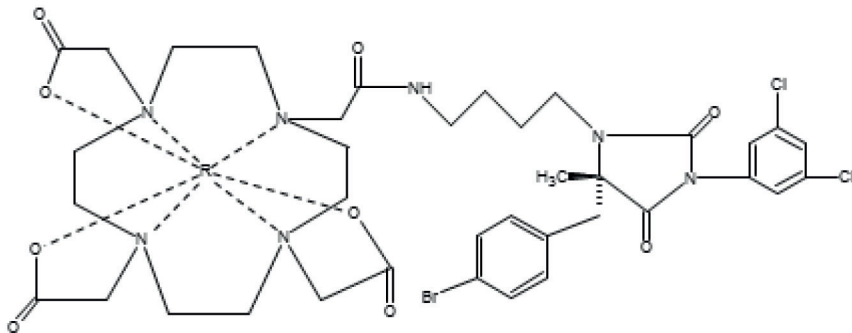


**Figure 1 | Chemical structure of *R-DANBIRT.** 1-(4-aminobutyl)-5-(4-bromobenzyl)-3-(3,5-dichlorophenyl)-5-methylimidazolidine-2,4-dione-DOTA. R, radiometal.

# Materials and Methods

## Animals and experimental setup

Female ApoE [-/-] mice on a C57BL/6J background (n=10) were purchased from Charles Rivers (Calco, Italy) at 6 weeks of age and were fed a high fat diet (0.3% cholesterol, Altromin Spezialfutter GmbH & Co. KG, Lage, Germany) *ad libitum* from 8 weeks of age onwards up to a maximum of 20 weeks. After SPECT/CT imaging, mice were sacrificed by an overdose of inhalation anaesthesia (isoflurane). All animal experiments were approved by the institutional animal studies committee and were in accordance with Dutch animal ethical legislation and the European Union Directive.

## Radiolabelling

^{111}In-DANBIRT (MW=886.5 g/mole) (provided by J.P. Norenberg) was radiolabelled with [111]In (Covidien, Petten, The Netherlands) with a specific activity of 200 MBq/nmol, as previously described (18). Radiochemical purity (>90%) and incorporation yield (>99%) were assessed using high-pressure liquid chromatography and instant thin-layer chromatography on silica gel. Quenchers (3.5 mM ascorbic acid, 3.5 mM gentisic acid, 10 mM methionine) were added to prevent radiolysis of the tracer (19).

## *In vivo* imaging

Mice were injected intravenously in the tail vein with ~40 MBq/200 pmol ^{111}In-DANBIRT in 0.1% Bovine serum albumin (BSA) in phosphate-buffered saline (PBS) (injection volume of 150 µL) (n=10). They were anesthetized (1.5–2% isoflurane) 2.5 hours post injection, after which they were injected with 100 µL CT-contrast agent (eXIA160, Binito Biomedical Inc, Ottawa, ON, Canada; or Exitron nano 12000 ,Milteny Biotec, Bergisch-Gladach, Germany). Immediately after contrast injection, a CT scan was performed (17 min, 615 mA, 55 KeV) followed by a SPECT scan (static scan, 1 hr, 2.0 mm pinhole collimator, 17 positions) on a hybrid SPECT/CT scanner (VECTor, MILabs, Utrecht, Netherlands) with a reported spatial resolution of 0.85 mm (20). SPECT images were reconstructed using photopeak windows of 214–262 and 152–185 KeV, with a background window on either side of the photopeak with a width of 2.5% of the corresponding photopeak, and a pixel-based ordered subset expectation maximization method (4 subsets and 30 iterations), a voxel size of 0.8 mm$^3$, and corrected for attenuation using the CT data. A post-reconstruction 3-dimensional Gaussian filter was applied (0.8 mm full width at half maximum). A blocking study was performed by co-injection with a100x or 850x excess of unlabelled DANBIRT in 2 mice.

## *Ex vivo* studies

After imaging, mice were euthanized and vasculature was flushed with PBS via the left ventricle, followed by excision of the aorta and carotid arteries. The arteries were cleaned from visceral fat and connective tissue and stained for lipids (Oil red O (ORO) according to standard protocol) to confirm plaque presence. After staining, the arteries were scanned *ex vivo* (CT: 5 min, 615 mA, 55 KeV; SPECT: static scan, 30 min, 2.0 mm pinhole collimator) on a SPECT/CT scanner (VECTor, MILabs, Utrecht, Netherlands). SPECT images were reconstructed as described above. Subsequently, arteries were used for *ex vivo* autoradiography (n=4) or embedded in tissue-tec and stored at -80° C for histological analysis (n=6). To determine the biodistribution of ^{111}In-DANBIRT in ApoE^{-/-} mice, selected organs were collected, weighed and measured for radioactivity in a gamma-counter (1480 Wizard, Gamma counter, Perkin Elmer). Radioactivity measured in the various tissues was expressed as percentage of injected dose per gram (%ID/g). ^{111}In-DANBIRT showed a biodistribution pattern according to expectation, with limited retention in major organs 24 hours post injection (Online Resource 1). After ~3 weeks, arteries used for *ex vivo* autoradiography were placed on a phosphor screen overnight

and read using a phosphor imager (Cyclone; Perkin Elmer). Plaque signal was quantified as digital light units/mm$^2$ (DLU/mm$^2$) using Optiquant software (Perkin Elmer), and compared to non-diseased arterial signal in the same sample to calculate a Target to Background Ratio (TBR).

## *Ex vivo* carotid endarterectomy study

To explore binding to human atherosclerotic plaques, we incubated a human carotid endarterectomy (CEA, acquired with informed consent and approved by the medical ethics committee) sample with ^{111}In-DANBIRT (~950 pmol, ~190 MBq) in 0.1% BSA in PBS for 2 hours. After incubation the specimen was washed in PBS and subsequently scanned on the SPECT/ CT scanner (CT: 5 min, 615 mA, 55 keV; SPECT: static scan, 30 min, 2.0 mm pinhole collimator). SPECT images were reconstructed as described above. Hereafter, the specimen was cut in transverse slices of 1 mm. Even slices were used for autoradiography, odd slice for histological evaluation. Histology was visually matched with transverse views of the SPECT/CT scan, to correlate ^{111}In-DANBIRT uptake with locations of cells expressing LFA-1 and CD68.

## Immunohistochemistry and *In vitro* autoradiography

Mouse aortic arch cryosections and human CEA cryosections (both 5 μm) were immuno-histochemically stained with anti-CD68, a pan-macrophage marker (human: 1:100, Abcam, ab955; mouse: 1:100 Biorad, MCA1957), and anti-LFA-1 (human: 1:100 Biorad, MCA1848; mouse: 1:1, Pont et al., 1986 [21]) to assess co-localization of LFA-1 and CD68 (macrophage)-positive cells. *In vitro* autoradiography was performed on mouse cryosections (10 μm) of aortic arch adjacent to slides used for immunohistochemistry, by incubating slides for 1 hr with 80 μL 10$^{-9}$ M ^{111}In-DANBIRT. Serially sectioned human CEA cryosections (10 μm) were incubated for 1 hr with 80 μL 10$^{-9}$ M ^{111}In-DANBIRT with or without excess (10$^{-6}$ M) unlabelled DANBIRT to determine non-specific binding. Slides were exposed to phosphor screens for 1 week and read using a phosphor imager (Cyclone; Perkin Elmer). The autoradiograms of human CEA cryosections were analysed by drawing fixed regions of interests (ROIs) around the sections using Optiquant software (Perkin Elmer). Signal was quantified as DLU/mm$^2$, after which blocked and unblocked sections were compared using a student's t-test.

## Quantification

SPECT data was analysed with Vivoquant (Invicro) by quantification of manually drawn regions of interests (ROIs) based on contrast-enhanced CT. On *in vivo* scans, ROIs were drawn in the aortic arch, vena cava inferior and jugular vein. ROIs on *ex vivo* scans were drawn in the aortic arch and non-diseased artery in the descending aorta or common carotid arteries. TBRs were calculated, and expressed as mean ± standard deviation.

# Results

## *In vivo* mouse plaque imaging

*In vivo* SPECT/CT imaging 3 hours after intravenous injection of ^{111}In-DANBIRT showed distinct focal spots of radioactivity, corresponding to common sites of plaque formation in the aortic arch of all animals (Figure 2 and Online Resource 4), with an average TBR of 1.7 ± 0.5. Uptake of ^{111}In-DANBIRT at plaque locations in the carotid bifurcations was not above background. Myocardial uptake was not above background in any of the animals. Co-injection of excess unlabelled DANBIRT reduced uptake of ^{111}In-DANBIRT in plaque areas of the aortic arch to background levels (Online Resource 2).
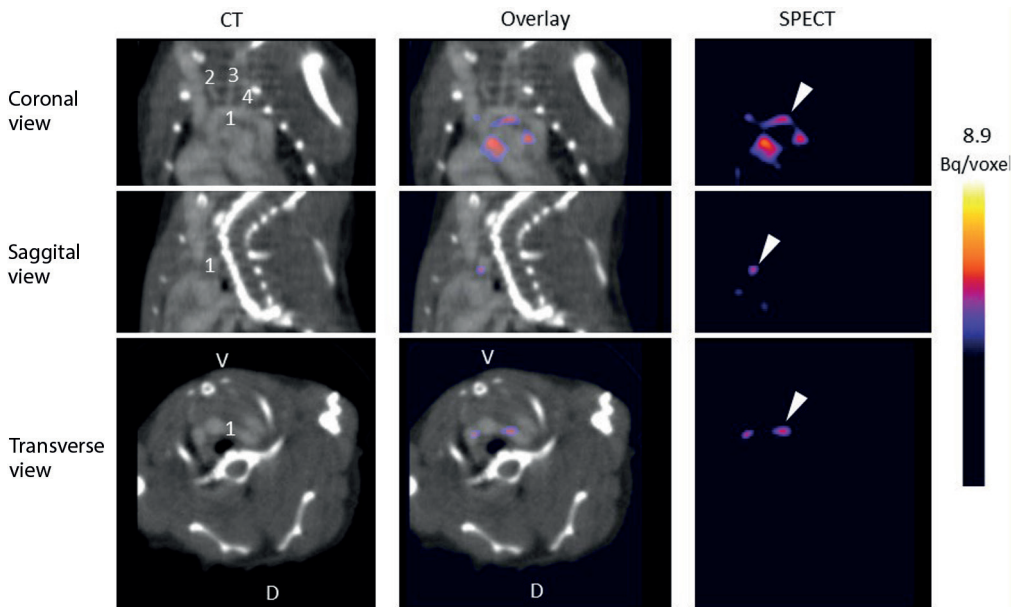


**Figure 2** | *In vivo* **uptake of ^{111}In-DANBIRT in atherosclerotic mice.** *In vivo* contrast enhanced Computed Tomography (CT), Single Photon Emission Computed Tomography (SPECT), and overlay images of ApoE^{-/-} mouse thorax in coronal, sagittal, and transverse view. Scans were made 3 hrs post injection. Exitron nano 12000 was used as contrast agent. 1=aortic arch; 2=right common carotid artery; 3=left common carotid artery; 4=left subclavian artery. V=ventral, D=dorsal. Arrowheads indicate radioactive hot spots (^{111}In-DANBIRT uptake) in the aortic arch.

## *Ex vivo* validation

After *in vivo* imaging, arteries were excised and scanned *ex vivo*. Focal uptake of ^{111}In-DANBIRT in the aortic plaques was evident (Figure 3A), with a TBR up to 11.5 (range: 2.6–11.5). To co-localize uptake to plaque locations, we performed *ex vivo* autoradiography and a lipid staining (ORO) on the excised arteries. The *ex vivo* autoradiography showed high ^{111}In-DANBIRT uptake in regions in the aortic arch, arterial branch points, descending aorta, and carotid bifurcations, corresponding to plaque locations as indicated by lipid staining (Figure 3A) with an average TBR of $19.0 \pm 7.9$. *In vitro* autoradiography and immunohistochemistry of mouse aorta containing plaque demonstrated ^{111}In-DANBIRT binding to plaque areas containing LFA-1-expressing inflammatory cells and CD68-positive macrophages (Figure 3B). Binding of ^{111}In-DANBIRT to human plaque cryosections could be blocked by addition of an excess of unlabelled DANBIRT (Online Resource 3).
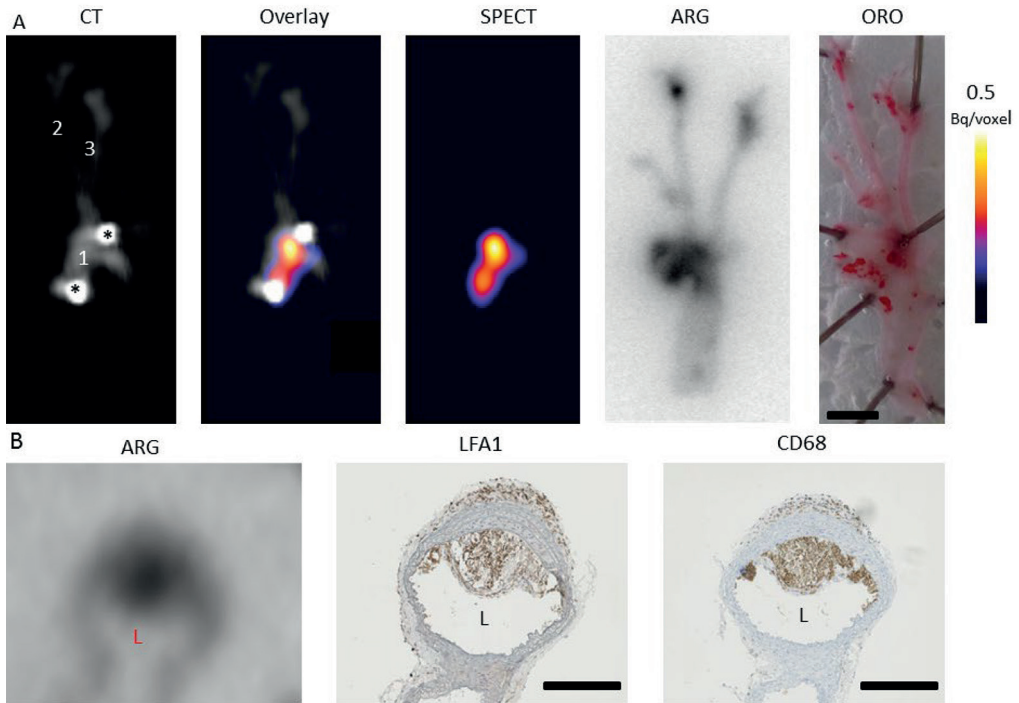


**Figure 3 | *Ex vivo* validation of ^{111}In-DANBIRT imaging of LFA-1.** Frontal view of *ex vivo* CT, SPECT, and overlay images of an excised artery of an ApoE^{-/-} mouse, autoradiography (ARG) and bright field photo of Oil Red O (ORO) stained, opened artery excised from another ApoE^{-/-} mouse, both injected with ^{111}In-DANBIRT. 1=aortic arch; 2=right common carotid artery; 3= left common carotid artery. Asterisks (*) indicate locations of needles used to pin down the artery. Scale bar=2 mm (panel A). *In vitro* autoradiography of 10 μm cryosection of mouse aortic arch. Adjacent 5 μm cryosections immunohistochemically stained for LFA-1 and CD68 expression. Scale bar=100 μm (panel B).

## Human plaque imaging

Incubation of a human CEA sample with ^{111}In-DANBIRT resulted in heterogeneous uptake of ^{111}In-DANBIRT seen as hot spots throughout the plaque in SPECT/CT scans (Figure 4 A, B, and Online Resource 5). Subsequent histological analysis of adjacent cryosections demonstrated co-localization of the hotspots of ^{111}In-DANBIRT uptake with LFA-1-expressing inflammatory cells and CD68-positive macrophages (Figure 4 C, D, E, F).
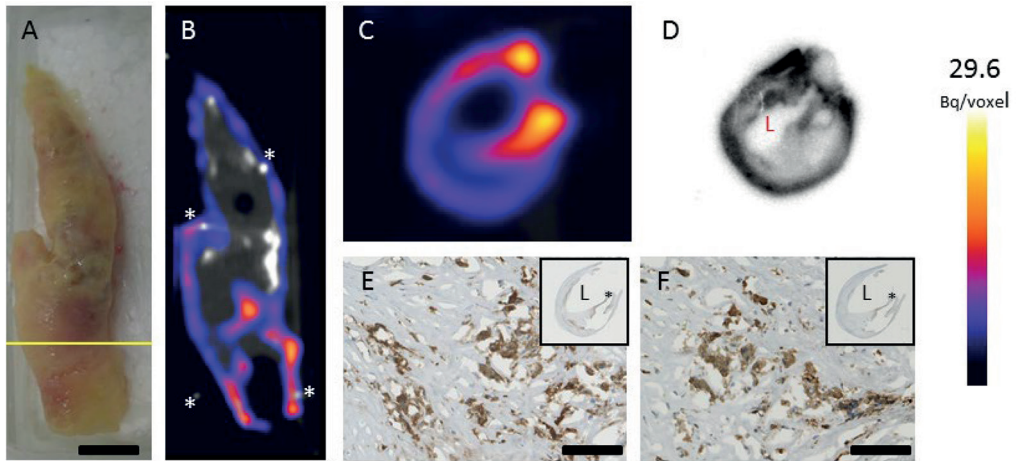


**Figure 4 |** *Ex vivo* **[111]In-DANBIRT imaging of LFA-1 in a human atherosclerotic plaque.** Bright field photo of a Carotid Endarterectomy specimen. Yellow line indicates location of transverse view of SPECT/CT scan in C, autoradiography of 1 mm thick transverse slide in D, and adjacent histologic sections in E and F. Scale bar=10mm **A)**. SPECT/CT imaging show heterogeneous uptake of ^{111}In-DANBIRT. Calcified regions of the plaque are visible in bright white in the CT views. Pins used as landmarks are indicated by asterisks (*). Coronal **B)**, and transverse views **C)** of SPECT/CT scan. *Ex vivo* autoradiography image **D)**. LFA-1 expression is visible in a slide adjacent to D, co-localizing with areas of high ^{111}In-DANBIRT uptake. Inset shows overview of the histological section, asterisk shows location of zoomed area. Scale bar=100 μm **E)**. CD68 expressing macrophages are present in an adjacent cryosection. Inset shows overview of the histological section, asterisk shows location of zoomed area. Scale bar=100 μm **F)**. L=Lumen.

# Discussion

In this study we show the feasibility of *in vivo* plaque detection using ^{111}In-DANBIRT SPECT/CT imaging of LFA-1. We demonstrated distinct focal uptake in the aortic arch of all animals 3 hours after intravenous injection of ^{111}In-DANBIRT, despite the small dimensions of murine arteries and plaques. This uptake was related to the presence of lipid rich plaques with inflammatory cells shown by ORO staining and immunohistochemistry. Moreover, we showed

uptake of ^{111}In-DANBIRT in an excised human carotid plaque. In addition, presence of LFA-1 positive cells in atherosclerotic plaque was confirmed by immunohistochemistry. The finding that ^{111}In-DANBIRT can detect plaques in murine aortas (vessel diameter <1 mm) point towards its possible applicability in human coronary arteries which have a common diameter of around 3 mm (22).

Various non-invasive imaging techniques are explored for the early detection of atherosclerosis and risk stratification of patients with cardiovascular disease, using various target-ligand combinations that are associated with atherosclerosis. The clinically most frequently explored technique is ^{18}F-FDG PET, which has limits in regards to its specificity and myocardial uptake. DANBIRT, in this study labelled with ^{111}In, solely binds to inflammatory cells and was not taken up by the myocardium in our atherosclerotic mouse model. As such, DANBIRT might surpass a limitation of ^{18}F-FDG. Moreover, DANBIRT might provide information on different stages of plaque development as all leukocytes express LFA-1. Furthermore, DANBIRT can be labelled with ^{68}Ga, which makes it suitable for PET imaging and enhances its clinical applicability.

^{111}In-DANBIRT signal was not visible by *in vivo* nor *ex vivo* SPECT/CT imaging of the plaque in the carotid artery bifurcations, whereas the more sensitive *ex vivo* autoradiography did demonstrate uptake. This could be due to a smaller plaque size and/or a lower number, or a more diffuse distribution of inflammatory cells, resulting in a signal below the detection threshold of our SPECT system.

^{111}In-DANBIRT exhibits specific uptake in plaques in atherosclerotic mice. Uptake of ^{111}In-DANBIRT occurs in plaque areas that contain LFA-1 expressing leukocytes and CD68 positive macrophages, indicating specific targeting of LFA-1 positive cells. We conclude that radiolabelled DANBIRT shows potential as a relevant nuclear imaging tracer to detect atherosclerotic inflammation. Upon confirmation of these findings in a patient population, this imaging tool may be used to improve risk assessment of cardiovascular disease by visualizing inflammation and for individualizing specific anti-inflammatory drug therapy.

## New knowledge gained

The novel LFA-1 targeting radioligand DANBIRT detects inflammation *in vivo* in atherosclerotic plaques in an ApoE$^{-/-}$ mouse model. DANBIRT uptake correlates to the presence of CD68 expressing macrophages and LFA-1 expressing inflammatory cells in the atherosclerotic plaque. In addition, *ex vivo* uptake of DANBIRT in a human carotid plaque correlates to the presence of CD68 expressing macrophages and LFA-1 expressing inflammatory cells, suggesting the potential of DANBIRT for non-invasive imaging of atherosclerotic plaque inflammation.

## Acknowledgements

## Authorship

Conceived and designed the experiments: B.J. Krenning, M. de Jong, M.R. Bernsen, K. van der Heiden. Performed the experiments: E.J. Meester. Provided DANBIRT: J.P. Norenberg. Performed radiolabelling: R.H. de Blois. Analysis or interpretation of data: E.J. Meester, B.J. Krenning, M. de Jong, M.R. Bernsen, K. van der Heiden. Wrote and revised the paper: E.J. Meester, B.J. Krenning, J.P. Norenberg, M. de Jong, M.R. Bernsen, K. van der Heiden.

## Disclosure

3

# References

1.  GBD 2015 Mortality and Causes of Death Collaborators I. Global, regional, and national life expectancy, all-cause mortality, and cause-specific mortality for 249 causes of death, 1980–2015: a systematic analysis for the Global Burden of Disease Study 2015. Lancet. 2016;380(9859):1459–1544.

2.  Moore KJ, Sheedy FJ, Fisher EA. Macrophages in Atherosclerosis: a Dynamic Balance. Nat Rev Immunol. 2013;13(10):709–721.

3.  Hansson GK. Inflammation, Atherosclerosis, and Coronary Artery Disease. N Engl J Med. 2005;352(16):1685–1695.

4.  Ridker PM, Everett BM, Thuren T, MacFayden JG, Chang WH, Ballantyne C, et al. Antiinflammatory Therapy with Canakinumab for Atherosclerotic Disease. N Engl J Med. 2017:1–13.

5.  Ridker PM. Clinical Application of C-Reactive Protein for Cardiovascular Disease Detection and Prevention. Circulation. 2003;107:363–369.

6.  Tawakol A, Migrino R, Hoffmann U, Abbara S, Houser S, Gewirtz H, et al. Noninvasive In Vivo Measurement of Vascular Inflammation with F-18 Fluorodeoxyglucose Positron Emission Tomography. J Nucl Cardiol. 2005;12(3):294–301.

7.  Rudd JHF, Narula J, Strauss HW, Virmani R, Machac J, Klimas M, et al. Imaging Atherosclerotic Plaque Inflammation by Fluorodeoxyglucose With Positron Emission Tomography. Ready for Prime Time? J Am Coll Cardiol. 2010;55(23):2527–2535.

8.  Figueroa AL, Subramanian SS, Cury RC, Truong QA, Gardecki JA, Tearney GJ, et al. Distribution of Inflammation Within Carotid Atherosclerotic Plaques With High-Risk Morphological Features A Comparison Between Positron Emission Tomography Activity, Plaque Morphology, and Histopathology. Circ Cardiovasc Imaging. 2012;5:69–77.

9.  Buettner C, Rudd JHF, Fayad ZA. Determinants of FDG Uptake in Atherosclerosis. JACC Cardiovasc Imaging. 2011;4(12):1302–1304.

10. Tarkin JM, Joshi FR, Rudd JHF. PET imaging of inflammation in atherosclerosis. Nat Rev Cardiol. 2014;11(8):443–457.

11. Libby P. History of Discovery : Inflammation in Atherosclerosis. Arterioscler Thromb Vasc Biol. 2012;32(9):2045–2051.

12. Salas A, Shimaoka M, Kogan AN, Harwood C, Andrian UH Von, Springer TA. Rolling Adhesion through an Extended Conformation of Integrin αLβ2 and Relation to αI and βI-like Domain Interaction. Immunity. 2004;20:393–406.

13. Watanabe T, Fan J. Atherosclerosis and Inflammation Mononuclear Cell Recruitment and Adhesion Molecules with Reference to the Implication of ICAM-1/LFA-1 Pathway in Atherogenesis. Int J Cardiol. 1998;66:S45–55.

14. Ma Y, Malbon CC, Williams DL, Thorngate FE. Altered Gene Expression in Early Atherosclerosis Is Blocked by Low Level Apolipoprotein E. PLoS One. 2008;3(6).

15. Kelly TA, Jeanfavre DD, Mcneil DW, Woska JR, Reilly PL, Mainolfi EA, et al. Cutting Edge: A Small Molecule Antagonist of LFA-1-Mediated Cell Adhesion. J Immunol. 1999;163:5173–5177.

16. Poria RB, Norenberg JP, Anderson TL, Erion J, Wagner CR, Arterburn JB, et al. Characterization of a Radiolabeled Small Molecule Targeting Leukocyte Function-Associated Antigen-1 Expression in Lymphoma and Leukemia. Cancer Biother Radiopharm. 2006;21(5):418–426.

17. Mumaw CL, Levesque S, Mcgraw C, obertson S, Lucas S, Stafflinger JE, et al. Microglial Priming Through the Lung – Brain Axis: the Role of Air Pollution – Induced Circulating Factors. FASEB J. 2016;30(5):1880–1891.

18. Blois E De, Schroeder RJ., de Ridder CMA, van Weerden W., Breeman WAP, de Jong M. Improving Radiopeptide Pharmacokinetics by Adjusting Experimental Conditions for Bombesin Receptor-Mediated Imaging of Prostate Cancer. Q J Nucl Med Mol Imaging. 2012;57:1–9.

19. de Blois E, Chan HS, Konijnenberg M, de Zanger R, Breeman WAP. Effectiveness of Quenchers to Reduce Radiolysis of 111In or 177Lu Labelled Methionin-Containing Regulatory Peptides. Maintaining Radiochemical Purity as Measured by HPLC. Currtent Top Med Chem. 2013;13(1).

20.	Ivashchenko O, Have F Van Der, Goorden MC, Ramakers RM, Beekman FJ. Ultra-High-Sensitivity Submillimeter Mouse SPECT. 2015;56(3):470–476.

21.	Pont S, Naquet P, Marchetto S, Regnier-vigouroux A, Blanc D, Pierres M. Identification of 5 Topographic Domains of the Mouse LFA-1 Molecule: Subunit Assignment and Functional Involvement in Lymphoid Cell Interactions. J Immunol. 1986;136(10):3750–3759.

22.	Dodge Jr. TJ, Brown GB, Bolson EL, Dodge HT. Lumen Diameter of Normal Human Coronary Arteries Influence of Age, Sex, Anatomic Variation4, and Left Ventricular Hypertrophy or Dilation. *Circulation*. 1992;86:232–246.

3

# Chapter 4

# Imaging Inflammation in Atherosclerotic Plaques, Targeting SST$_2$ with [$^{111}$In]In-DOTA-JR11

Authors: **E.J. Meester** MSc[1,2]; B.J. Krenning, MD, PhD[3]; E. de Blois PhD[2], M. de Jong PhD[2], A.F.W. van der Steen PhD[1]; M.R. Bernsen PhD[2]*, K. van der Heiden, PhD[1]*

Author affiliations:

[1] Department of Biomedical Engineering, ThoraxCenter, Erasmus MC, Rotterdam, The Netherlands

[2] Department of Radiology & Nuclear Medicine, Erasmus MC, Rotterdam, The Netherlands

[3] Department of Cardiology, ThoraxCenter, Erasmus MC, Rotterdam, The Netherlands

* These authors contributed equally to this work

# Abstract

**Background |** Imaging Somatostatin Subtype Receptor 2 (SST$_2$) expressing macrophages by [DOTA,Tyr$^3$]-octreotate (DOTATATE) has proven successful for plaque detection. DOTA-JR11 is a SST$_2$ targeting ligand with a five times higher tumour uptake than DOTATATE, and holds promise to improve plaque imaging. The aim of this study was to evaluate the potential of DOTA-JR11 for plaque detection.

**Methods and Results |** Atherosclerotic ApoE$^{-/-}$ mice (n=22) fed an atherogenic diet were imaged by SPECT/CT two hours post injection of [$^{111}$In]In-DOTA-JR11 (~200pmol, ~50MBq). *In vivo* plaque uptake of [$^{111}$In]In-DOTA-JR11 was visible in all mice, with a Target-to-Background-Ratio (TBR) of 2.23 ± 0.35. Post mortem scans after thymectomy and *ex vivo* scans of the arteries after excision of the arteries confirmed plaque uptake of the radioligand with TBRs of 2.46 ± 0.52. and 3.43 ± 1.45 respectively. Oil red O lipid-staining and *ex vivo* autoradiography of excised arteries showed [$^{111}$In]In-DOTA-JR11 uptake at plaque locations. Histological processing showed CD68 (macrophages) and SST$_2$ expressing cells in plaques. SPECT/CT, *in vitro* autoradiography and immunohistochemistry performed on slices of a human carotid endarterectomy sample showed [$^{111}$In]In-DOTA-JR11 uptake at plaque locations containing CD68 and SST$_2$ expressing cells.

**Conclusions |** The results of this study indicate DOTA-JR11 as a promising ligand for visualization of atherosclerotic plaque inflammation.

## Abbreviations

| | |
|---|---|
| SST$_2$ | Somatostatin subtype receptor 2 |
| SPECT | Single photon emission tomography |
| CT | Computed tomography |
| ORO | Oil red O |
| CEA | Carotid Endarterectomy |
| TBR | Target to background ratio |

Key words: SPECT, atherosclerosis, inflammation, molecular imaging

# Introduction

Cardiovascular disease is the leading cause of death worldwide (1). Most cardiovascular events are caused by atherosclerosis, in which plaques form over time due to continuous inflammation and lipid deposition in the arterial wall. Current imaging techniques focus on plaque morphology or measures such as calcium score, which are used for cardiovascular risk assessment to improve clinical risk scores (2). Inflammation is a crucial factor in atherosclerotic plaque and plays a crucial role in plaque initiation, progression, and destabilization (3,4). Imaging plaque inflammation may complement traditional imaging methods, providing a better risk stratification of patients at risk of future cardiovascular events.

2-deoxy-2-[$^{18}$F]fluoro-D-glucose ([$^{18}$F]FDG) has proven a reliable non-invasive imaging method not only to detect, but even to quantify the degree of inflammation in plaques (5-7). $^{18}$F-FDG, therefore, provides a valuable tool to assess and monitor disease burden (8). However, background uptake in normal tissue and high uptake of $^{18}$F-FDG in the myocardium severely hinders detection of coronary plaques (9,10), and warrants the search for novel radioligands.

Somatostatin Subtype Receptor 2 (SST$_2$) is highly expressed on activated macrophages (11,12). As macrophages are the main inflammatory cell type in atherosclerotic plaque, SST$_2$ has been proposed as a relevant imaging target for inflammation-based plaque detection. A number of studies have reported on the use of SST$_2$ for inflammation-based imaging of atherosclerosis (13-19). Moreover, Tarkin et al. recently prospectively validated [$^{68}$Ga]Ga-[DOTA, Tyr$^3$]-octreotate (DOTATATE) as a marker for plaque inflammation (20) in a clinical study. They demonstrated the feasibility to detect both carotid and coronary plaques with [$^{68}$Ga]Ga-DOTATATE. Moreover, [$^{68}$Ga]Ga-DOTATATE could better discriminate between high-risk and low-risk lesions compared to [$^{18}$F]FDG.

Various radioligands, based on SST$_2$ agonists, for SST$_2$-targeted imaging and therapy have been developed and used over the past 20 years for detection and treatment of SST$_2$-expressing tumors (21). More recently, a new generation of radioligands based on SST$_2$ antagonists has been developed and described, showing more favourable pharmacokinetics and higher tumour uptake than agonists like DOTATATE. Of these, the compound JR11 (Cpac[D-Cys-Aph(Hor)-D-Aph(Cbm)-Lys-Thr-Cys]-D-Tyr-NH$_2$) performed best in preclinical and clinical studies as an imaging as well as a therapeutic agent (21-24). Based on the reported favourable biodistribution and targeting efficiency of DOTA-JR11, we studied the potential of DOTA-JR11 in inflammation imaging for atherosclerotic plaque detection as it could yield higher TBRs than agonistic radioligands. We therefore used [$^{111}$In]In-DOTA-JR11 Single Photon Emission Computed Tomography/Computed Tomography (SPECT/CT) to image plaques *in vivo* in an atherosclerotic mouse model, and assessed target binding in human plaque material.

4

# Materials and Methods

## Animals and experimental setup

Atherosclerotic female ApoE$^{-/-}$ mice on a C67BL/6J background (n=22) were purchased from Charles Rivers (Calco, Italy) at 6 weeks of age, and were fed a high fat diet (0.3% cholesterol, Altromin Spezialfutter GmbH & Co. KG, Lage, Germany) ad libitum from an age of 8 weeks up to 20 weeks. All animal experiments were approved by the institutional animal studies committee and were in accordance with Dutch animal ethical legislation and the European Union Directive.

## Radiolabelling

[$^{111}$In]In-DOTA-JR11 (MW=1690 g/mol) (kindly provided by Dr. Helmut Maecke) was radiolabelled with [$^{111}$In]InCl$_3$ (Covidien, Petten, The Netherlands) with a specific activity of 200 MBq/nmol as described previously (25). Radiochemical purity (>95%) and incorporation yield (>99%) were evaluated with high-pressure liquid chromatography and instant thin-layer chromatography on silica gel. Quenchers (3.5 mM gentisic acid, 3.5 mM ascorbic acid, 7% ethanol) were added to prevent radiolysis as described previously (26).

## *In vivo* imaging and validation

Mice (n=22) were injected with 50 MBq/200 pmol [$^{111}$In]In-DOTA-JR11 in Phosphate Buffered Saline (PBS) with 0.1% Bovine Serum Albumin (BSA), with a total injection volume of 150 µL. Four mice were co-injected with a 100x excess of unlabelled DOTA-JR11 to test the specificity of the radioligand. Mice were anesthetized with 1.5% isofluorane two hours post injection, after which they were injected with 50 µL CT-contrast agent (Exitron Nano 12000, Milteny Biotec, Bergisch-Gladbach, Germany). Immediately after contrast agent injection, mice were transferred to a VECTor5/CT scanner (MILabs B.V. Utrecht, The Netherlands) on which a CT scan was made followed by a SPECT scan. The time between radioligand injection and imaging was based on pilot experiments (data not shown). The CT scan was made with the following settings: full scan angle; accurate scan mode; 50 kV tube voltage; 0.24 mA tube current; 3.5 minute scan time. CT scans were reconstructed at a resolution of 80 µm. SPECT was performed with the M3.0 pinhole collimator (resolution <1.3 mm, sensitivity >30000 cps/MBq). Data were acquired in list-mode using the following acquisition parameters: 1 hour scan; 15 positions; spiral scan mode; fine step mode. Scans were reconstructed with energy windows incorporating a width of 20% of the In-111 photo peaks of 171 and 245 keV with background windows of 2.5% on either side of the photo peak windows, and scatter correction was applied according to (27). Reconstructions were performed with a SROSEM (Similarity Regulated Ordered Subset Expectation Maximization (28) algorithm with 9 iterations, 128 subsets, with a voxel size of 0.4 mm and a post reconstruction 3-dimensional Gaussian filter was applied (1 mm full width at half maximum).

After *in vivo* imaging, mice were euthanized with an overdose of isoflurane, after which the vasculature was flushed with PBS via the left ventricle, and thymectomy was performed. In this state, the thorax of the euthanized mice was scanned '*in situ*' to circumvent signal interference from thymic uptake of [111In]In-DOTA-JR11 with signal from plaque uptake. CT and SPECT settings for *in situ* imaging were the same as for *in vivo* imaging, except for a shorter SPECT scan duration of 30 minutes.

The arteries were removed after *in situ* imaging, and cleaned of remaining connective tissue. They were then stained for lipids (Oil Red O (ORO) according to standard protocol) to confirm plaque presence, and scanned *ex vivo* with SPECT/CT. The scan settings for *ex vivo* imaging were the same as *in situ* settings except for four SPECT positions due to a smaller field of view. Subsequently, the arteries were cut open and used for *ex vivo* autoradiography (n=4) or embedded in Tissue-Tek O.C.T. compound (Sakura Finetek Europe B.V., Alphen aan den Rijn, The Netherlands) and stored at -80° C for histological analysis (n=14). After ~2weeks, arteries used for *ex vivo* autoradiography were placed on a phosphor screen overnight and read using a phosphor imager (Cyclone, Perkin Elmer).

## *Ex vivo* carotid endarterectomy study

To investigate binding of [111In]In-DOTA-JR11 to and its potential for imaging of human plaque tissue, we performed an *ex vivo* study with human carotid endarterectomy (CEA) tissue slices. For this purpose we sliced a CEA sample (acquired with informed consent and approved by the medical ethics committee of the Erasmus MC, MEC 2008-147) into 2 mm slices. Even-numbered slices were embedded in O.C.T. compound and stored at -80° C for later *in vitro* binding assays and histological evaluation. Odd-numbered slices were incubated with 200 MBq/1 nmol [111In]In-DOTA-JR11 in 20 mL PBS with 0.1% BSA for one hour. After incubation, the slices were washed in PBS with 0.1% BSA until no residual radioactivity remained in the washing medium as measured by a dose calibrator (Dose calibrator VDC-405, Comecer Netherlands, Joure, The Netherlands). The slices were subsequently placed on a holder, and imaged with the VECTor5/CT. CT and SPECT settings were the same as for the *in vivo* mouse scan, except a mouse 1.6 pinhole collimator (resolution <1.6 mm, sensitivity >1500 cps/MBq) was used with 38 scan positions, and the scans were reconstructed with a Gaussian filter of 0.5 mm full width at half maximum.

## Immunohistochemistry and *in vitro* binding assays

Embedded mouse arteries and CEA slices were sectioned into 5 µm sections, which were immunohistochemically stained for CD68 (Mouse: 1:100, Biorad, MCA1848; human: 1:100, Abcam, ab955) and $SST_2$ (1:100, Abcam, clone UMB-1) to assess target presence and presence of macrophages. In short, sections were fixed in cold acetone for 5 minutes, endogenous peroxidase was blocked with 0.3% $H_2O_2$, and non-specific binding was blocked with 1% BSA

4

for mouse CD68 staining and 2% normal goat serum for SST and human CD68 staining. The primary antibody was omitted from the protocol in negative controls.

10 μm sections, adjacent to the 5 μm sections used for immunohistochemistry, were cut from the embedded CEA slices to assess radioligand uptake via an *in vitro* competition binding assay (autoradiography). Sections were incubated for 1 hour with 10$^{-9}$ M [$^{111}$In]In-DOTA-JR11 with or without an excess of 10$^{-6}$ M unlabelled DOTA-JR11 to asses specific binding. Slides were exposed to phosphor screens overnight and read with a phosphor imager (Cyclone, Perkin Elmer). Haematoxylin-eosin staining according to standard protocol was performed on the sections afterwards.

## Quantification and statistics

SPECT/CT data were analysed with Vivoquant (Invicro) by quantification of the activity within manually drawn regions of interests (ROIs) based on contrast-enhanced CT images. *In vivo* ROIs were drawn for the aortic arch and the brachiocephalic artery, whereas the vena cava inferior and jugular vein were used as background regions. *In situ* ROIs were the aortic arch and brachiocephalic artery, and the heart ventricles were taken as background tissue. ROIs on *ex vivo* images were also the aortic arch and brachiocephalic artery for plaque areas, and the relatively healthy descending thoracic aorta as background. Target to background ratios (TBRs) were calculated and expressed as mean ± standard deviation.

*In vitro* autoradiography analysis was performed by drawing ROIs around tissue sections in Optiquant (Perkin Elmer), quantifying the signal as Digital Light Units (DLU)/mm$^2$ and comparing non-blocked to blocked tissue sections.

The Shapiro-Wilk test was used to test data for normality. The student's t-test was used to compare means of normally distributed data, the Mann-Whitney U test was used for non-parametric data.

# Results

## Mouse plaque imaging

*In vivo* SPECT/CT imaging 2 hours after intravenous injection of [$^{111}$In]In-DOTA-JR11 showed focal uptake at locations of plaque formation in the vasculature of all animals (Figure 1A-D), with an average TBR of 2.23 ± 0.35. Thymic uptake (average TBR of 2.28 ± 0.51) of [$^{111}$In]In-DOTA-JR11 masked plaque signal and therefore complicated visualization and quantification. Therefore, '*in situ*' scans were made in post-mortem thymectomized animals. *In situ* SPECT/CT imaging confirmed plaque uptake of [$^{111}$In]In-DOTA-JR11 as seen in *in vivo* images (Figure 1E-H), with a TBR of 2.46 ± 0.52. Blocking studies with an 100x excess of DOTA-JR11 significantly
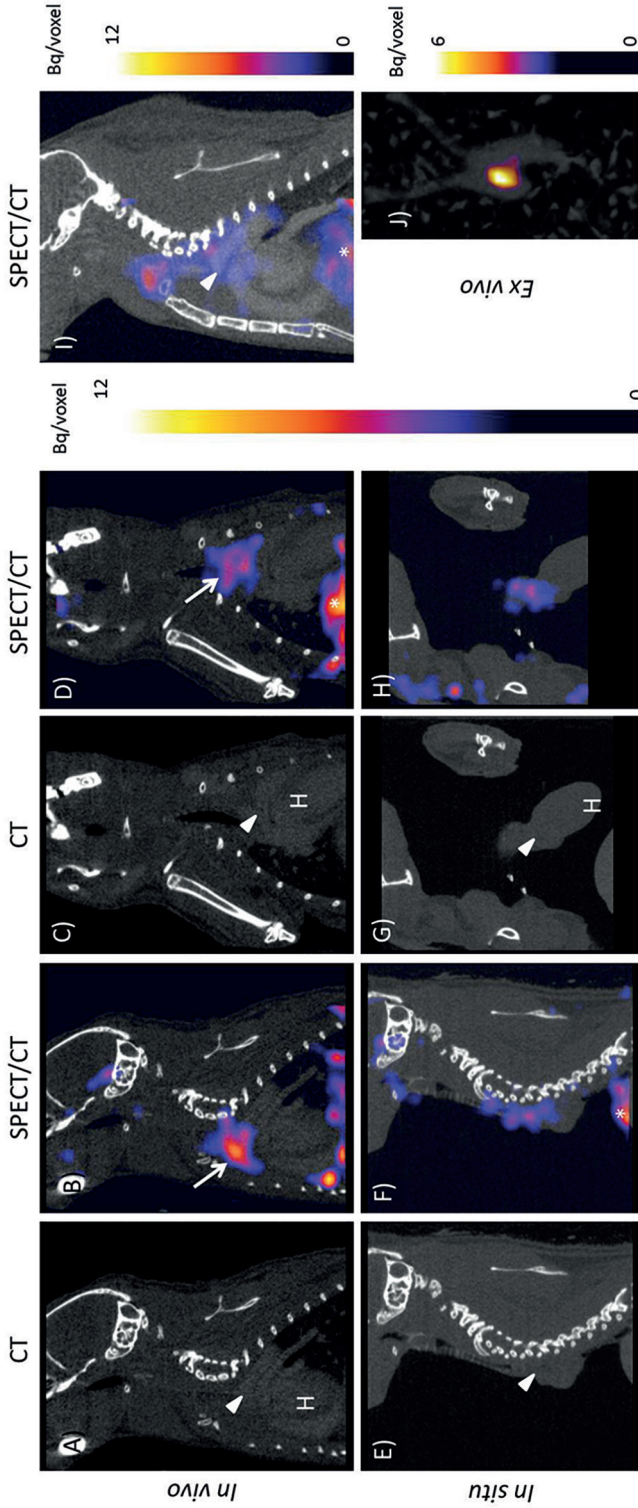
**Figure 1 | [¹¹¹In]In-DOTA-JR11 uptake in mouse atherosclerotic plaque two hours post injection of 200 pmol [¹¹¹In]In-DOTA-JR11. A)** Sagittal CT, **B)** saggital SPECT/CT, **C)** coronal CT, and **D)** coronal SPECT/CT image of [¹¹¹In]In-DOTA-JR11 uptake *in vivo* in an atherosclerotic mouse. **E)** Sagittal CT, **F)** saggital SPECT/CT, **G)** coronal CT, and **H)** coronal SPECT/CT image of [¹¹¹In]In-DOTA-JR11 uptake *in situ* in the mouse displayed in (**A-C**) scanned post mortem after thymectomy and flushing of the vasculature with PBS. **I)** Sagittal SPECT/CT image of a mouse two hours post injection of 50 MBq/200 pmol [¹¹¹In]In-DOTA-JR11 plus a 100x excess of unlabelled DOTA-JR11. Plaque uptake was strongly reduced by blocking. **J)** Maximum intensity projection image of the excised arteries of the mouse shown in (**A-H**). Focal uptake of [¹¹¹In]In-DOTA-JR11 is visible at the plaque location. Arrowheads indicates the location of the aortic arch containing plaque, arrows indicates thymic uptake of [¹¹¹In]In-DOTA-JR11, * indicates uptake in the liver, H indicates the heart.

reduced the arterial signal (TBR *in vivo* blocked: 1.47 ± 0.36; TBR *in situ* blocked: 1.36 ± 0.15, p=0.05, see Figure 1I and Online Resource 1) Likewise, blocking significantly reduced uptake in the thymus (TBR 1.32 ± 0.43, p=0.05).

Presence of plaque in excised arteries was confirmed by ORO staining of excised arteries. *Ex vivo* SPECT/CT imaging of the mouse arteries showed uptake of [$^{111}$In]In-DOTA-JR11 at plaque locations in the aortic arch and brachiocephalic artery with a TBR of 3.43 ± 1.45 (Figure 1J). *Ex vivo* autoradiography and ORO staining of excised, cut open arteries confirmed uptake of [$^{111}$In]In-DOTA-JR11 in plaque (Figure 2A and B). Immunohistochemistry of the arteries confirmed presence of SST$_2$ and CD68 expressing cells in plaque (Figure 2C-F).
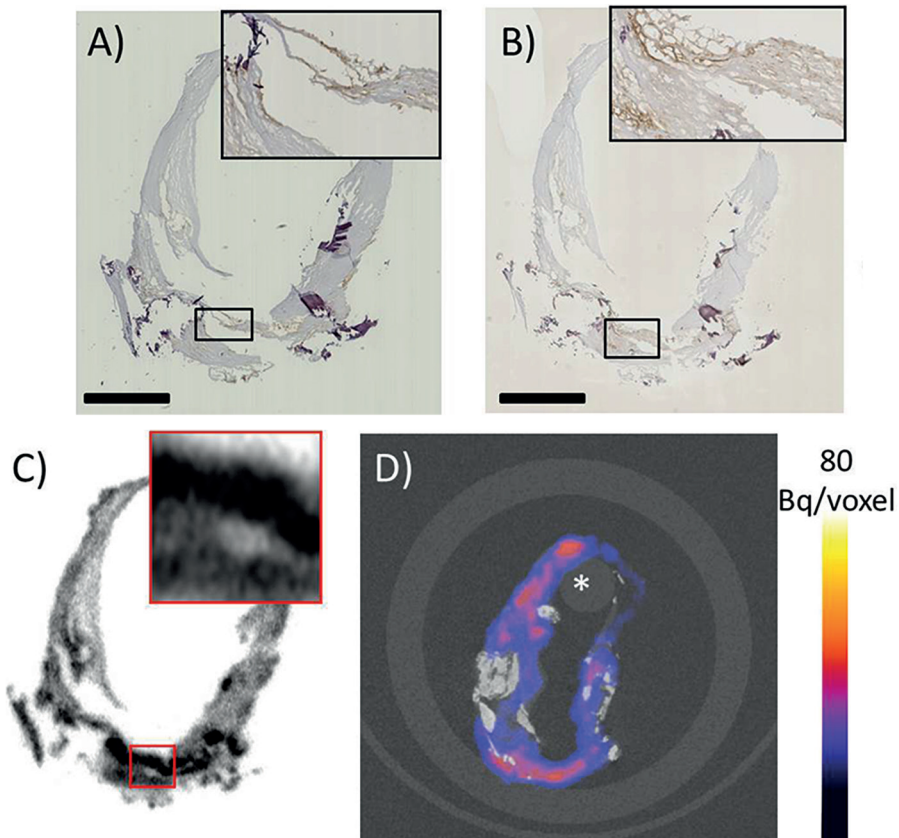


**Figure 2 | A)** Excised, cut open and Oil red O stained arteries of a mouse injected with 200 pmol [$^{111}$In]In-DOTA-JR11. Scale bar indicates 2 mm. **B)** Matching high resolution *ex vivo* autoradiogram to the arteries shown in (**A**), showing [$^{111}$In]In-DOTA-JR11 uptake at plaque locations. **C)** and **D)** show immunohistochemistry for CD68 (macrophages) and Somatostatin Subtype Receptor 2 (SST$_2$) expressing cells in mouse plaque, respectively. Scale bar indicates 100 μm. **E)** and **F)** show the overview of the histological sections shown in (**C**) and (**D**); the asterisk marks the location of the zoomed area in (**C**) and (**D**). Scale bar indicates 2.5 mm.

## Human plaque imaging

Two millimetre thick slices of a human carotid endarterectomy sample incubated with [$^{111}$In] In-DOTA-JR11 showed focal hotspots of radioligand uptake detectable by SPECT, reflecting the presence of SST$_2$ as determined by immunohistochemistry (Figure 3). Noticeably, no radioligand uptake or SST$_2$ expression was visible in areas of macrocalcifications visible in CT. *In vitro* autoradiography performed on 10 µm sections of adjacent 2 mm slices showed specific binding of [$^{111}$In]In-DOTA-JR11 when compared to adjacent sections incubated with a 1000x excess of unlabelled DOTA-JR11 (non blocked=$35*10^6 \pm 90*10^5$, blocked=$25*10^6 \pm 63*10^5$ DLU/mm$^2$, p=0.005, see Online Resource 2 and Figure 3). Moreover, radioligand uptake visualized on *in vitro* autoradiography co-localized with CD68 and SST$_2$ expression on adjacent sections, and signal as seen on the SPECT/CT images of the adjacent 2 mm slices (Figure 3B-E).
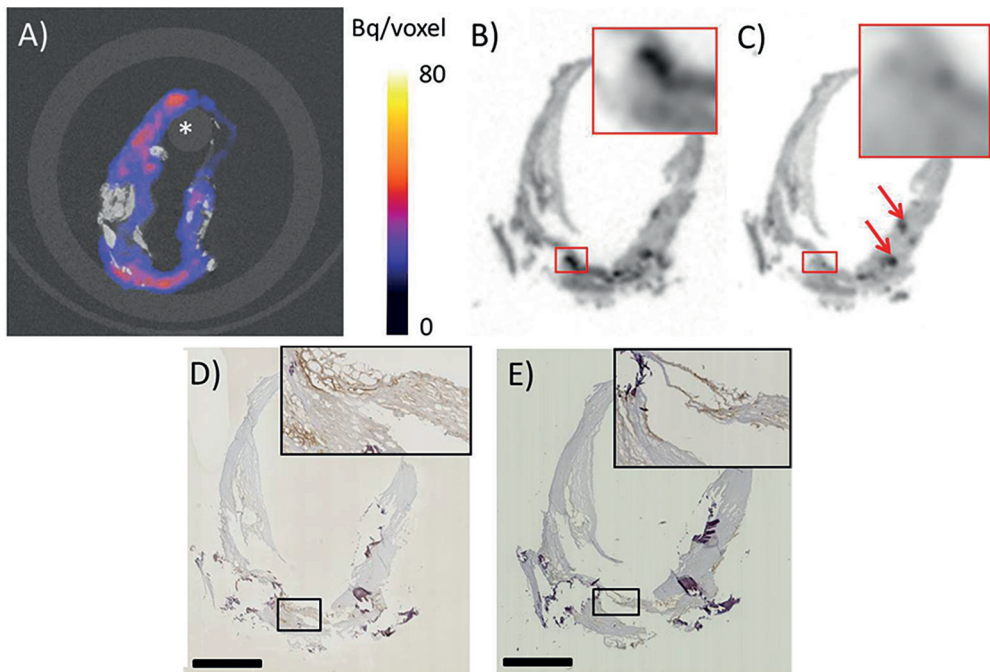


**Figure 3 | [$^{111}$In]In-DOTA-JR11 uptake in human carotid endarterectomy (CEA) tissue after incubation with [$^{111}$In]In-DOTA-JR11. A**) Transverse SPECT/CT image of a two mm slice of a CEA sample. Calcifications are visible in CT in white, the asterisk indicates the holder used to keep the two mm slice in place. **B**) and **C**) *In vitro* autoradiography of adjacent 10 µm sections made of an adjacent two mm slice of the same CEA sample seen in (**A**). The section in **B**) was incubated with $10^{-9}$ M [$^{111}$In]In-DOTA-JR11, the section in **C**) was incubated with $10^{-9}$ M [$^{111}$In]In-DOTA-JR11 plus a blocking dose of $10^{-6}$ M unlabelled DOTA-JR11. The inset shows the boxed region at higher magnification, the red arrows indicate sectioning artefacts (tissue folds). **D**) SST$_2$ and **E**) CD68 immunohistochemistry on 5 µm sections adjacent to **B**) and **C**), with matching insets. Scale bar indicates two mm.

# Discussion

We have demonstrated the feasibility of imaging atherosclerotic plaques by targeting SST$_2$ with DOTA-JR11, by visualizing plaque with In-111 labelled DOTA-JR11 in a mouse model of atherosclerosis and in human plaque tissue. We showed that radioligand uptake is located in plaque regions in the mouse vasculature as evidenced by *in vivo* and *in situ* SPECT/CT imaging, autoradiography, and ORO staining. [$^{111}$In]In-DOTA-JR11 uptake in human plaque tissue co-localizes with SST$_2$ and CD68 expressing cells, whereas blocking studies show target-specific uptake *in vivo* and *in situ* in mouse plaque, and *in vitro* in human tissue.

High thymic uptake of [$^{111}$In]In-DOTA-JR11, visible in the *in vivo* SPECT images and in line with reported SST$_2$ expression in mice in this tissue (29), is problematic when visualizing plaque in the used atherosclerotic model. Nevertheless, we demonstrated that the *in vivo* signal visible next to the thymus did originate from plaque, by comparing the intensity and the localization of plaque signal in the *in vivo*, *in situ*, and *ex vivo* SPECT scans, as well as the *ex vivo* autoradiography. Thymic uptake is not expected to interfere with human plaque imaging as thymic activity wanes during adolescence, and little SST$_2$–ligand binding has been found in dedicated studies (30). *Ex vivo* imaging of a human CEA sample showed that SPECT imaging using [$^{111}$In]In-DOTA-JR11 is feasible in human plaque tissue and that radioligand uptake co-localizes to regions of inflammation as evidenced by CD68 and SST$_2$ immunohistochemistry. These results indicate that DOTA-JR11 has potential for imaging of inflammation in human plaques.

Oncological studies reported a five times higher uptake of DOTA-JR11 over DOTATATE in SST$_2$ positive tumours (21-23). It is hypothesized that antagonistic ligands such as DOTA-JR11 have more binding sites on the receptor than agonistic ligands such as DOTATATE (31). Although the exact mechanism for this difference in uptake remains to be elucidated, the growing amount of studies using SST$_2$-mediated imaging in atherosclerosis (13-19) indicate DOTA-JR11 as an interesting candidate for further studies.

DOTATATE and DOTA-JR11 have not been compared for the detection of atherosclerotic plaque. Two preclinical studies have tested [$^{68}$Ga]Ga-DOTATATE for plaque imaging in mouse models, however. Although it is difficult to compare studies using different animal models and different imaging systems, the results found in (14,15) indicate that [$^{68}$Ga]Ga-DOTATATE has a lower TBR compared to [$^{111}$In]In-DOTA-JR11 our study. Rinne et al. found an aorta to blood ratio of 0.67 ± 0.04 using [$^{68}$Ga]Ga-DOTATATE *in vivo* in IFG-II/LDLR$^{-/-}$ApoB$^{100/100}$ mice (15), indicating low radioligand uptake in plaque. However, they also reported a high plaque to wall ratio of 2.1 ± 0.5 for [$^{68}$Ga]Ga-DOTATATE in autoradiographic studies. Li et al. found a similar plaque to non plaque ratio of ~1.8 after autoradiographic analysis of ApoE$^{-/-}$ arteries incubated with [$^{68}$Ga]Ga-DOTATATE (14). We found an *in vivo* TBR of 2.23 ± 0.35 and an *in situ* TBR of 2.46 ± 0.52, and in

the autoradiogram of the mouse arteries we found a TBR of 3.43 ± 1.45. Taken together, these studies warrant further investigations into the added value of DOTA-JR11 over DOTATATE in atherosclerotic patients.

If a five times higher uptake of DOTA-JR11, as was found in oncological studies, would be found in atherosclerosis as well, DOTA-JR11 could offer possibilities for visualization of less inflamed plaques or plaques with lower $SST_2$ expression. Moreover, the DOTA chelator of JR11 allows labelling with different radionuclides including Ga-68, making DOTA-JR11 attractive for PET imaging. Although different radiometals result in differences in binding affinity of DOTA-JR11 (32), the attractive pharmacokinetics of DOTA-JR11 are conserved when labelled with Ga-68 (24).

Because inflammation in different plaque regions can have a substantial effect on the rupture risk of atherosclerotic plaques, future studies should investigate whether DOTA-JR11 uptake can be correlated to different plaque phenotypes. A better interpretation of radioligand uptake related to plaque phenotype could be a major step in patient risk stratification.

# Conclusion

4

Our results indicate DOTA-JR11 as a promising ligand for atherosclerosis imaging based on our promising *in vivo* results and *ex vivo* validation studies. DOTA-JR11 could be a valuable improvement in imaging of inflammation in atherosclerotic disease.

## New Knowledge Gained

The $SST_2$ targeting radioligand [111In]In-DOTA-JR11 can be used to detect plaques in a mouse model of atherosclerosis by visualizing plaque inflammation. [111In]In-DOTA-JR11 uptake in human plaque tissue indicates the translational potential of this radioligand for human imaging. Recent success of $SST_2$ imaging in atherosclerosis with DOTATATE, and a five times higher TBR of DOTA-JR11 than DOTATATE in oncological studies, make DOTA-JR11 an interesting ligand for further studies in atherosclerosis.

## Disclosure

## Sources of funding

# References

1. GBD 2015 Mortality and Causes of Death Collaborators I. Global, regional, and national life expectancy, all-cause mortality, and cause-specific mortality for 249 causes of death, 1980–2015: a systematic analysis for the Global Burden of Disease Study 2015. Lancet. 2016;380(9859):1459–1544. doi:10.1016/S0140-6736(16)31012-1

2. Quillard T, Libby P. Molecular imaging of atherosclerosis for improving diagnostic and therapeutic development. Circ Res. 2012;111(2):231-244. doi:10.1161/CIRCRESAHA.112.268144

3. Hansson GK. Inflammation, Atherosclerosis, and Coronary Artery Disease. N Engl J Med. 2005;352(16):1685–1695. doi:10.1056/NEJMra043430

4. Moore KJ, Sheedy FJ, Fisher EA. Macrophages in atherosclerosis: a dynamic balance. Nat Rev Immunol. 2013;13(10):70–721. doi:10.1038/nri3520

5. Rudd JHF, Warburton EA, Fryer TD, et al. Imaging atherosclerotic plaque inflammation with [18F]-fluorodeoxyglucose positron emission tomography. Circulation. 2002;105(23):2708–2711. doi:10.1161/01.CIR.0000020548.60110.76

6. Tawakol A, Migrino R, Hoffmann U, et al. Noninvasive in vivo measurement of vascular inflammation with F-18 fluorodeoxyglucose positron emission tomography. J Nucl Cardiol. 2005;12(3):294–301. doi:10.1016/j.nuclcard.2005.03.002

7. Figueroa AL, Subramanian SS, Cury RC, et al. Distribution of Inflammation Within Carotid Atherosclerotic Plaques With High-Risk Morphological Features A Comparison Between Positron Emission Tomography Activity, Plaque Morphology, and Histopathology. Circ Cardiovasc Imaging. 2012;5:69–77. doi:10.1161/CIRCIMAGING.110.959478

8. Rudd JHF, Narula J, Strauss HW, et al. Imaging Atherosclerotic Plaque Inflammation by Fluorodeoxyglucose With Positron Emission Tomography. Ready for Prime Time? J Am Coll Cardiol. 2010;55(23):2527–2535. doi:10.1016/j.jacc.2009.12.061

9. Buettner C, Rudd JHF, Fayad ZA. Determinants of FDG Uptake in Atherosclerosis. JACC Cardiovasc Imaging. 2011;4(12):1302–1304. doi:10.1016/j.jcmg.2011.09.011

10. Tarkin JM, Joshi FR, Rudd JHF. PET imaging of inflammation in atherosclerosis. Nat Rev Cardiol. 2014;11(8):443–457. doi:10.1038/nrcardio.2014.80

11. Elliott DE, Li J, Blum a M, Metwali A, Patel YC, Weinstock JV. SSTR2A is the dominant somatostatin receptor subtype expressed by inflammatory cells, is widely expressed and directly regulates T cell IFN-gamma release. Eur J Immunol. 1999;29(8):2454–2463. doi:10.1002/(SICI)1521-4141(199908)29:08&#60;2454::AID-IMMU2454&#62;3.0.CO;2-H

12. Dalm V a SH, van Hagen PM, van Koetsveld PM, et al. Expression of somatostatin, cortistatin, and somatostatin receptors in human monocytes, macrophages, and dendritic cells. Am J Physiol Endocrinol Metab. 2003;285(2):E344-E353. doi:10.1152/ajpendo.00048.2003

13. Rominger A, Saam T, Vogl E, et al. In vivo imaging of macrophage activity in the coronary arteries using 68Ga-DOTATATE PET/CT: correlation with coronary calcium burden and risk factors. J Nucl Med. 2010;51(2):193–197. doi:10.2967/jnumed.109.070672

14. Li X, Bauer W, Kreissl MC, et al. Specific somatostatin receptor II expression in arterial plaque: 68Ga-DOTATATE autoradiographic, immunohistochemical and flow cytometric studies in apoE-deficient mice. Atherosclerosis. 2013;230(1):33–39. doi:10.1016/j.atherosclerosis.2013.06.018

15. Rinne P, Hellberg S, Kiugel M, et al. Comparison of Somatostatin Receptor 2-Targeting PET Tracers in the Detection of Mouse Atherosclerotic Plaques. Mol Imaging Biol. 2015;18(1):99–108. doi:10.1007/s11307-015-0873-1

16. Mojtahedi A, Alavi A, Thamake S, et al. Assessment of vulnerable atherosclerotic and fibrotic plaques in coronary arteries using 68 Ga-DOTATATE PET/CT. Am J Nucl Med Mol Imaging. 2015;5(1):65–71.

17. Malmberg C, Ripa RS, Johnbeck CB, et al. 64Cu-DOTATATE for non-invasive assessment of atherosclerosis in large arteries and its correlation with risk factors: head-to-head comparison with 68Ga-DOTATOC in 60 patients. J Nucl Med. 2015:1–33. doi:10.2967/jnumed.115.161216

18. Pedersen SF, Sandholt BV, Keller SH, et al. [64] Cu-DOTATATE PET/MRI for Detection of Activated Macrophages in Carotid Atherosclerotic PlaquesSignificance. Arterioscler Thromb Vasc Biol. 2015;35(7):1696–1703. doi:10.1161/ATVBAHA.114.305067

19. Wan MYS, Endozo R, Michopoulou S, et al. PET/CT Imaging of Unstable Carotid Plaque with ^{68}Ga-Labeled Somatostatin Receptor Ligand. J Nucl Med. 2017;58(5):774–780. doi:10.2967/jnumed.116.181438

20. Tarkin JM, Joshi FR, Evans NR, et al. Detection of Atherosclerotic Inflammation by 68Ga-DOTATATE PET Compared to [18F]FDG PET Imaging. J Am Coll Cardiol. 2017;69(14):1774–1791. doi:10.1016/j.jacc.2017.01.060

21. Fani M, Nicolas GP, Wild D. Somatostatin Receptor Antagonists for Imaging and Therapy. J Nucl Med. 2017;58(Supplement 2):61S–66S. doi:10.2967/jnumed.116.186783

22. Wild D, Fani M, Fischer R, et al. Comparison of Somatostatin Receptor Agonist and Antagonist for Peptide Receptor Radionuclide Therapy: A Pilot Study. 2014;55(8):1248–1253. doi:10.2967/jnumed.114.138834

23. Dalm SU, Nonnekens J, Doeswijk GN, et al. Comparison of the Therapeutic Response to Treatment with a 177Lu-Labeled Somatostatin Receptor Agonist and Antagonist in Preclinical Models. J Nucl Med. 2016;57(2):260–266. doi:10.2967/jnumed.115.167007

24. Krebs S, Pandit-Taskar N, Reidy D, et al. Biodistribution and radiation dose estimates for 68 Ga-DOTA-JR11 in patients with metastatic neuroendocrine tumors. Eur J Nucl Med Mol Imaging. 2019;46(3):677–685. doi:10.1007/s00259-018-4193-y

25. Blois E De, Schroeder RJ., de Ridder CMA, van Weerden W., Breeman WAP, de Jong M. Improving radiopeptide pharmacokinetics by adjusting experimental conditions for bombesin receptor-mediated imaging of prostate cancer. Q J Nucl Med Mol Imaging. 2012;57:1–9.

26. de Blois E, Chan HS, de Zanger R, Konijnenberg M, Breeman WAP. Application of single-vial ready-for-use formulation of 111In- or 177Lu-labelled somatostatin analogs. Appl Radiat Isot. 2014;85:28–33. doi:10.1016/j.apradiso.2013.10.023

27. Ogawa K, Harata Y, Ichihara T, Kubo A, Hashimoto S. A practical method for position-dependent Compton-scatter correction in single photon emission CT. IEEE Trans Med Imaging. 1991;10(3):408–412. doi:10.1109/42.97591

28. Vaissier PEB, Beekman FJ, Goorden MC. Similarity-regulation of OS-EM for accelerated SPECT reconstruction. Phys Med Biol. 2016;61(11):4300–4315. doi:10.1088/0031-9155/61/11/4300

29. Hofland LJ, Lamberts SWJ, Martin Van Hagen P, et al. Crucial role for somatostatin receptor subtype 2 in determining the uptake of [111In-DTPA-D-Phe1]octreotide in somatostatin receptor-positive organs. J Nucl Med. 2003;44(8):1315–1321.

30. Ferone D, Pivonello R, Kwekkeboom DJ, et al. Immunohistochemical localization and quantitative expression of somatostatin receptors in normal human spleen and thymus: Implications for the in vivo visualization during somatostatin receptor scintigraphy. J Endocrinol Invest. 2012;35(5):528–534. doi:10.3275/7871

31. Ginj M, Zhang H, Waser B, et al. Radiolabeled somatostatin receptor antagonists are preferable to agonists for in vivo peptide receptor targeting of tumors. Proc Natl Acad Sci. 2006;103(44):16436–16441. doi:10.1073/pnas.0607761103

32. Fani M, Braun F, Waser B, et al. Unexpected Sensitivity of sst 2 Antagonists to N-Terminal Radiometal Modifications. 2012:1481–1490. doi:10.2967/jnumed.112.102764

4

# Chapter 5

# Imaging of Inflammatory Cellular Protagonists in Human Atherosclerosis: a Dual-isotope SPECT Approach

Authors: H.E. Barrett PhD[1,2]; **E.J. Meester** Msc[1,2]; K. van Gaalen Bsc[1]; K. van der Heiden PhD[1];

B.J. Krenning MD, PhD[3]; F.J. Beekman PhD[5,6,7]; E. de Blois PhD[2]; J. de Swart[2]; H.J. Verhagen MD, PhD[4];

T. Maina PhD[8]; B.A. Nock PhD[8]; J.P. Norenberg PhD, PharmD[9]; M. de Jong PhD[2]; F.J.H. Gijsen PhD[1];

M.R. Bernsen PhD[2,10]


Author affiliations:

[1] Biomedical Engineering, Department of Cardiology, Erasmus MC, Rotterdam, the Netherlands

[2] Department of Radiology & Nuclear Medicine, Erasmus MC, Rotterdam, the Netherlands

[3] Department of Cardiology, Erasmus MC, Rotterdam, the Netherlands

[4] Department of Vascular Surgery, Erasmus MC, Rotterdam, the Netherlands

[5] MiLabs, B.V., Utrecht, the Netherlands

[6] Section Biomedical Imaging, Delft University of Technology, Delft, the Netherlands

[7] Department of Translational Neuroscience, Brain Centre Rudolf Magnus, University Medical Centre Utrecht, Utrecht, the Netherlands

[8] Molecular Radiopharmacy, INRASTES, NCSR "Demokritos", 15310 Athens, Greece

[9] Radiopharmaceutical Sciences, University of New Mexico, Albuquerque, NM, USA

[10] Applied Molecular Imaging Erasmus Core Facility Erasmus MC, Rotterdam, the Netherlands

# Abstract

**Purpose** | Atherosclerotic plaque development and progression signifies a complex inflammatory disease mediated by a multitude of proinflammatory leukocyte subsets. Using single photon emission computed tomography (SPECT) coupled with computed tomography (CT), this study tested a new dual-isotope acquisition protocol to assess each radiotracer's capability to identify plaque phenotype and inflammation levels pertaining to leukocytes expressing leukocyte function-associated antigen-1 (LFA-1) and the leukocyte subset of proinflammatory macrophages expressing somatostatin receptor subtype-2 ($SST_2$). Individual radiotracer uptake was quantified and the presence of corresponding immunohistological cell markers was assessed.

**Methods** | Human symptomatic carotid plaque segments were obtained from endarterectomy. Segments were incubated in dualisotope radiotracers [111In]In-DOTA-butylamino-NorBIRT ([111In]In-Danbirt) and [99mTc]Tc-[$N^{0-1}_4$,$Asp^0$,$Tyr^3$]-octreotate ([99mTc]Tc-Demotate 2) before scanning with SPECT/CT. Plaque phenotype was classified as pathological intimal thickening, fibrous cap atheroma or fibrocalcific using histology sections based on distinct morphological characteristics. Plaque segments were subsequently immuno-stained with LFA-1 and $SST_2$ and quantified in terms of positive area fraction and compared against the corresponding SPECT images.

**Results** | Focal uptake of co-localising dual-radiotracers identified the heterogeneous distribution of inflamed regions in the plaques which co-localised with positive immuno-stained regions of LFA-1 and SST2. [111In]In-Danbirt and [99mTc]TcDemotate 2 uptake demonstrated a significant positive correlation (r=0.651; p=0.001). Fibrous cap atheroma plaque phenotype correlated with the highest [111In]In-Danbirt and [99mTc]Tc-Demotate 2 uptake compared with fibrocalcific plaques and pathological intimal thickening phenotypes, in line with the immunohistological analyses.

**Conclusion** | A dual-isotope acquisition protocol permits the imaging of multiple leukocyte subsets and the pro-inflammatory macrophages simultaneously in atherosclerotic plaque tissue. [111In]In-Danbirt may have added value for assessing the total inflammation levels in atherosclerotic plaques in addition to classifying plaque phenotype.

Keywords: Atherosclerosis, Inflammation, Carotid artery, Macrophage, Leukocyte, SPECT imaging, Dual-isotope

# Introduction

Atherosclerosis is derived from an inflammatory cycle that forms in response to the deposition of cholesterol rich, apolipoprotein B-containing lipoproteins in the intimal layer of the arterial wall (1). Inflammation controls all stages of the disease starting from the initiating atheroma development to the advanced, and potentially rupture-prone, plaque. Inflammation is instrumental in causing the clinical complications resulting in life-threatening stroke and myocardial infarction (2). Detection of this inflammatory activity is a high clinical priority. If the atherosclerosis-associated inflammation can be detected early a considerable reduction in the occurrence of these cardiovascular events could be made possible.

From the initiating phase of the disease, leukocytes, including monocyte-derived macrophages, lymphocytes and neutrophils, adhere to activated endothelium and are recruited into the developing atheroma (3). The proinflammatory leukocytes elicit a cascade of biological processes which renders the plaque susceptible to structural disruptions including fibrous cap ruptures (4). Following rupture, exposure of the thrombogenic plaque core to blood components can result in catastrophic cardiovascular events (5). The search for methods that can specifically target the inflammatory activity in atherosclerotic tissue and identify the high-risk vulnerable plaque phenotype is a high clinical priority (6).

Molecular imaging techniques including positron emission tomography (PET) and single photon emission computed tomography (SPECT) have the unique capability to target specific biological processes at the molecular level. Numerous radiotracers, capable of targeting leukocytes and the inflammatory subsets, have been developed and imaged in human atherosclerotic plaque vessels (7). [^{111}In]In-DOTA-butylamino-NorBIRT also known as [^{111}In]In-Danbirt is a novel radiotracer which can specifically target the leukocytes which express leukocyte function-associated antigen-1 (LFA-1). The value of this radiotracer has been initially demonstrated in *in vivo* animal studies utilising atherosclerosis disease models and also in a human atherosclerotic plaque case (8,9). Targeted imaging of atherosclerotic plaque with [^{68}Ga]Ga-DOTA-[Tyr[3]]octreotate, a somatostatin receptor subtype 2 (SST$_2$)-targeting radiotracer, detects the presence of activated (proinflammatory) macrophages (10). The clinical utilisation of this radiotracer has revealed its ability to achieve more focal imaging of inflamed atherosclerotic plaques in comparison to 2-deoxy-2-[^{18}F]fluoro-D-glucose ([^{18}F]FDG) and thereby presenting another viable radiotracer (10-12). Clinical studies indicated that the detection of proinflammatory macrophages with a SST$_2$ targeting radiotracer could help discriminate culprit plaques which have an overall higher uptake (10,11). Notwithstanding, there are conflicting results reported for this radiotracer. For example, comparing symptomatic culprit vessels to the contralateral vessels in the carotid vasculature can result in little to no differences in terms of uptake levels (13,14). The detection of 'culprit' inflamed vessels is partially

impeded by the paucity of information linking radiotracer uptake with respect to the specific plaque phenotype.

Furthermore, the simultaneous use of two radiotracers, targeting different molecular processes, with dual-isotope acquisition SPECT imaging has provided an enhancement in the understanding of specific diseases (15-17). The utilisation of a dual-isotope acquisition protocol for atherosclerotic plaque tissue assessment may also provide improved information and in terms of aiding the detection of specific plaque phenotype. In this regard, this study aims to assess the added value of simultaneously targeting all leukocytes expressing LFA-1 and the subset of proinflammatory macrophages expressing $SST_2$ in order to identify plaque phenotype. To investigate this, a dual-isotope acquisition protocol of [$^{111}$In]In-Danbirt and [$^{99m}$Tc]Tc-[$N^0_4$, Tyr$^3$]-octreotate also known as [$^{99m}$Tc]Tc-Demotate 2 (18) is utilised to image *ex vivo* human carotid artery plaques. Additionally, the two radiotracers are compared to investigate if targeting all leukocytes provides pertinent information regarding the inflammatory status of the plaque that could be overlooked with current clinical protocols targeting the subset of proinflammatory macrophages alone.

# Materials and Methods

## Study design

A cross-sectional molecular imaging study was performed with excised human carotid plaques. This exploratory research examines the uptake of two radiotracers pertaining to inflammatory populations involved in plaque progression. The plaque samples were obtained from seven atherosclerotic/symptomatic patients through endarterectomy procedures in the Erasmus MC, Rotterdam, The Netherlands, in a manner that conformed to the declaration of Helsinki and was approved by the hospital's ethical research committee (MEC 2008-147). The carotid plaques were divided into segments of 2 mm thickness (n=23) for SPECT/CT imaging followed by immunohistochemistry. In another set of experiments, adjacent Carotid endarterectomy (CEA) segments (n=7) were sectioned for autoradiography followed by immunohistochemistry.

## Radiolabelling

To target the two plaque's inflammatory cell populations, [$^{111}$In]In-Danbirt (MW=886.5 g/mole) (9) and [$^{99m}$Tc]Tc-Demotate 2 (18) were used (Figure 1). Each peptide was radiolabelled with a molar activity of 100 MBq/nmol, the radiochemical purity was >90% and the incorporation yield was >99%, as determined by high-pressure liquid chromatography and instant thin-layer chromatography on silica gel. For [$^{111}$In]In-Danbirt Quenchers (3.5 mM ascorbic acid, 3.5 mM gentisic acid, 10 mM methionine) were present during labelling to prevent radiolysis of the radiotracers (19). The radiotracers were mixed in a solution of phosphate-buffered saline (PBS) containing 0.1% v/v bovine serum albumin (BSA). The plaque samples were incubated

in a mixed solution of the 2 radiotracers for 1h at room temperature. The plaque samples were then washed in PBS five times and assembled on a sealed perspex sample holder for scanning (Figure 2).
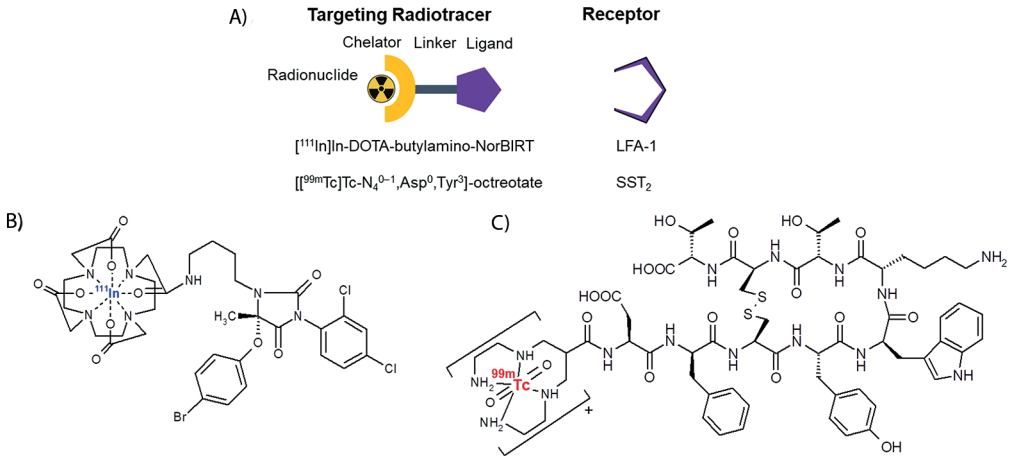


**Figure 1 | A**) Schematic of the two radiotracers targeting the receptors of leukocytes expressing leukocyte function-associated antigen-1 (LFA-1) and proinflammatory macrophages expressing somatostatin receptor subtype-2 (SST$_2$). Chemical structures of the two radiotracers **B**) [$^{111}$In][In-DOTA-butylamino-NorBIRT] ([$^{111}$In] In-Danbirt) and **C**) [[$^{99m}$Tc]Tc-[N$_4^{0-1}$,Asp$^0$,Tyr$^3$]octreotate ([$^{99m}$Tc]TcTc-Demotate 2).

5
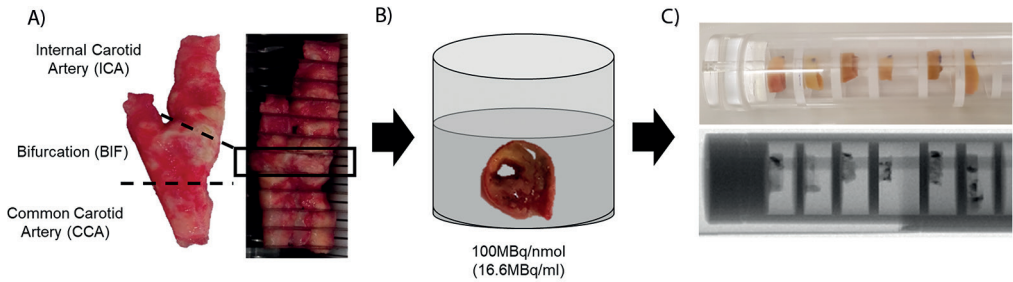


**Figure 2 | A**) Carotid plaque sample sectioned into 2 mm segments, **B**) incubation step involved immersing segment in mixture of dual-radiotracers [$^{111}$In]In-Danbirt) and [$^{99m}$Tc]Tc-Demotate 2 and **C**) live and x-ray view of plaque segments (2 mm) mounted on a custom made holder for dual-isotope acquisition SPECT/CT scanning.

## Dual-isotope SPECT/CT imaging

For SPECT/CT imaging a VECTor5/CT system (MILabs B.V. Utrecht, The Netherlands) was used equipped with a high-energy ultra-high resolution mouse (HE-UHR-M) collimator. The system equipped with this collimator yields a 0.5 mm reconstructed SPECT resolution and a SPECT sensitivity of ~0.3 % (20,21). Each scan was acquired in list mode using the same scan parameters; spiral scan mode (22), and fine step mode at 30 seconds per bed position yielding a total acquisition time of 90 minutes for a field of view of 26 mm in diameter and 48 mm in length. This permitted scanning six 2 mm plaque segments, placed in the sample holder, during a single scan. For the CT, scanner settings were identical for all scans. Ultra-focus magnification was applied with a full scan angle, at 0.24 mA, 50 kV and 75 ms yielding a total scan time of 15 minutes. The scans were reconstructed using filtered back projection at a resolution of 20 µm and down sampled to a reconstructed resolution of 80 µm for registration to SPECT scans.

To accomplish quantification of $^{99m}$Tc and $^{111}$In from dual isotope acquisitions, two separate reconstructions were performed. For $^{99m}$Tc, a width of 20% of the gamma photopeak at 140 keV was incorporated in the reconstruction. For $^{111}$In, two photopeak windows were set incorporating a width of 20% of the each gamma photopeak at 171 and 245 keV (23). For scatter correction the triple-energy-window method was (24) applied to each photo peak. Phantom experiments with dual-isotopes acquisitions for $^{99m}$Tc and $^{111}$In were performed using the small-animal SPECT phantom SPECT IQ phantom which verified that the cross-talk within the relevant energy ranges was negligible (25).

SPECT scans were reconstructed at 0.2 mm voxel size using the Similarity Regulated Ordered Subset Expectation Maximization (SROSEM) algorithm (22). For this, 9 iterations, 128 subsets and a 3D Gaussian post filter of 0.5 mm (FWHM) were utilised. The VECTor5/CT system was calibrated to a standard of known activity that was measured in a dose calibrator, for absolute SPECT quantification for both radionuclides. All analysis of SPECT/CT scans was performed using PMOD (PMOD Technologies LLC, Zürich, Switzerland, Version 3.4). After imaging, the tissue segments were embedded in tissue-tek medium and stored at -80° C for immunohistological analysis after the radioactivity contained in the samples had decayed.

## Immunohistological analyses

Each 2 mm plaque segment was cryo-sectioned into four 500 µm blocks in line with the SPECT resolution. Within each 500 µm block, sequential adjacent sections of 5 µm were made which overall yielded a total of 262 sections for quantification and analysis with respect to the SPECT/CT scan data. Sections were immunohistochemically stained with anti-LFA-1 (mouse anti-human CD11a 1:100 Biorad, MCA1848 clone 38), and anti-SST$_{2A}$ (human tissue: rabbit anti-human SSTR2A 1:50, clone UMB1, Abcam). Haematoxylin and eosin staining was used to determine the plaques overall structural morphology. The slides were photographed using a NanoZoomer Digital slide scanner (Hamamatsu, Photonics K.K). All images were exported to

BioPix iQ 3.3.5 software for quantitative analysis. The areas of positively stained LFA-1 and $SST_2$ were quantified using the dedicated hue, saturation and brightness selection tool and positive areas were measured as a percent fraction of the total plaque tissue area.

## Plaque classification

The twenty-three carotid plaque segments were classified into 3 groups according to the American Heart Association (AHA) plaque classification (4), based on distinct morphological characteristics, identified with histology. Segments with pathological intimal thickening (n=4, 17%) contained areas of inflammatory infiltration without necrotic tissue and were present in the bifurcation and internal carotid region. The fibrous cap atheroma segments (n=9, 39%) morphologically consisted of a well-formed necrotic core and an overlying fibrous cap containing a high infiltration of inflammatory cells and were mainly found in the internal and common carotid regions. The fibrocalcific segments (n=10, 43%) contained large areas of calcification within the necrotic core and were all located in the bifurcation region.

## Autoradiography

Segments of the carotid plaques, adjacent to those used for scanning, were cryo-sectioned at 10 μm and examined by *ex vivo* autoradiography and immunohistochemistry. Slides were washed in a washing buffer consisting of 1 M Tris-HCl (pH=7.6) containing 0.25% v/v BSA for 10 minutes. The samples were incubated with 80 μL of radiotracer ($10^{-9}$ M), with and without excess ($10^{-6}$ M) matching unlabelled tracer for blocking. Slides were then washed and allowed to dry in an incubator at 37° C. High sensitivity phosphor screens were placed over the tissue sections for 48 h, after which the screens were read using a Packard Cyclone (Perkin Elmer) resolution 600 DPI. Quantification of the plaque sections was performed in terms of digital light units per mm² ($DLU/mm^2$) using Optiquant (Perkin Elmer).

## Statistical analysis

Statistical analysis was performed using IBM SPSS statistics 21. Shapiro–Wilk tests were performed to assess the distribution of the data and select the most appropriate statistical test. Pearson's correlation (r) and Spearman's rho correlation ($r_s$) were used to compare the correlation between the uptake levels of the radiotracers. A Mann-Whitney U test was used for non-parametric datasets to compare differences between uptake and positive area fraction for the three plaque morphology groups.

5

# Results

## Expression of LFA-1 and $SST_2$ in carotid plaque segments

Figure 3 illustrates the distinct morphological characteristics and positive immuno-stained regions of LFA-1 and $SST_2$ in three plaque phenotypes classified as pathological intimal thickening, fibrous cap atheroma and fibrocalcific. In the inflamed fibrous cap atheroma phenotype, immunohistological analyses revealed large clusters of colocalising LFA-1 and $SST_2$ expressing inflammatory cells concentrated in the atheroma, at the fibrous caps and along shoulders (Figure 3 f, h) (Figure 4 c-d). Quantification of the areas with positive immuno-staining for LFA-1 and $SST_2$, within the representative 4 cryosections taken at intervals of 500 μm within each of the 2 mm plaque segments, revealed that the overall area fraction of LFA-1-positive leukocytes was significantly larger in comparison with the area fraction positive for $SST_2$-expressing macrophages independent of plaque phenotype. A large degree of variation was detected for fibrous cap atheroma segments in terms of the degree of positive LFA-1, reflecting the diverse inflammation status associated with this phenotype. The fibrous cap atheroma segments contained a significantly higher degree of inflammatory cells expressing LFA-1 compared to the fibrocalcific plaque segments and the pathological intimal thickening segments (Figure 5A). For $SST_2$, fibrous cap atheroma segments and fibrocalcific segments contained comparable area fraction levels of $SST_2$ positive cells. Pathological intimal thickening segments contained a significantly lower amount of $SST_2$ positive area (Figure 5B).

## Radiotracer targeting of LFA-1 and $SST_2$ in different plaque phenotypes assessed by SPECT

High-resolution SPECT images portray the local specificity of the dual-radiotracer's binding to inflamed regions in the plaques which also co-localises with positive immuno-stained regions of LFA-1 and $SST_2$ (Figure 3). An example of the focal high uptake of both radiotracers in the atheroma core and fibrous cap region of a fibrous cap atheroma plaque is illustrated in the SPECT images in Figure 4 whereby regions of [^{111}In]In-Danbirt uptake co-localised with [^{99m}Tc]Tc-Demotate 2 uptake. The [^{111}In]In-Danbirt uptake is significantly higher compared to the [^{99m}Tc]Tc-Demotate 2 for all plaque samples analysed in this cohort (p=0.001). There is a significant positive correlation in uptake between the radiotracers targeting the cells expressing LFA-1 and $SST_2$ receptors (r=0.651; p=0.001) as illustrated in Figure 6. Quantification of each radiotracer's total uptake (MBq/g) in each 2mm plaque segment with distinct plaque phenotype revealed that the highest uptake of [^{111}In]In-Danbirt is correlated to plaque phenotype with fibrous cap atheroma (20.39 ± 3.97 MBq/g) (Figure 7A). The uptake is significantly higher compared to both the pathological intimal thickening (14.70 ± 3.23 MBq/g) and fibrocalcific plaque (14.05 ± 4.89 MBq). For [^{99m}Tc]Tc-Demotate 2 the mean uptake is significantly higher in the fibrous cap atheroma segments (7.98 ± 1.10 MBq/g) compared to the fibrocalcific segments (6.36 ± 2.39 MBq/g) (Figure 7B). However, a significant difference was not reached between the fibrous cap atheroma and pathological intimal thickening (6.38 ± 2.23 MBq/g) for the [^{99m}Tc]Tc-Demotate 2 uptake (p=0.142).
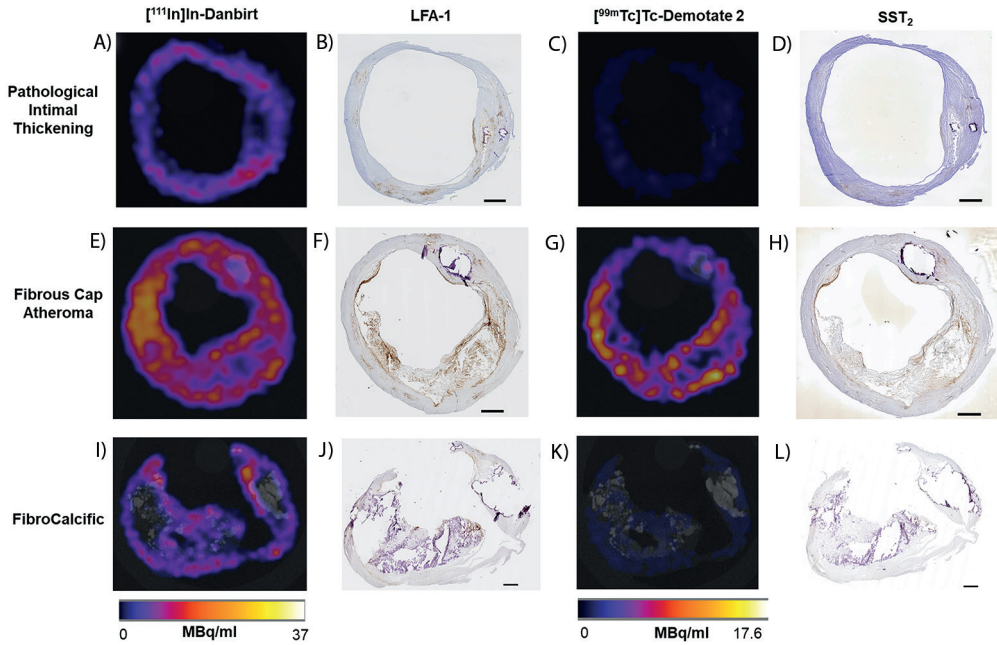
**Figure 3** | SPECT images of uptake for [$^{111}$In]In-Danbirt (left panel 0–37 MBq/ml) and [$^{99m}$Tc]Tc-Demotate 2 (right panel 0–17.5 MBq/ml) and the corresponding immunohistological sections classified according to plaque phenotype; pathological intimal thickening (**A-D**), fibrous cap atheroma (**E-H**) and fibrocalcific (**I-L**) (Scale bar=1mm).

5
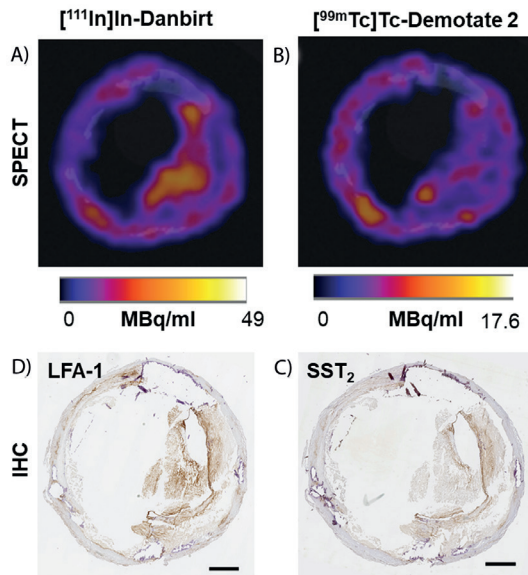


**Figure 4** | SPECT co-localisation of radiotracer uptake **A**) [$^{111}$In]In-Danbirt) and **B**) [$^{99m}$Tc]Tc-Demotate 2 and corresponding immunohistochemistry sections with positive immunostaining for **C**) LFA-1 and **D**) SST$_2$ in a plaque segment classified with fibrous cap atheroma phenotype (Scale bar=1 mm).
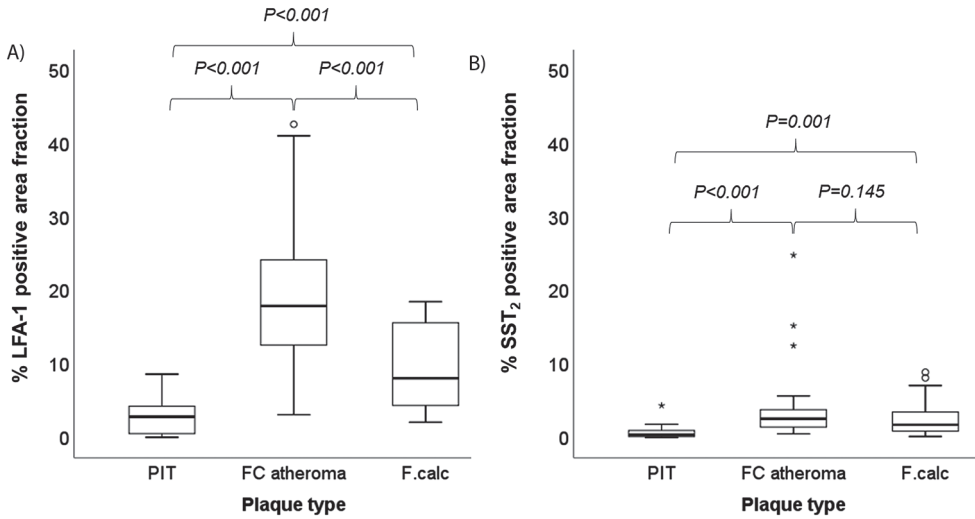
**Figure 5** | Box-plot of percent area fraction of positive immuno-staining for **A**) LFA-1 and **B**) SST$_2$ in segments classified according to plaque phenotype (PIT, pathological intimal thickening; FC atheroma, fibrous cap atheroma and F.calc, fibrocalcific)
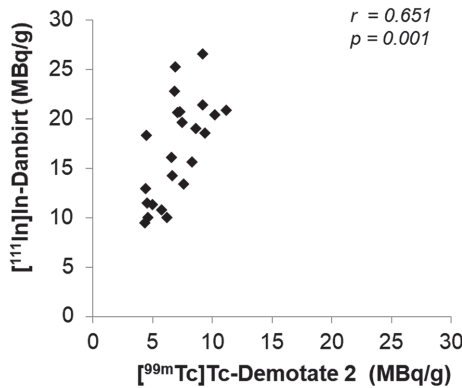


**Figure 6** | Positive correlation between [$^{99m}$Tc]Tc-Demotate 2 and [$^{111}$In]In-Danbirt and in terms of total uptake (MBq/g) per plaque segment

Comparing the sections with and without excess (10–6 M) radiotracer, revealed the substantial reduction in uptake in the CEA sections. The autoradiography analysis of [$^{111}$In]In-Danbirt and [$^{99m}$Tc]Tc-Demotate 2 uptake also revealed the focal regions of high radiotracer binding in the fibrous cap atheroma segments in line with the immuno-positive regions for LFA-1 and SST$_2$ respectively (Figure 8).
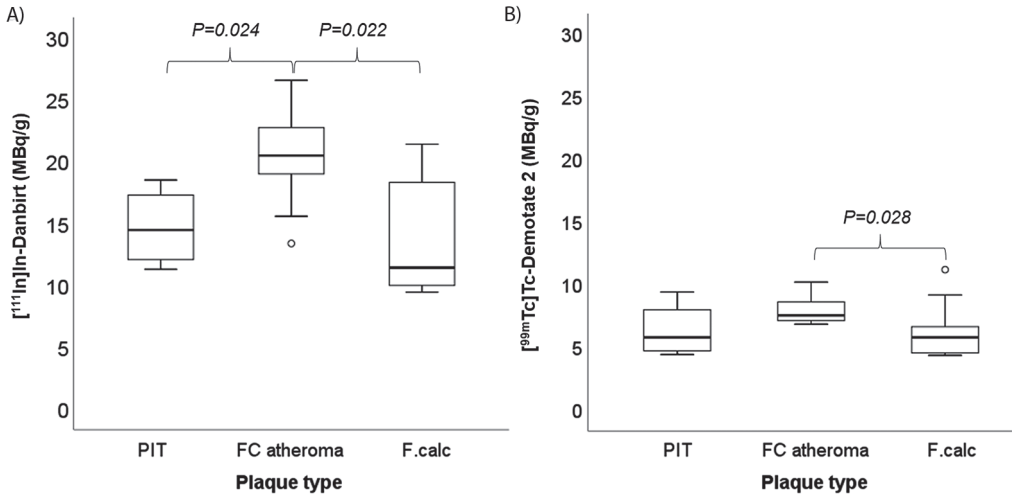
**Figure 7** | Box-plot of radiotracer uptake (MBq/g) for **A**) [$^{111}$In]In-Danbirt and **B**) [$^{99m}$Tc]Tc-Demotate 2 in each carotid plaque segment type classified according to plaque phenotypes; PIT, pathological intimal thickening; FC, fibrous cap atheroma and F.calc, fibrocalcific
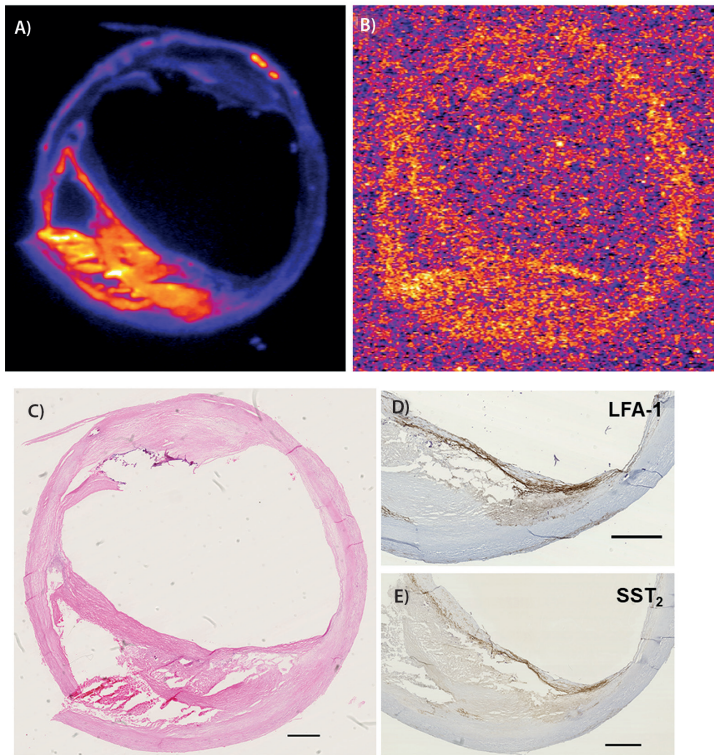


**Figure 8** | Uptake of dual-radiotracers in fibrous cap atheroma section; Autoradiography images showing focal regions of high radiotracer binding for **A**) [$^{111}$In]In-Danbirt **B**) [$^{99m}$Tc]Tc-Demotate 2, **C**) Hematoxylin and eosin stain demonstrating morphology of fibrous cap atheroma section and corresponding immuno-sections showing positive staining in the fibrous cap for **D**) leukocytes (LFA-1) and **E**) macrophages (SST$_2$) (scale bar=1mm).

# Discussion

In this study, a dual-isotope acquisition SPECT imaging protocol was tested to assess radiotracer uptake in distinct plaque phenotypes pertaining to two inflammatory cell populations involved in atherosclerosis. We demonstrated the unique capability of the [$^{111}$In]In-Danbirt to identify inflamed plaque phenotype using human carotid plaques acquired through endarterectomy procedures. The mean [$^{111}$In]In-Danbirt and [$^{99m}$Tc]Tc-Demotate 2 uptake was highest in fibrous cap atheroma plaque compared to pathological intimal thickening and fibrocalcific plaques. A comparison of the uptake for the two radiotracers revealed that [$^{111}$In]In-Danbirt uptake was significantly higher compared to [$^{99m}$Tc]Tc-Demotate 2 uptake for all plaque samples analysed in this cohort, independent of plaque phenotype. These findings were in line with the immunohistological findings and detailed examination of the corresponding immunohistological sections revealed co-localization with LFA-1 and SST$_2$ expressing cells.

The atherosclerotic inflammatory activity is driven by multiple key leukocyte subsets including the monocyte derived macrophages, lymphocytes and neutrophils (26,27). In this regard, it is important to detect the presence of all leukocyte subsets, encapsulating the total inflammation activity, as a means for early atherosclerotic disease detection and potential prevention of adverse cardiovascular events (28). SPECT imaging showed focal uptake of [$^{111}$In]In-Danbirt in the carotid plaque tissue which varied in accordance with the degree of inflammation that was heterogeneously distributed throughout the plaque as indicated by the co-localising areas of positive immuno-staining for LFA-1. The overall higher degree of [$^{111}$In]In-Danbirt uptake compared to [$^{99m}$Tc]Tc-Demotate 2 uptake for all plaque samples analysed in this cohort is indicative of the successful detection of all leukocytes which are playing a key role in the disease progression. In a clinical setting, PET scanning is the preferred methodology in atherosclerosis imaging in terms of nuclear medicine due to the superior spatial resolution and quantification capabilities compared to clinical SPECT. For example, Moto et al. recently demonstrated that Danbirt labelled with the PET radioisotope Gallium-68 is highly stable *in vitro* in conditions that closely emulate those found during *in vivo* tracer delivery (9). For clinical use, the equivalents to SPECT imaging with [$^{99m}$Tc]Tc-Demotate 2 for targeting SST2 expressing proinflammatory macrophages *in vivo* are, [$^{68}$Ga]Ga-DOTA-TATE and [$^{64}$Cu]64Cu-DOTA-TATE which have both been shown to be potentially relevant tracers for plaque imaging with PET in cardiovascular disease patients.

From a pathological point of view, the atherosclerotic plaque composition is heterogeneous even within the same phenotype as identified for the [$^{111}$In]In-Danbirt uptake in the fibrous cap atheroma segments. This is a consequence of the fact that inflammation levels vary considerably depending on the disease phase and inflammatory activity. Notably, this large variation in inflammation intensity was less pronounced in the [$^{99m}$Tc]Tc-Demotate 2 uptake, likely as proinflammatory macrophages (SST$_2$) represents a small subset of the inflammatory

cells present in the plaque. While [111In]In-Danbirt imaging alone is very informative regarding atherosclerotic plaque phenotype detection, the ratio of [99mTc]Tc-Demotate 2 to [111In]In-Danbirt advocates a potential role for dual-isotope acquisition in the assessment of plaque inflammation advancing the understanding towards the atherosclerotic disease development. For example, in the fibrous cap atheroma segments the ratio of [99mTc]Tc-Demotate 2 to [111In]In-Danbirt is lower compared to the fibrocalcific segments. This implicates a higher level of involvement of the other leukocyte subsets with the proinflammatory macrophages in the fibrous cap atheroma phenotype compared to the more advanced fibrocalcific phenotype. In this regard, a dual-isotope acquisition protocol could provide added diagnostic benefit for the assessment of inflamed atherosclerotic vessels which could be useful for patient-specific therapeutic intervention.

Moreover, studies have reported the performance of [111In]In-Danbirt *in vivo* utilisingthe ApoE^{-/-} mouse model. These studies provide evidence that the [111In]In-Danbirt is adequately taken up in local athero-prone regions, including the aortic arch. These atherosclerotic regions of uptake further co-localise with immunohistochemistry LFA-1 expressing cells (8). Importantly, the myocardial uptake signal is sufficiently low with respect to the background levels so as to not interfere with the imaging quantification of the aorta's inflammation (8).

Pathological studies have classified the fibrous cap atheroma phenotype as the 'culprit' part of the vessel (29-31). Interestingly, in this study the intensity of radiotracer uptake correlated to plaque phenotype. The highest [111In]In-Danbirt uptake (MBq/g), correlates to inflamed fibrous cap atheroma plaque segments. This differentiates these highly inflamed plaque segments from fibrocalcific and pathological intimal thickening segments which are considerably less inflamed, and considered to have a lower risk of rupture. Similarly, the mean [99mTc]Tc-Demotate 2 uptake was also highest in the fibrous cap atheroma segments and also significantly higher compared to the fibrocalcific phenotype in line with the immunohistochemistry. Notwithstanding, to make a distinction in specific atherosclerotic plaque phenotype and the identification of vulnerable plaque characteristics remains a challenge based on the current radiotracers used in the clinic (13,32,33). For example, clinical studies have reported difficulty in differentiating symptomatic carotid vessels compared to the contralateral asymptomatic diseased side where there is a high degree of disease present in the contralateral carotid vessel (13). Consequently, delineation of the culprit vulnerable plaque is not always possible. The typical morphological features of a vulnerable plaque have been determined from pathological studies and can be characterised using MRI scanning. These include the presence of a large lipid-rich necrotic core, an overlying thin fibrous cap layer and intraplaque haemorrhage (34-36). However, morphological plaque data alone is also not enough for risk prediction of plaque rupture. In this regard, combining a measurement of the inflammation imaging (9) and the plaque morphology information from MRI may permit assessing the degree of inflammation activity coupled with vulnerable plaque characteristics in order to delineate high-risk vessels (37,38).

5

There are inherent limitations associated with this study that must be taken into account. The clinical translational aspect of the dual-isotope acquisition imaging protocol utilised in this *ex vivo* setting needs to be assessed *in vivo*. Notably, the acquisition of SPECT/CT imaging involved using a HE-UHR-M collimator which resulted in a considerably higher in-plane resolution of 0.5mm compared to the resolution capabilities of the clinical PET scanner which are approximately 10 times lower (33). In a clinical setting, the opposite occurs whereby PET resolution outperforms SPECT. Thus, PET isotopes Fluorine-18 and Gallium-68 are more favourable in the clinical setting compared to Indium-111 or Technitium-99m, although there is no current option for dual isotope imaging with the PET isotopes. Moreover, in order to incorporate a dual-isotope acquisition for SPECT imaging [$^{99m}$Tc]Tc-Demotate 2 was used simultaneously with [$^{111}$In]In-Danbirt in this study. In the clinical setting, [$^{68}$Ga]Ga-DOTA-TATE is utilised for PET imaging of SST$_2$ expressing proinflammatory macrophages. The TATE differs from octreotate by the amino acid in position 3, being Tyr or Phe, respectively. It is important to take into account the application of different analogue radiotracers as they may lead to different quantitative results. Irrespective of the radiotracer applied, the fundamental principle of targeting the SST$_2$ in atherosclerotic plaque tissue remains the same. Thus, the relative trend in uptake differences is expected to be comparable in the *ex vivo* and *in vivo* setting. In an in-vivo situation a larger degree of down scatter is to be expected in the [$^{99m}$Tc] window from [$^{111}$In]. This will subsequently increase the background signal for [$^{99m}$Tc] but should not deter from the image quality when scatter is corrected for. An increased amount of scattering from the tissue in an *in-vivo* situation would also increase the background. The administration of two radionuclides will increase the radiation dose to the patient compared to the use of only one. Since both [$^{99m}$Tc] and [$^{111}$In] radionuclides radiate mainly low to medium energy gamma rays, and the absence of alpha and beta radiation, radiation issues are not expected when a diagnostic amount of these radionuclides are administered to the patient. In terms of the analysis, in an attempt to normalise the plaque segments for comparison, the radiotracer uptake was reported with respect to the weight of each plaque segment. In one plaque segment, classified with the pathological intimal thickening phenotype, a negligible degree of inflammation was present whereby positive area fraction of staining for LFA-1 and SST$_2$ were 0.09% and 0.01% respectively on immunohistochemistry. As a consequence, it is likely that this ratio approach resulted in a false high uptake (MBq/g) for this one segment due to the extremely low uptake (MBq) in this segment and the low weight (g). Due to the small sample size in this phenotype group (n=4) a significant difference therefore was not reached for [$^{99m}$Tc]Tc-Demotate 2 uptake compared to the fibrous cap atheroma segments.

In conclusion, a dual-isotope acquisition SPECT scanning protocol was tested to assess the capability of [$^{111}$In]In-Danbirt and [$^{99m}$Tc]Tc-Demotate 2 to determine atherosclerotic plaque inflammation and phenotype. The novel [$^{111}$In]In-Danbirt detects the presence of multiple leukocyte subsets and appears to be able to strongly discriminate plaque phenotype of fibrous cap atheroma from pathological intimal thickening and fibrocalcific plaque segments. This

information provides a proof of concept basis for the [111In]In-Danbirt as a potential candidate for total inflammation imaging and plaque phenotype classification. Detecting the presence of all leukocytes in addition to leukocyte subset of proinflammatory macrophages may further enhance the pathological understanding of the inflammation involvement in atherosclerosis progression. Thus, further studies that evaluate the clinical benefit of utilising this radiotracer *in vivo* with clinical SPECT scanners are recommended.

## Acknowledgments

## Disclosure

F.J. Beekman is founder, CEO and shareholder of MILabs. B.V., the vendor of the VECTor5/CT system and J. Norenberg holds the patent on [111In]In-Danbirt.

## Ethical approval

All procedures performed in studies involving human participants were in accordance with the ethical standards of the Erasmus Medical Centre's research committee (MEC 2008-147) and with the 1964 Helsinki declaration and its later amendments or comparable ethical standards.

5

# References

1.  Moore KJ, Sheedy FJ, Fisher EA. Macrophages in atherosclerosis: A dynamic balance. Nat Rev Immunol. 2013;13:709–21.

2.  Naghavi M, Libby P, Falk E, Casscells SW, Litovsky S, Rumberger J, et al. From Vulnerable Plaque to Vulnerable Patient. Circulation. 2003;108:1664–72.

3.  Libby P. Inflammation in atherosclerosis. Nature. 2002;420:868–74.

4.  Virmani R, Kolodgie FD, Burke AP, Farb A, Stephen SM. Lessons From Sudden Coronary Death. Arterioscler Thromb Vasc Biol. 2000;20:1262–75.

5.  Tabas I, Lichtman AH. Monocyte-Macrophages and T Cells in Atherosclerosis. Immunity. Elsevier Inc.; 2017;47:621–34.

6.  Bucerius J, Dijkgraaf I, Mottaghy FM, Schurgers LJ. Target identification for the diagnosis and intervention of vulnerable atherosclerotic plaques beyond 18F-fluorodeoxyglucose positron emission tomography imaging: promising tracers on the horizon. Eur J Nucl Med Mol Imaging. 2019;46:251–65.

7.  Meester EJ, Krenning BJ, de Swart J, Segbers M, Barrett HE, Bernsen MR, et al. Perspectives on Small Animal Radionuclide Imaging; Considerations and Advances in Atherosclerosis. Front Med. 2019;6:1–11.

8.  Meester EJ, Krenning BJ, Blois RH De. Imaging of atherosclerosis, targeting LFA-1 on inflammatory cells with 111In-DANBIRT. J Nucl Cardiol. 2018;13:1–8.

9.  Mota R, Campen MJ, Cuellar ME, Garver WS, Hesterman J, Qutaish M, et al. 111InIn-Danbirt in Vivo Molecular Imaging of Inflammatory Cells in Atherosclerosis. Contrast Media Mol Imaging. 2018;2018.

10. Tarkin JM, Joshi FRJ, Evans NR, Chowdhury MM, Figg NL, Shah A V, et al. Detection of Atherosclerotic Inflammation by 68 Ga-DOTATATE PET Compared to [18F]FDG PET Imaging. J Am Coll Cardiol. 2017;69:1774–91.

11. Li X, Samnick S, Lapa C, Israel I, Buck AK, Kreissl MC, et al. Ga-DOTATATE PET/CT for the detection of inflammation of large arteries: correlation with 18F-FDG , calcium burden and risk factors. Eur J Nucl Med Mol Imaging. 2012;2:1–10.

12. Rominger A, Saam T, Vogl E, Ubleis C, Fougere L, Forster S, et al. In Vivo Imaging of Macrophage Activity in the Coronary Arteries Using 68 Ga-DOTATATE PET / CT : Correlation with Coronary Calcium Burden and Risk Factors. J Nucl Med. 2010;51:193–7.

13. Wan SMY, Endozo R, Michopoulou S, Shortman R, Rodriguez-justo M, Menezes L, et al. PET/CT Imaging of Unstable Carotid Plaque with 68 Ga-Labeled Somatostatin Receptor Ligand. J Nucl Med. 2017;58:774–81.

14. Pedersen SF, Vikj B, Keller SH, Hansen AE, Clemmensen AE, Sillesen H, et al. Cu-DOTATATE PET / MRI for Detection of Activated Macrophages in Carotid Atherosclerotic Plaques Studies in Patients Undergoing Endarterectomy. Arter Thromb Vasc Biol. 2015;7:1696–703.

15. Hsieh PC, Lee IH, Yeh TL, Chen KC, Huang HC, Chen PS, et al. Distribution volume ratio of serotonin and dopamine transporters in euthymic patients with a history of major depression – a dual-isotope SPECT study. Psychiatry Res – Neuroimaging. Elsevier Ireland Ltd; 2010;184:157–61.

16. Berman DS, Kang X, Tamarappoo B, Wolak A, Hayes SW, Nakazato R, et al. Stress Thallium-201/Rest Technetium-99m Sequential Dual Isotope High-Speed Myocardial Perfusion Imaging. JACC Cardiovasc Imaging [Internet]. Elsevier Inc.; 2009;2:273–82. Available from: http://dx.doi.org/10.1016/j.jcmg.2008.12.012

17. Heiba SI, Kolker D, Mocherla B, Kapoor K, Jiang M, Son H, et al. The optimized evaluation of diabetic foot infection by dual isotope SPECT/CT imaging protocol. J Foot Ankle Surg. Elsevier Ltd; 2010;49:529–36.

18. Maina T, Nock BA, Cordopatis P, Bernard BF, Breeman WAP, Gameren A Van, et al. Original article [99m Tc] Demotate 2 in the detection of sst2-positive tumours: a preclinical comparison with [111 In] DOTA-tate. Eur J Nucl Med Mol Imaging. 2006;33:831–840.

19. de Blois E, Sze Chan H, A.P. Breeman W. Iodination and Stability of Somatostatin Analogues: Comparison of Iodination Techniques. A Practical Overview. Curr Top Med Chem. 2012;12:2668–76.

20. Walker MD, Goorden MC, Dinelle K, Ramakers RM, Blinder S, Shirmohammad M, et al. Performance Assessment of a Preclinical PET Scanner with Pinhole Collimation by Comparison to a Coincidence-Based Small-Animal PET Scanner. J Nucl Med. 2014;55:1368–74.

21. Goorden MC, van der Have F, Kreuger R, Ramakers RM, Vastenhouw B, Burbach JPH, et al. VECTor: A Preclinical Imaging System for Simultaneous Submillimeter SPECT and PET. J Nucl Med. 2013;54:306–12.

22. Vaissier PEB, Beekman FJ, Goorden MC. Similarity-regulation of OS-EM for accelerated SPECT reconstruction. Phys Med Biol. 2016;61:4300–15.

23. Cervo M, Gerbaudo VH, Park MA, Moore SC. Quantitative simultaneous 111In/99mTc SPECT-CT of osteomyelitis. Med Phys. 2013;40:1–11.

24. Ogawa K, Harata Y, Ichihara T, Kubo A, Hashimoto S. A practical method for position-dependent Compton-scatter correction in single photon emission CT. IEEE Trans Med Imaging. 1991;10:408–12.

25. Visser EP, Harteveld AA, Meeuwis APW, Disselhorst JA, Beekman FJ, Oyen WJG, et al. Image quality phantom and parameters for high spatial resolution small-animal SPECT. Nucl Instruments Methods Phys Res A. Elsevier; 2011;654:539–45.

26. Andersson J, Libby P, Hansson GK. Adaptive immunity and atherosclerosis. Clin Immunol. 2010;134:33–46.

27. Tsouknos A, Nash GB, Rainger GE. Monocytes initiate a cycle of leukocyte recruitment when cocultured with endothelial cells. Atherosclerosis. 2003;170:49–58.

28. Kounis NG, Soufras GD, Tsigkas G, Hahalis G. White blood cell counts, leukocyte ratios, and eosinophils as inflammatory markers in patients with coronary artery disease. Clin Appl Thromb. 2015;21:139–43.

29. Virmani R, Burke AP, Farb A, Kolodgie FD. Pathology of the Vulnerable Plaque. J Am Coll Cardiol. 2006;47:7–12.

30. Narula J, Nakano M, Virmani R, Kolodgie FD, Petersen R, Newcomb R, et al. Histopathologic characteristics of atherosclerotic coronary disease and implications of the findings for the invasive and noninvasive detection of vulnerable plaques. J Am Coll Cardiol. 2013;61:1041–51.

31. Falk E. Why do plaques rupture? Circulation. 1992;86:30–42.

32. Hyafil F, Pelisek J, Laitinen I, Schottelius M, Mohring M, Yvonne D, et al. Imaging the Cytokine Receptor CXCR4 in Atherosclerotic Plaques with the Radiotracer 68 Ga-Pentixafor for PET. J Nucl Med. 2017;58:499–507.

33. Masteling MG, Zeebregts CJ, Tio RA, Breek JC, Tietge UJF, De Boer JF, et al. High-resolution imaging of human atherosclerotic carotid plaques with micro 18F-FDG PET scanning exploring plaque vulnerability. J Nucl Cardiol. 2011;18:1066–75.

34. Watanabe Y, Nagayama M. MR plaque imaging of the carotid artery. Neuroradiology. 2010;52:253–74.

35. Mitsumori LM, Hatsukami TS, Ferguson MS, Kerwin WS, Cai J, Yuan C. In vivo accuracy of multisequence MR imaging for identifying unstable fibrous caps in advanced human carotid plaques. J Magn Reson Imaging. 2003;17:410–20.

36. Singh N, Moody AR, Roifman I, Bluemke DA, Zavodni AEH. Advanced MRI for carotid plaque imaging. Int J Cardiovasc Imaging. 2016;32:83–9.

37. Robson PM, Dweck MR, Trivieri MG, Karakatsanis NA, Contreras J, Gidwani U, et al. Coronary Artery PET/MR Imaging: Feasibility, Limitations, and Solutions. JACC Cardiovasc Imaging. 2018;10:1103–12.

38. Li X, Heber D, Leike T, Beitzke D, Lu X, Zhang X, et al. [68Ga]Pentixafor-PET/MRI for the detection of Chemokine receptor 4 expression in atherosclerotic plaques. Eur J Nucl Med Mol Imaging. 2018;45:558–66.

5

# Chapter 6

# Autoradiographical Assessment of Inflammation-targeting Radioligands for Atherosclerosis Imaging: Potential for Plaque Phenotype Identification

Authors: **E.J. Meester** MSc[1,2]; E. de Blois PhD[2]; B.J. Krenning MD PhD[3]; A.F.W. van der Steen PhD[1]; J.P. Norenberg PhD , PharmD[4]; K. van Gaalen[1]; M.R. Bernsen PhD[2]; M. de Jong PhD[2]; and K. van der Heiden PhD[a]

Author affiliations:

[1] Department of Biomedical Engineering, Thorax Center, Erasmus MC, Rotterdam, The Netherlands

[2] Department of Radiology & Nuclear Medicine, Erasmus MC, Rotterdam, The Netherlands

[3] Department of Cardiology, Thorax Center, Erasmus MC, Rotterdam, The Netherlands

[4] Radiopharmaceutical Sciences, University of New Mexico, Albuquerque, NM, USA

# Abstract

**Purpose** | Many radioligands have been developed for the visualization of atherosclerosis by targeting inflammation. However, interpretation of *in vivo* signals is often limited to plaque identification. We evaluated binding of some promising radioligands in an *in vitro* approach in atherosclerotic plaques with different phenotypes.

**Methods** | Tissue sections of carotid endarterectomy tissue were characterized as early plaque, fibro-calcific plaque, or phenotypically vulnerable plaque. *In vitro* binding assays for the radioligands [111In]In-DOTATATE; [111In]In-DOTA-JR11; [67Ga]Ga-Pentixafor; [111In]In-DANBIRT; and [111In]In-EC0800 were conducted, the expression of the radioligand targets was assessed via immunohistochemistry. Radioligand binding and expression of radioligand targets was investigated and compared.

**Results** | In sections characterized as vulnerable plaque, binding was highest for [111In]In-EC0800; followed by [111In]In-DANBIRT; [67Ga]Ga-Pentixafor; [111In]In-DOTA-JR11; and [111In]In-DOTATATE (0.064 ± 0.036; 0.052 ± 0.029; 0.011 ± 0.003; 0.0066 ± 0.0021; 0.00064 ± 0.00014 %Added activity/mm$^2$, respectively). Binding of [111In]In-DANBIRT and [111In]In-EC0800 was highest across plaque phenotypes, binding of [111In]In-DOTA-JR11 and [67Ga]Ga-Pentixafor differed most between plaque phenotypes. Binding of [111In]In-DOTATATE was lowest across plaque phenotypes. The areas positive for cells expressing the radioligand's target differed between plaque phenotypes for all targets, with lowest percentage area of expression in early plaque sections and highest in phenotypically vulnerable plaque sections.

**Conclusions** | Radioligands targeting inflammatory cell markers showed different levels of binding in atherosclerotic plaques and among plaque phenotypes. Different radioligands might be used for plaque detection and discerning early from vulnerable plaque. [111In]In-EC0800 and [111In]In-DANBIRT appear most suitable for plaque detection, while [67Ga]Ga-Pentixafor and [111In]In-DOTA-JR11 might be best suited for differentiation between plaque phenotypes.

Key words: atherosclerosis, inflammation, molecular imaging, autoradiography

# Introduction

Inflammation plays a crucial role in atherosclerotic plaque formation, progression, and destabilization (1,2). Therefore, inflammation is an attractive imaging target for plaque detection (3). Different plaque compositions present a different likelihood of rupture and subsequent cardiovascular events like myocardial infarction or stroke (4,5). Hence, there is a need for A) plaque detection, and B) a distinction between plaques in risk of rupture and in need of treatment as opposed to plaques which do not require intervention. As inflammation is a major factor in plaque destabilization, the level of inflammation might be used to identify vulnerable, rupture prone plaques.

2-deoxy-2-[$^{18}$F]fluoro-D-glucose ([$^{18}$F]FDG) Positron Emission Tomography/Computed Tomography (PET/CT) is taken up by metabolically active macrophages in plaque, and has been shown to detect plaque inflammation *in vivo* (6). However, [$^{18}$F]FDG lacks specificity for inflammatory cells, and high uptake in the myocardium complicates image interpretation limiting the use of [$^{18}$F]FDG in the coronary arteries (6,7). Therefore, recent research has focussed on the evaluation of other inflammation targeting radioligands.

A number of radioligands have shown good results for plaque detection in recent literature (8-10). Especially imaging of the somatostatin subtype receptor 2 (SST$_2$) and chemokine CXC motif receptor type 4 (CXCR4) seem promising. Coronary plaques were successfully detected by targeting SST$_2$ on activated macrophages with [$^{68}$Ga]Ga-[DOTA, Tyr$^3$]-octreotate ([$^{68}$Ga]Ga-DOTATATE) (11). DOTA-JR11 (DOTA-Cpac[D-Cys-Aph(Hor)-D-Aph(Cbm)-Lys-Thr-Cys]-D- Tyr-NH$_2$) also targets SST$_2$ but has a reported five times higher uptake in tumours than DOTATATE in oncological studies, and a more favourable biodistribution resulting in a higher target to background ratio (TBR) (12-15). Recently, we have reported on the successful use of [$^{111}$In]In-DOTA-JR11 for plaque detection in atherosclerotic mice (16). CXCR4 can be targeted with Pentixafor, which has shown favourable results for plaque visualization in a number of studies (17-21). We found that targeting leukocyte function associated antigen-1 (LFA-1) with radiolabelled DOTA-butylamino-NorBIRT (DANBIRT) was well suited for plaque detection (22,23). Moreover, we recently found higher uptake of radiolabelled DANBIRT than of an SST$_2$-targeting radioligand *ex vivo* in human plaque tissue, as well as different levels of uptake in different plaque phenotypes (24). Another promising radioligand is radiolabelled DOTA-Bz-EDA-folate (EC0800), which binds to the Folate Receptor (FR). We and others showed the feasibility of FR imaging for plaque detection with a number of different radioligands (25-27).

Previous studies mostly focused on plaque detection, and radioligand uptake is usually correlated to plaque presence, symptomatic plaque, or culprit plaque in the event of e.g. myocardial infarction. To our knowledge few studies relate radioligand uptake to plaque phenotype or composition (e.g. (28-30)). Ideally, future nuclear imaging methods relate

6

radioligand uptake to plaque phenotype, ultimately identifying plaques requiring intervention before a major adverse cardiovascular event occurs. Therefore, we investigated radioligand binding in human plaque samples with different phenotypes.

## Methods

### Study material
Human carotid plaques were obtained with informed consent via carotid endarterectomy from eight patients in the Erasmus MC. Sample acquisition was approved by the medical ethics committee of the Erasmus MC (MEC 2008-147). The samples were snap frozen in liquid nitrogen and stored in -80° C until the experiment started. The samples were embedded in Tissue-Tek O.C.T. compound (Sakura Finetek Europe B.V, Alpen aan den Rijn, The Netherlands) and stored in -80° C, after which tissue sections for *in vitro* binding assays and immunohistochemistry were sectioned at 4 mm intervals (n=37).

### Tissue sectioning
Tissue was sectioned at 5 μm for immunohistochemical (IHC) analysis and at 10 μm for *in vitro* binding assays (autoradiography (ARG)). *In vitro* binding assays were performed on adjacent sections for optimal comparison. Similarly, IHC was performed on sections adjacent to the sections used for *in vitro* binding assays.

### Radiolabelling
DOTATATE, DOTA-JR11 (provided by Helmut Maecke), DANBIRT, and EC0800 (provided by Auspep, Tullamarine, Australia) were labelled with $[^{111}In]InCl_3$ (Covidien, Petten, The Netherlands) with a molar activity of 200 MBq/nmol as described previously (31). Pentixafor (provided by Hans-Jürgen Wester) was labelled with Gallium-67 (Curium, Petten, The Netherlands), as Indium-111 labelling results in reduced binding affinity (32,33). Although Pentixafor is regularly labelled with Ga-68, we used Ga-67 due to its preferable characteristics for autoradiography in terms of half-life and resolution. Labelling with Gallium-67 was performed with a molar activity of 100 MBq/nmol as described (34). Radiochemical purity (>95%) and incorporation yield (>99%) were evaluated with high-pressure liquid chromatography and instant thin-layer chromatography on silica gel. Quenchers were added to prevent radiolysis as described previously (35,36).

### *In vitro* binding assays and competition binding assays
Sections were incubated for 1 hour with $10^{-9}$ M radiolabelled ligand. Specificity of the radioligands was demonstrated previously (11,16,17,37-41). Additionally, we confirmed specific binding in our tissue via competition binding experiments by blocking with $10^{-6}$ M unlabelled

compound. Slides were exposed to phosphor screens overnight and read with a phosphor imager (Cyclone, Perkin Elmer).

## Immunohistochemistry

Sections were immunohistochemically stained for $SST_2$ (ab134152, Abcam), CXCR4 (ab124824, Abcam), LFA-1 (MCA1848, AbD SeroTec), or FR (AP5032a, Abgent). In short, sections were fixed in cold acetone for 5 minutes ($SST_2$, CXCR4, LFA-1) or 10% formalin for 10 min (FR), endogenous peroxidase was blocked with 0.3% $H_2O_2$ for 30 minutes ($SST_2$, LFA-1, FR) or 0.15% $H_2O_2$ for 20 min (CXCR4), and non-specific binding was blocked with 1% BSA for 20 minutes (CXCR4) or 2% normal goat serum for 20 minutes ($SST_2$, LFA-1, FR). The primary antibody was omitted from the protocol in negative controls.

Haematoxylin-eosin staining according to standard protocol was performed on the sections used for *in vitro* binding assays after radioactivity had sufficiently decayed. These sections were later used for plaque classification.

## Plaque classification

Haematoxylin-eosin stained plaque sections where classified by two independent observers according to the criteria used in the adapted American Heart Association (AHA) classification (4,5,42). Plaque phenotypes were categorized into three groups: early plaque; fibro-calcific (FCALC) as stable plaque; and phenotypically vulnerable plaque.

## Quantification and statistical analysis

Radioactive signal in plaque sections was quantified with Optiquant (Perkin Elmer) and expressed in digital light units per $mm^2$ ($DLU/mm^2$). Signal was corrected for radionuclide half-life, and exposure time of the phosphor screen to the tissue sections. $DLU/mm^2$ was converted to percentage added activity per $mm^2$ ($\%AA/mm^2$) by normalizing data to standards included in the binding assays.

6

For immunohistochemically-stained sections, Biopix software (Biopix AB, Gothenburg, Sweden) was used to calculate the percentage DAB (3,3'-diminobenzidine) positive area per tissue section.

The data were analysed with SPSS 21.0 (SPSS Inc, Chicago, IL). The data was tested for normality using the Shapiro-Wilk test. Differences between groups were analysed with the Kruskal-Wallis test, with Dunn's post hoc test to account for multiple comparisons. P values below 0.05 were considered significant. Data are presented as mean ± standard deviation.

# Results

## Plaque classification

Plaque sections were classified as early plaque (12 samples), stable plaque (10 samples), or phenotypically vulnerable plaque (15 samples) with an interobserver agreement of 97%.

## Area of DAB positive staining & radioligand binding

*Area of cells expressing radioligand targets*

Figure 1A shows the average DAB-positive area for each studied radioligand target and plaque category. All radioligand targets were expressed in larger areas in more advanced plaques than in early plaques (Figure 1A). No significant differences in areas were observed in early plaque sections. In FCALC plaque sections, the areas containing LFA-1 expressing cells were significantly higher than the areas of FR expressing cells (p<0.05). In vulnerable plaque sections, FR was expressed in significantly less area than LFA-1 (p<0.001) and CXCR4 (p<0.001).

*Binding of [$^{111}$In]In-DANBIRT and [$^{111}$In]In-EC0800 was highest across plaque phenotypes*

Figure 1B shows radioligand binding of the different radioligands across plaque categories. Binding of [$^{111}$In]In-DANBIRT and [$^{111}$In]In-EC0800 was highest, followed by [$^{67}$Ga]Ga-Pentixafor, [$^{111}$In]In-DOTA-JR11, and [$^{111}$In]In-DOTATATE. In sections of early plaque lesions, [$^{111}$In]In-DOTATATE signal (0.00047 ± 0.00017 %AA/mm$^2$) was significantly lower than [$^{67}$Ga]Ga-Pentixafor (0.0053 ± 0.0012 %AA/mm$^2$ p<0.01), [$^{111}$In]In-DANBIRT (0.026 ± 0.013 %AA/mm$^2$) and [$^{111}$In]In-EC0800 (0.027 ± 0.018 %AA/mm$^2$) signal (p<0.001). [$^{111}$In]In-DOTA-JR11 signal (0.0027 ± 0.00085 %AA/mm$^2$) was also significantly lower than [$^{111}$In]In-DANBIRT and [$^{111}$In]In-EC0800 signals (p<0.001).

In FCALC sections, [$^{111}$In]In-DOTATATE signal (0.00053 ± 0.000076 %AA/mm$^2$) was also significantly lower compared to [$^{67}$Ga]Ga-Pentixafor (0.0066 ± 0.0014 %AA/mm$^2$ p<0.05), [$^{111}$In]In-DANBIRT (0.032 ± 0.015 %AA/mm$^2$) and [$^{111}$In]In-EC0800 (0.068 ± 0.050 %AA/mm$^2$) (p<0.001). [$^{111}$In]In-DOTA-JR11 signal (0.0033 ± 0.0015 %AA/mm$^2$) was also significantly lower than [$^{111}$In]In-DANBIRT (p<0.01) and [$^{111}$In]In-EC0800 (p<0.001).

In vulnerable plaque sections, [$^{111}$In]In-DOTATATE signal (0.00064 ± 0.00014 %AA/mm$^2$) was again lower than that of [$^{67}$Ga]Ga-Pentixafor (0.011 ± 0.003 %AA/mm$^2$ p<0.05), [$^{111}$In]In-DANBIRT (0.052 ± 0.029 %AA/mm$^2$) and [$^{111}$In]In-EC0800 (0.064 ± 0.036 %AA/mm$^2$ p<0.001). [$^{111}$In]In-DOTA-JR11 signal (0.0066 ± 0.0021 %AA/mm$^2$) was significantly lower than those of [$^{111}$In]In-DANBIRT (p<0.01) and [$^{111}$In]In-EC0800 (p<0.001), whereas [$^{111}$In]In-EC0800 signal was significantly higher than [$^{67}$Ga]Ga-Pentixafor signal (p<0.05).
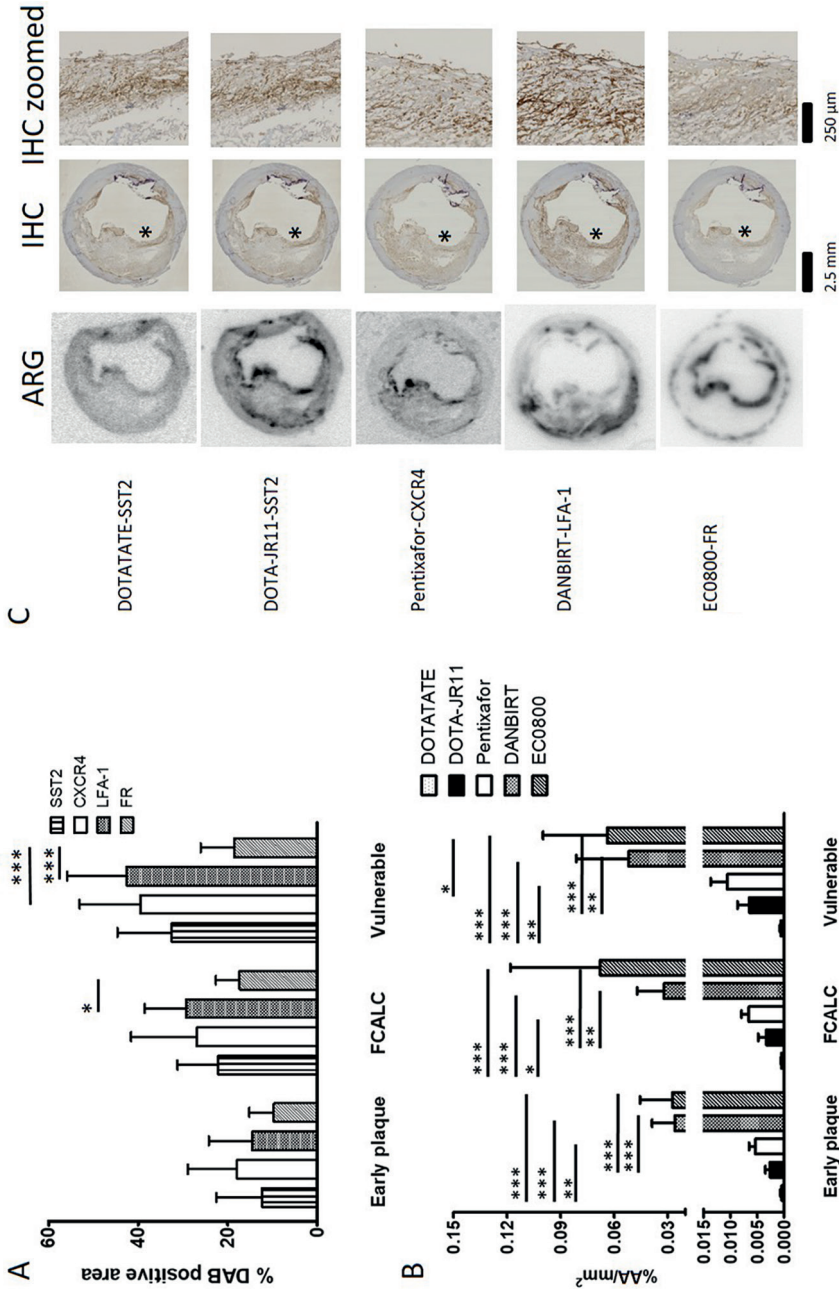
**Figure 1 | A)** % DAB positive area in sections categorised as early plaque, stable plaque, and vulnerable plaque. **B)** % Added activity/mm² (%AA/mm²) per radioligand in different plaque categories. Note that the y-axis consists of two segments. **C)** Representative examples of autoradiograms of the different radioligands and immunohistochemistry of adjacent sections stained for the radioligand target. The autoradiograms are not uniformly scaled, but scaled for visibility per image. DOTATATE, DOTA-JR11, DANBIRT, and EC0800 were labelled with Indium-111, Pentixafor was labelled with Gallium-67. ARG, autoradiography; IHC, immunohistochemistry; $SST_2$, somatostatin subtype receptor 2; CXCR4, chemokine CXC motif receptor type 4; LFA-1, leukocyte associated antigen 1; FR, folate receptor; FCALC, fibro-calcific; DAB, 3,3'-Diaminobenzidine. * indicates $p < 0.05$, ** indicates $p < 0.01$, *** indicates $p = < 0.001$.

6

*Radioligand binding was higher in advanced plaque phenotypes than in early plaque*

Figure 2 shows radioligand binding per radioligand across plaque phenotypes. All radioligands showed more signal in advanced than in early plaque sections. [$^{111}$In]In-DOTATATE signal was significantly higher in vulnerable sections than in sections classified as early plaque (0.00064 ± 0.00014 and 0.00047 ± 0.00017 %AA/mm$^2$ p<0.01). [$^{111}$In]In-DANBIRT and [$^{111}$In]In-EC0800 also had significantly higher signal in vulnerable sections compared to early plaque (0.052 ± 0.029 vs 0.026 ± 0.013 and 0.064 ± 0.036 vs 0.027 ± 0.018 %AA/mm$^2$, respectively. p<0.05). [$^{111}$In]In-DOTA-JR11 bound significantly more to vulnerable sections compared to early (0.0066 ± 0.0021 vs 0.0027 ± 0.00085 %AA/mm$^2$ p<0.001) and FCALC sections (0.0033 ± 0.0015 %AA/mm$^2$ p<0.01). [$^{67}$Ga]Ga-Pentixafor showed a similar binding pattern as [$^{111}$In]In-DOTA-JR11, with binding in vulnerable sections being higher (0.011 ± 0.003 %AA/mm$^2$) than binding in early plaque sections (0.0053 ± 0.0012 %AA/mm$^2$ p<0.001) and FCALC sections (0.0066 ± 0.0014 %AA/mm$^2$ p<0.05).

*[$^{111}$In]In-DOTA-JR11 binding is higher than [$^{111}$In]In-DOTATATE*

There was a clear difference in binding amongst the SST$_2$ targeting radioligands, but the differences were not statistically significant. [$^{111}$In]In-DOTA-JR11 showed a 5.6 fold higher signal than [$^{111}$In]In-DOTATATE in early plaque sections, a 6.3 fold higher signal in stable plaques, and a 10.2 fold higher signal in vulnerable plaque sections (Figure 1B).

*Location of binding differs between radioligands*

Figure 1C illustrates the differences in radioligand signal and target receptor distribution in vulnerable plaque sections. Figure 2 displays representative examples of radioligand binding and target receptor distribution. Expression of SST$_2$ and signal of [$^{111}$In]In-DOTATATE and [$^{111}$In]In-DOTA-JR11 was mostly located in cap areas of plaque. [$^{67}$Ga]Ga-Pentixafor signal and CXCR4 expression was located in cap areas as well as around calcified nodes. [$^{111}$In]In-DANBIRT signal and LFA-1 expression was visible on the medial side of the necrotic core, in cap areas, and around calcium deposits. Signal of [$^{111}$In]In-EC0800 and expression of FR was mostly located at areas close to the artery lumen, and in areas at the edge of the tunica media. Signal of [$^{67}$Ga]Ga-Pentixafor and [$^{111}$In]In-DOTA-JR11 differed most between vulnerable plaque sections and early or stable plaque sections.

**Figure 2** | % added activity/mm$^2$ (%AA/mm$^2$) in plaque sections for each radioligand across plaque categories. Representative examples of IHC and ARG are shown below each radioligand graph. Note that the graphs and autoradiograms are not uniformly scaled, but scaled for visibility per image. DOTATATE, DOT-JR11, DANBIRT, and EC0800 were labelled with Indium-111, Pentixafor was labelled with Gallium-67. ARG,autoradiography, IHC,immunohistochemistry, SST$_2$,somatostatin subtype receptor 2, CXCR4, chemokine CXC motif receptor type 4; LFA-1, leukocyte associated antigen 1; FR, folate receptor; * indicates p<0.05, ** indicates p<0.01, *** indicates p=<0.001.
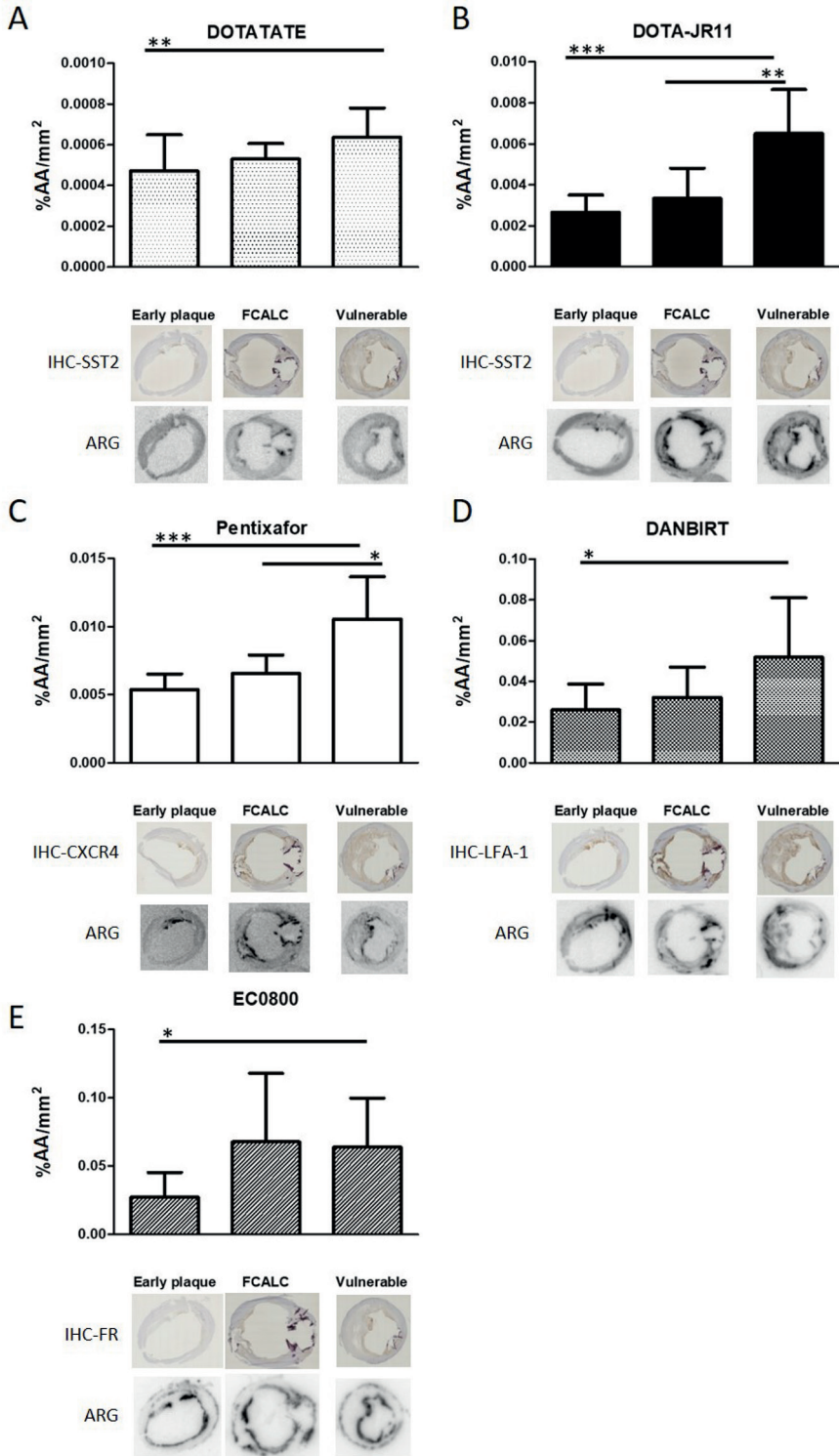
# Discussion

A large number of inflammation targeted radioligands has been studied for atherosclerotic plaque detection (8-10). We examined the binding of several promising inflammation targeted radioligands and the distribution of cells expressing the radioligand targets in sections of different plaque phenotypes. For all radioligands, we found higher levels of binding in advanced, vulnerable plaque sections than in early plaque sections. The same pattern was visible for the portion of plaque area expressing the radioligand targets. Moreover, we found significantly higher binding of [111In]In-DANBIRT and [111In]In-EC0800 across plaque phenotypes compared to the other radioligands. Binding of [111In]In-DOTA-JR11 and [67Ga]Ga-Pentixafor differed most between vulnerable plaque sections and sections of the other plaque phenotypes.

We studied *in vitro* binding of radioligands in tissue sections of atherosclerotic plaque. Binding differs strongly between *in vitro* assays and *in vivo*. The mechanisms of uptake could differ, expression of receptors might be influenced differently *in vivo*, and radioligands *in vivo* often only get a limited number of passes along tissues to reach their target receptor before being cleared from the blood. Moreover, background signal from other tissues might be high *in vivo*. Also, the effects of freezing or tissue degradation can play a role in *in vitro* binding. Despite these important differences between *in vitro* and *in vivo*, our approach provides valuable information. The targets are optimally reachable in 10 μm sections, the radioligands get sufficient time to bind to available receptors, and there are no imaging artefacts related to resolution, spill over, or attenuation. Therefore, our approach mimics the potential binding of the radioligands in the examined tissues and might give an indication of an idealized uptake that might be achieved *in vivo*.

Recent studies suggest that $SST_2$ targeting with DOTATATE is a viable strategy for plaque detection (37,43-47). Tarkin and colleagues showed that [68Ga]Ga-DOTATATE could better discriminate between high-risk and low-risk plaques compared to [18F]FDG (11). However, another study found that imaging with [68Ga]Ga-DOTATATE could not differentiate between symptomatic plaque and the contralateral artery, and in line with these results found no $SST_2$ expressing cells in plaque (48). Furthermore, the aorta to blood ratio of [68Ga]Ga-DOTATATE found by Rinne et al. (44) was lower than one, which further indicates that *in vivo* imaging with this radioligand requires optimization. Our *in vitro* results could in part explain these discrepancies. We clearly demonstrated the presence of $SST_2$ expressing cells in human carotid tissues and found localized binding of [111In]In-DOTATATE. However, [111In]In-DOTATATE signal was much lower than signal of the other studied radioligands. Moreover, binding of [111In]In-DOTATATE between sections of different plaque phenotypes showed the least difference of all investigated radioligands. Although imaging of atherosclerosis with DOTATATE is valid for plaque detection, these results confirm the need for further optimization.

DOTA-JR11 could provide a significant improvement in $SST_2$ imaging. Oncological studies reported a much higher uptake and TBR of DOTA-JR11 than DOTATATE, ranging from 2–20 fold more (12–15). The mechanism for this difference in uptake between the $SST_2$ targeting radioligands remains to be elucidated, it is hypothesized that antagonistic ligands such as DOTA-JR11 bind more binding sites than agonistic ligands such as DOTATATE (49). We recently found that [$^{111}$In]In-DOTA-JR11 could be used to detect atherosclerotic plaques *in vivo* in an animal model of atherosclerosis with high specificity (16). Our current results showed a 10.2 fold higher signal of [$^{111}$In]In-DOTA-JR11 over [$^{111}$In]In-DOTATATE in vulnerable plaque sections. Moreover, binding of [$^{111}$In]In-DOTA-JR11 differed significantly between plaque phenotypes, which indicates that DOTA-JR11 could be useful to discriminate between different plaque phenotypes. These results strongly suggest that imaging $SST_2$ with DOTA-JR11 is a relevant strategy for plaque detection and characterization.

Similarly to DOTA-JR11, we found high binding of [$Ga^{67}$]Ga-Pentixafor, and significantly different binding between plaque phenotypes. In line with our findings, Derlin et al. (18) found more CXCR4 expressing cells in symptomatic plaques than in asymptomatic plaque tissue. Similar findings were reported via mRNA and IHC assays, with more CXCR4 expression in late stage plaque (21,50,51). Combined with our data these and other studies mark Pentixafor as an important radioligand for atherosclerosis detection and characterization (17,19,20,52-54).

[$^{111}$In]In-DANBIRT binding differed strongly from binding of [$^{111}$In]In-DOTATATE, [$^{111}$In]In-DOTA-JR11, and [$Ga^{67}$]Ga-Pentixafor. Binding of [$^{111}$In]In-DANBIRT was located at the same locations, but was in addition high at the medial side of the necrotic core. The high signal and binding in more areas compared to the other radioligands was in line with the target findings. Whereas $SST_2$ and CXCR4 are expressed on a subset of inflammatory cells, LFA-1 can be considered a leukocyte marker and is therefore present on various types of inflammatory cells. Earlier studies showed high specificity of DANBIRT, and *in vivo* experiments in animal models of atherosclerosis show promising results (23,40,55). Moreover, our group also found different levels of [$^{111}$In]In-DANBIRT uptake in phenotypically different plaque tissues *ex vivo* (24). Combined with the high binding of [$^{111}$In]In-DANBIRT in our tissue sections this suggests that this radioligand is relevant for plaque detection and characterization.

[$^{111}$In]In-EC0800 binding was highest across plaque phenotypes in the examined panel of radioligands, and its signal was significantly higher in sections classified as vulnerable plaque than in early plaque sections. Imaging of FR is extensively studied in atherosclerosis with different imaging probes *in vivo* in animal models of atherosclerosis (26,27,56,57) and *in vitro* in human tissue (27,58-60). Müller et al. found higher FR expression and higher signal of a FR targeting radioligand in sections of plaque compared to normal arterial wall, but no significant differences between sections of plaque classified as stable or vulnerable (60). In contrast, our group showed *in vivo* uptake of [$^{111}$In]In-EC0800 in a mouse model of atherosclerosis, and found

6

higher [$^{111}$In]In-EC0800 uptake in stable plaque compared to vulnerable plaque (26). Jager *et al.* linked FR expression to presence of M1-like macrophages (58). None of the studies examining *in vitro* expression or imaging of FR reported uptake or binding in the edges of tissue sections, like we observed in our study. FR staining confirmed FR expression in these locations, therefore binding of EC0800 in these locations is not an artefact. However, additional staining for CD68 (data not shown) shows no presence of macrophages in these areas. FR expression is not limited to macrophages, further studies into the binding or uptake of FR targeting radioligands are therefore recommended.

Few imaging studies make head-to-head comparisons between radioligands or relate radioligand uptake to plaque composition beyond identification of clinically identified culprit plaque. Our and various other studies can aid the development of new imaging strategies (29,44), and are useful to translate *in vivo* signal to characterization of plaque status. For example, Rinne *et al.* examined multipe radioligands in an *in vivo* model of atherosclerosis, and Borchert et al. investigated uptake of multiple radioligands *in vitro* in different leukocyte subtypes (29,44). Such studies can be used to identify which radioligands are most suited for plaque detection and for identification of vulnerable plaques in need of intervention. Our results warrant further clinical translation studies of plaque imaging using these new radioligands.

# Conclusion

This *in vitro* study indicates that DANBIRT and EC0800 are most suited for plaque detection given the high levels of binding. DOTA-JR11 and Pentixafor are best suited to differentiate between stable and vulnerable plaque based on the high differences in binding of these radioligands in phenotypically stable and vulnerable plaques. As *in vivo* studies with these radioligands show promising results for plaque detection, our findings indicate that further clinical evaluation for plaque characterization are warranted.

## Declarations, Disclosure
This work was supported by a grant from the University Medical Center Erasmus MC.

## Conflict of interest
J.P. Norenberg holds patents on DANBIRT (US patent nos. 8,097,237; 8,435,489; 8,623,322; 8,834,838; 9,352,059; 9,546,186).

## *Ethical approval*
All procedures performed in studies involving human participants were in accordance with the ethical standards of the Erasmus Medical Centre's research committee (MEC 2008-147) and with the 1964 Helsinki declaration and its later amendments or comparable ethical standards.

# References

1.   Moore KJ, Sheedy FJ, Fisher EA. Macrophages in atherosclerosis: a dynamic balance. Nat Rev Immunol. 2013;13:709–21.

2.   Hansson GK. Inflammation, Atherosclerosis, and Coronary Artery Disease. N Engl J Med. 2005;352:1685–95.

3.   Libby P, DiCarli M, Weissleder R. The vascular biology of atherosclerosis and imaging targets. J Nucl Med. 2010;51 Suppl 1:33S-37S.

4.   Virmani R, Kolodgie FD, Burke AP, Farb A, Schwartz SM. Lessons From Sudden Coronary Death A Comprehensive Morphological Classification Scheme for Atherosclerotic Lesions. Arter Thromb Biol. 2000;20:1262–75.

5.   Schaar JA, Muller JE, Falk E, Virmani R, Fuster V, Serruys PW, et al. Terminology for high-risk and vulnerable coronary artery plaques. Eur Heart J. 2004;25:1077–82.

6.   Tarkin JM, Joshi FR, Rudd JHF. PET imaging of inflammation in atherosclerosis. Nat Rev Cardiol. 2014;11:443–57.

7.   Buettner C, Rudd JHF, Fayad ZA. Determinants of FDG Uptake in Atherosclerosis. JACC Cardiovasc Imaging. 2011;4:1302–4.

8.   Meester EJ, Krenning BJ, Swart J De, Segbers M, Barrett HE. Perspectives on Small Animal Radionuclide Imaging; Considerations and Advances in Atherosclerosis Animal Models of Atherosclerosis. Front. Med. 2019;6:1–11.

9.   Leccisotti L, Nicoletti P, Cappiello C, Indovina L, Giordano A. PET imaging of vulnerable coronary artery plaques. Clin Transl Imaging. 2019;7:267–84.

10.  MacAskill MG, Newby DE, Tavares AAS. Frontiers in positron emission tomography imaging of the vulnerable atherosclerotic plaque. Cardiovasc Res. 2019;115:1952–62.

11.  Tarkin JM, Joshi FR, Evans NR, Chowdhury MM, Figg NL, Shah AV, et al. Detection of Atherosclerotic Inflammation by 68Ga-DOTATATE PET Compared to [18F]FDG PET Imaging. J Am Coll Cardiol. 2017;69:1774–91.

12.  Fani M, Nicolas GP, Wild D. Somatostatin Receptor Antagonists for Imaging and Therapy. J Nucl Med. 2017;58:61S-66S.

13.  Wild D, Fani M, Fischer R, Pozzo L Del, Kaul F, Krebs S, et al. Comparison of Somatostatin Receptor Agonist and Antagonist for Peptide Receptor Radionuclide Therapy: A Pilot Study. J Nucl Med. 2014;55:1248–53.

14.  Dalm SU, Nonnekens J, Doeswijk GN, Blois E De, Gent DC Van, Konijnenberg MW, et al. Comparison of the Therapeutic Response to Treatment with a 177Lu-Labeled Somatostatin Receptor Agonist and Antagonist in Preclinical Models. J Nucl Med. 2016;57:260–6.

15.  Krebs S, Pandit-Taskar N, Reidy D, Beattie BJ, Lyashchenko SK, Lewis JS, et al. Biodistribution and radiation dose estimates for 68 Ga-DOTA-JR11 in patients with metastatic neuroendocrine tumors. Eur J Nucl Med Mol Imaging. 2019;46:677–85.

16.  Meester EJ, Krenning BJ, Blois E De, Jong M De, Bernsen MR, Heiden K Van Der. Imaging inflammation in atherosclerotic plaques, targeting SST2 with [111In]In-DOTA-JR11. J Nucl Cardiol.; 2020;https://doi.org/10.1007/s12350-020-02046-y.

17.  Hyafil F, Pelisek J, Laitinen I, Schottelius M, Mohring M, Yvonne D, et al. Imaging the Cytokine Receptor CXCR4 in Atherosclerotic Plaques with the Radiotracer 68 Ga-Pentixafor for PET. J Nucl Med. 2017;58:499–506.

18.  Derlin T, Sedding DG, Dutzmann J, Haghikia A, König T, Napp LC, et al. Imaging of chemokine receptor CXCR4 expression in culprit and nonculprit coronary atherosclerotic plaque using motion-corrected [68Ga]pentixafor PET/CT. Eur J Nucl Med Mol Imaging.2018;45:1934–44.

19.  Weiberg D, Thackeray JT, Daum G, Sohns JM, Kropf S, Wester H-J, et al. Clinical Molecular Imaging of Chemokine Receptor CXCR4 Expression in Atherosclerotic Plaque using 68 Ga-Pentixafor PET: Correlation with Cardiovascular Risk Factors and Calcified Plaque Burden. J Nucl Med. 2018;59:266–72.

20.  Li X, Heber D, Leike T, Beitzke D, Lu X, Zhang X, et al. [68Ga]Pentixafor-PET/MRI for the detection of Chemokine receptor 4 expression in atherosclerotic plaques. Eur J Nucl Med Mol Imaging. 2018;45:558–66.

21.  Li X, Yu W, Wollenweber T, Lu X, Wei Y, Beitzke D, et al. [68Ga]Pentixafor PET/MR imaging of chemokine receptor 4 expression in the human carotid artery. Eur J Nucl Med Mol Imaging. 2019;46:1616–25.

22.  Meester EJ, Krenning BJ, de Blois RH, Norenberg JP, de Jong M, Bernsen MR, et al. Imaging of atherosclerosis, targeting LFA-1 on inflammatory cells with 111In-DANBIRT. J Nucl Cardiol. 2019;26:1697–704.

6

23. Mota R, Campen MJ, Cuellar ME, Garver WS, Hesterman J, Qutaish M, et al. In-DANBIRT In Vivo Molecular Imaging of Inflammatory Cells in Atherosclerosis. Contrast Media Mol Imaging. 2018. doi:10.1155/2018/6508724

24. Barrett HE, Meester EJ, van Gaalen K, van der Heiden K, Krenning BJ, Beekman FJ, et al. Imaging of inflammatory cellular protagonists in human atherosclerosis: a dual-isotope SPECT approach. Eur J Nucl Med Mol Imaging. 2020

25. Ayala-lopez W, Xia W, Varghese B, Low PS. Imaging of Atherosclerosis in Apoliprotein E Knockout Mice : Targeting of a Folate-Conjugated Radiopharmaceutical to Activated Macrophages. J Nucl Med. 2010;51:768–74.

26. Winkel LCJ, Groen HC, van Thiel BS, Müller C, van der Steen AFW, Wentzel JJ, et al. Folate receptor–targeted single-photon emission computed tomography/computed tomography to detect activated macrophages in atherosclerosis: can it distinguish vulnerable from stable atherosclerotic plaques? Mol Imaging. 2013;13:1–5.

27. Silvola JMU, Li X-G, Virta J, Marjamäki P, Liljenbäck H, Hytönen JP, et al. Aluminum fluoride-18 labeled folate enables in vivo detection of atherosclerotic plaque inflammation by positron emission tomography. Sci Rep. 2018;8:9720.

28. Wenning C, Kloth C, Kuhlmann MT, Jacobs AH, Schober O, Hermann S, et al. Serial F-18-FDG PET / CT distinguishes in fl amed from stable plaque phenotypes in shear-stress induced murine atherosclerosis. Atherosclerosis. 2014;234:276–82.

29. Borchert T, Beitar L, Langer LBN, Polyak A, Wester HJ, Ross TL, et al. Dissecting the target leukocyte subpopulations of clinically relevant inflammation radiopharmaceuticals. J Nucl Cardiol. 2019;

30. Youn T, Al'Aref SJ, Narula N, Salvatore S, Pisapia D, Dweck MR, et al. 18F-Sodium Fluoride Positron Emission Tomography/Computed Tomography in Ex Vivo Human Coronary Arteries With Histological Correlation. Arterioscler Thromb Vasc Biol. 2020;40:404–11.

31. Blois E De, Schroeder RJ., de Ridder CMA, van Weerden W., Breeman WAP, de Jong M. Improving radiopeptide pharmacokinetics by adjusting experimental conditions for bombesin receptor-mediated imaging of prostate cancer. Q J Nucl Med Mol Imaging. 2012;57:1–9.

32. Dalm SU, Sieuwerts AM, Look MP, Melis M, Deurzen CHM Van, Foekens JA, et al. Clinical Relevance of Targeting the Gastrin-Releasing Peptide Receptor, Somatostatin Receptor 2, or Chemokine C-X-C Motif Receptor 4 in Breast Cancer for Imaging and Therapy. J Nucl Med. 2015;1487–94.

33. Poschenrieder A, Schottelius M, Schwaiger M, Kessler H, Wester HJ. The influence of different metal-chelate conjugates of pentixafor on the CXCR4 affinity. EJNMMI Res. 2016;6:4–11.

34. de Blois E, Blaauw E, Koyuncu C, Boedhram S, Seimbille Y. P108: Purification of Gallium-67 for (pre)clinical application as surrogate for Gallium-68. 23rd Int Symp Radiopharm Sci (ISRS 2019) Beijing, China, 26–31 May 2019. 2019. p. S262–3.

35. de Blois E, Chan HS, de Zanger R, Konijnenberg M, Breeman WAP. Application of single-vial ready-for-use formulation of 111In- or 177Lu-labelled somatostatin analogs. Appl Radiat Isot. 2014;85:28–33.

36. de Blois E, Chan HS, Konijnenberg M, de Zanger R, Breeman WAP. Effectiveness of Quenchers to Reduce Radiolysis of 111In or 177Lu Labelled Methionin-Containing Regulatory Peptides. Maintaining Radiochemical Purity as Measured by HPLC. Curr Top Med Chem. 2012;12(23):2677-2685.

37. Li X, Bauer W, Kreissl MC, Weirather J, Bauer E, Israel I, et al. Specific somatostatin receptor II expression in arterial plaque: 68Ga-DOTATATE autoradiographic, immunohistochemical and flow cytometric studies in apoE-deficient mice. Atherosclerosis. 2013;230:33–9.

38. Fani M, Braun F, Waser B, Beetschen K, Cescato R, Erchegyi J, et al. Unexpected Sensitivity of sst 2 Antagonists to N-Terminal Radiometal Modifications. 2012;1481–90.

39. Poria RB, Norenberg JP, Anderson TL, Erion J, Wagner CR, Arterburn JB, et al. Characterization of a radiolabeled small molecule targeting leukocyte function-associated antigen-1 expression in lymphoma and leukemia. Cancer Biother Radiopharm. 2006;21:418–26.

40. Meester EJ, Krenning BJ, de Blois RH, Norenberg JP, de Jong M, Bernsen MR, et al. Imaging of atherosclerosis, targeting LFA-1 on inflammatory cells with111In-DANBIRT. J Nucl Cardiol. 2018;1–8.

41. de Visser HM, Korthagen NM, Müller C, Ramakers RM, Krijger GC, Lafeber FPJG, et al. Imaging of Folate Receptor Expressing Macrophages in the Rat Groove Model of Osteoarthritis: Using a New DOTA-Folate Conjugate. Cartilage. 2018;9:183–91.

42. Redgrave JN, Gallagher P, Lovett JK, Rothwell PM. Critical cap thickness and rupture in symptomatic carotid plaques: The oxford plaque study. Stroke. 2008;39:1722–9.

43. Rominger A, Saam T, Vogl E, Ubleis C, la Fougère C, Förster S, et al. In vivo imaging of macrophage activity in the coronary arteries using 68Ga-DOTATATE PET/CT: correlation with coronary calcium burden and risk factors. J Nucl Med. 2010;51:193–7.

44. Rinne P, Hellberg S, Kiugel M, Virta J, Li X, Käkelä M, et al. Comparison of Somatostatin Receptor 2-Targeting PET Tracers in the Detection of Mouse Atherosclerotic Plaques. Mol Imaging Biol. 2015;18:99–108.

45. Mojtahedi A, Alavi A, Thamake S, Amerinia R, Ranganathan D, Tworowska I, et al. Assessment of vulnerable atherosclerotic and fibrotic plaques in coronary arteries using 68 Ga-DOTATATE PET/CT. Am J Nucl Med Mol Imaging. 2015;5:65–71.

46. Malmberg C, Ripa RS, Johnbeck CB, Knigge U, Langer SW, Mortensen J, et al. 64Cu-DOTATATE for non-invasive assessment of atherosclerosis in large arteries and its correlation with risk factors: head-to-head comparison with 68Ga-DOTATOC in 60 patients. J Nucl Med. 2015;1895–901.

47. Pedersen SF, Sandholt BV, Keller SH, Hansen AE, Clemmensen AE, Sillesen H, et al. 64Cu-DOTATATE PET/MRI for Detection of Activated Macrophages in Carotid Atherosclerotic PlaquesSignificance. Arterioscler Thromb Vasc Biol. 2015;35:1696–703.

48. Wan MYS, Endozo R, Michopoulou S, Shortman R, Rodriguez-Justo M, Menezes L, et al. PET/CT Imaging of Unstable Carotid Plaque with 68Ga-Labeled Somatostatin Receptor Ligand. J Nucl Med. 2017;58:774–80.

49. Ginj M, Zhang H, Waser B, Cescato R, Wild D, Wang X, et al. Radiolabeled somatostatin receptor antagonists are preferable to agonists for in vivo peptide receptor targeting of tumors. Proc Natl Acad Sci. 2006;103:16436–41.

50. Bot I, Daissormont ITMN, Zernecke A, van Puijvelde GHM, Kramp B, de Jager SCA, et al. CXCR4 blockade induces atherosclerosis by affecting neutrophil function. J Mol Cell Cardiol. 2014;74:44–52.

51. Merckelbach S, Van Der Vorst EPC, Kallmayer M, Rischpler C, Burgkart R, Döring Y, et al. Expression and Cellular Localization of CXCR4 and CXCL12 in Human Carotid Atherosclerotic Plaques. Thromb Haemost. 2018;118:195–206.

52. Thackeray JT, Derlin T, Haghikia A, Napp LC, Wang Y, Ross TL, et al. Molecular Imaging of the Chemokine Receptor CXCR4 after Acute Myocardial Infarction. JACC Cardiovasc Imaging. 2015;8:1417–26.

53. Reiter T, Kircher M, Schirbel A, Werner RA, Kropf S, Ertl G, et al. Imaging of C-X-C Motif Chemokine Receptor CXCR4 Expression After Myocardial Infarction With [68Ga]Pentixafor-PET/CT in Correlation With Cardiac MRI. JACC Cardiovasc Imaging. 2018;11(10)1541–1543.

54. Döring Y, Pawig L, Weber C, Noels H. The CXCL12/CXCR4 chemokine ligand/receptor axis in cardiovascular disease. Front Physiol. 2014;5:1–23.

55. Poria RB, Norenberg JP, Anderson TL, Erion J, Wagner CR, Arterburn JB, et al. Characterization of a radiolabeled small molecule targeting leukocyte function-associated antigen-1 expression in lymphoma and leukemia. Cancer Biother Radiopharm. 2006;21:418–26.

56. Ayala-López W, Xia W, Varghese B, Low PS. Imaging of atherosclerosis in apoliprotein e knockout mice: targeting of a folate-conjugated radiopharmaceutical to activated macrophages. J Nucl Med. 2010;51:768–74.

57. Poh S, Chelvam V, Ayala-López W, Putt KS, Low PS. Selective liposome targeting of folate receptor positive immune cells in inflammatory diseases. Nanomedicine Nanotechnology, Biol Med. 2018;14:1033–43.

58. Jager N a., Westra J, Golestani R, van Dam GM, Low PS, Tio R a., et al. Folate Receptor- Imaging Using 99mTc-Folate to Explore Distribution of Polarized Macrophage Populations in Human Atherosclerotic Plaque. J Nucl Med. 2014;55:1945–51.

59. Jager N a., Westra J, van Dam GM, Teteloshvili N, Tio R a., Breek J-CJ-C, et al. Targeted Folate Receptor Fluorescence Imaging as a Measure of Inflammation to Estimate Vulnerability Within Human Atherosclerotic Carotid Plaque. J Nucl Med. 2012;53:1222–9.

60. Müller A, Mu L, Meletta R, Beck K, Rancic Z, Drandarov K, et al. Towards non-invasive imaging of vulnerable atherosclerotic plaques by targeting co-stimulatory molecules. Int J Cardiol. 2014;174:503–15.

6

# Chapter 7

**Summary, Discussion, and Future Outlook**

# Summary

Cardiovascular disease remains the leading cause of death worldwide (1,17), the incidence of cardiovascular disease is expected to further increase due to the rise in longevity and increase in western type life style in Asian and South American countries (18). As atherosclerosis is the main contributor to ischemic cardiovascular events like myocardial infarction and stroke (6), diagnosis and treatment of atherosclerotic plaques remains of paramount importance. Innovative detection methods such as those discussed in this thesis (see Figure 1 for a visual overview) may guide treatment to prevent major adverse cardiovascular events. Further research, as discussed in the final chapters of this thesis, may be used to identify the most promising imaging methods to be evaluated in clinical studies.
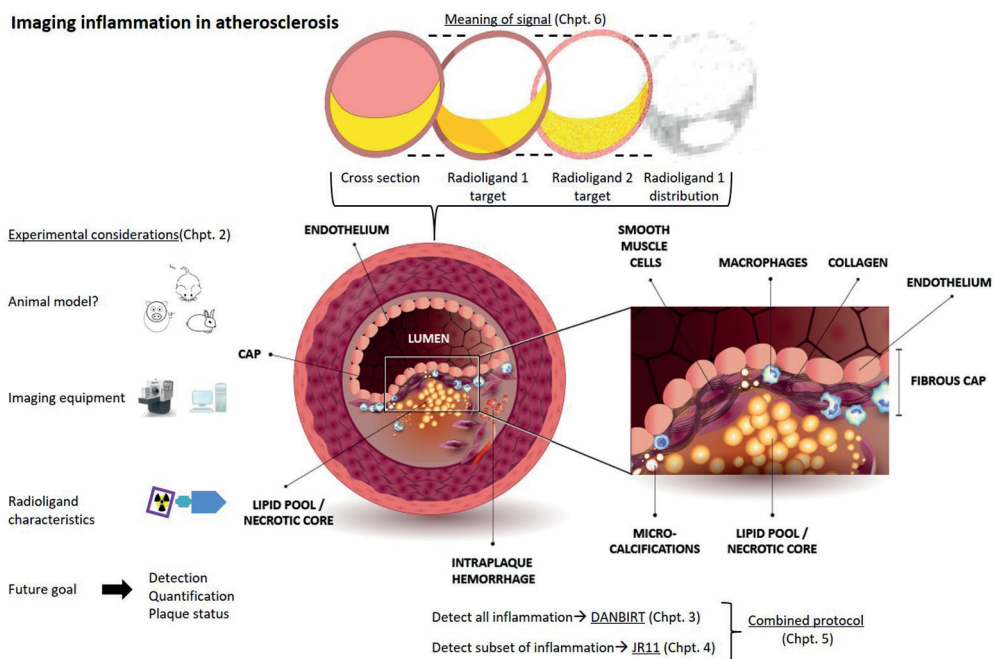
**Figure 1** | A schematic overview of the work discussed in this thesis. Chapter 2 discusses relevant considerations in preclinical radionuclide evaluation. The studies presented in Chapters 3 and 4 focussed on detection of inflammatory cells in atherosclerotic plaque. Chapter 5 shows a novel protocol, which combines the approaches discussed in Chapters 3 and 4. The work presented in Chapter 6 assessed the prevalence and distribution of the targets of a selection of promising radioligands, and how the respective radioligand binding localizes in these tissues.

Nuclear medicine has improved patient care in many ways in the past decades. The use of nuclear imaging procedures still increases because of rising incidence of cancer but also increasing prevalence of cardiovascular disease. Application of imaging procedures has become fairly standardized, and widespread expertise for existing imaging platforms and radioligand applications is present. However, testing of novel methods as discussed in this thesis requires new perspectives, new approaches, and often new expertise. In **Chapter 2** we reviewed a number of the important considerations regarding the use of small animal models for studying novel imaging techniques for atherosclerosis. When performing new imaging procedures on the edge of what is possible regarding e.g. spatial resolution and sensitivity, optimizing every aspect of imaging is necessary to reach the highest standard. We firstly discussed the need and potential for novel imaging methods in atherosclerosis imaging. Secondly, we described animal models of atherosclerosis, and discussed differences between human and murine atherosclerosis regarding aspects of plaque composition and location, as well as differences between immune cell subsets. We also covered different technical considerations like quantification and image reconstruction and discussed opportunities in hybrid imaging and differences between clinical and preclinical PET and SPECT. Finally, we argued which traits are relevant when developing novel radiolabelled tracers and provided a future outlook on preclinical imaging.

In the following two chapters we covered two novel imaging approaches for plaque evaluation. In **Chapter 3** we evaluated the novel radioligand [111In]In-DANBIRT, a radioligand targeting Leukocyte Function-associated Antigen-1 (LFA-1). This is a highly attractive imaging target because it is present on all leukocytes. Whereas many studies investigate radioligands targeted at macrophage subsets, this target can give a complete overview of the inflammatory status of a plaque. This is relevant as many leukocytes, such as neutrophils, dendritic cells, and monocytes play a role in plaque formation and destabilization besides macrophages (19-22). In this study we found that [111In]In-DANBIRT successfully visualized plaque *in vivo* in mice with a high target to background ratio (TBR) and high specificity. Moreover, we confirmed that the uptake of the radioligand, and expression of LFA-1, co-localizes with regions of inflammation as evidenced by staining for macrophages with immunohistochemistry (CD68). As we showed this co-localization and specificity in both human and mouse tissue, we concluded that this radioligand has high potential for plaque imaging in a clinical study.

In **Chapter 4** we report our findings on [111In]In-DOTA-JR11, a radioligand which targets soma-tostatin receptor subtype 2 ($SST_2$). $SST_2$ is highly expressed on activated macrophages and therefore it is an attractive imaging target to detect inflammation in plaques. As discussed in the previous paragraph, many studies focus on macrophages for atherosclerotic plaque detection as macrophages are the most prevalent inflammatory cell type in plaques. Moreover, radioligands targeted at more ubiquitously expressed inflammatory markers, like [18F]FDG,

often lack target specificity. Earlier $SST_2$ imaging studies with [$^{68}$Ga]Ga-[DOTA,Tyr3]-octreotate (DOTATATE) in patients have successfully visualized plaques *in vivo* in the coronary (23) and carotid (24) arteries. DOTA-JR11 is a somatostatin receptor antagonist however, as opposed to most radioligands like [DOTA,Tyr3]-octreotate (DOTATATE), which are receptor agonists. Recent studies (reviewed in (25)) have reported that DOTA-JR11 has a five to ten times higher uptake than DOTATATE in tumour tissue. We therefore considered DOTA-JR11 a valuable candidate to improve plaque imaging, as higher radioligand uptake would lower the detection threshold. We examined the feasibility of plaque imaging with [$^{111}$In]In-DOTA-JR11 *in vivo* in a mouse model of atherosclerosis and *ex vivo* in human and mouse plaque tissue. We found high levels of specific uptake *in vivo*, which was confirmed by *ex vivo* and *in vitro* experiments. Given the earlier results on imaging $SST_2$ in atherosclerosis, we believe that clinical studies with DOTA-JR11 and head to head comparisons between DOTATATE and DOTA-JR11 are justified.

Current nuclear imaging most often applies a single radioligand for an imaging procedure. We hypothesize that using multiple radioligands in one scan procedure could be an effective way to more thoroughly assess disease characteristics in clinical practice and help to identify which plaques may require intervention before an acute event occurs. In **Chapter 5** we described our first step in this direction. In this study, we use an imaging protocol which visualizes both targets described in **Chapters 3** and **4** by combined SPECT/CT. Both LFA-1 and $SST_2$ show high potential as targets for clinical plaque identification. Therefore, an imaging protocol which ascertains the degree of inflammation by imaging LFA-1 and provides information on macrophages by imaging $SST_2$ could be of value to differentiate between less-inflamed or calcified plaque via CT, inflamed plaque via LFA-1 imaging, and plaque vulnerability by adding $SST_2$ imaging. Our results firstly showed that such a combined imaging protocol is feasible in human plaque tissue. Secondly, we observed that [$^{111}$In]In-DANBIRT is taken up in all plaque types, with a higher uptake in phenotypically vulnerable plaques. Thirdly, we found that although imaging $SST_2$ with [$^{99m}$Tc]Tc-[$N_4$,Asp$^0$,Tyr$^3$]-octreotate ([$^{99m}$Tc]Tc-Demotate 2) was feasible, there were no significant differences between different plaque phenotypes. Finally, we confirmed that radioligand uptake co-localized with immunohistochemistry for the radioligand targets. These results indicate that dual isotope imaging is feasible in atherosclerosis, that [$^{111}$In]In-DANBIRT has discriminatory power for different plaque phenotypes, whereas the $SST_2$ targeting moiety does not discriminate between plaque phenotypes in this research setting.

Assessment of plaque characteristics is an important research aim besides plaque detection. In **Chapter 6** we present results for the most promising radioligands in our field. We examined [$^{111}$In]In-DOTATATE and [$^{111}$In]In-DOTA-JR11 for $SST_2$, [$^{111}$In]In-DANBIRT for LFA-1, [$^{67}$Ga]Ga-Pentixafor for chemokine CXC motif receptor type 4 (CXCR4), and [$^{111}$In]In-EC0800 for the Folate Receptor (FR). We used *in vitro* autoradiography and immunohistochemistry to examine the presence of radioligand targets in different phenotypes of human plaque as well as binding of radioligands to these targets. Our results indicated that the radioligands targeting FR and

LFA-1 had the highest radioligand binding across all plaque phenotypes and may therefore be most useful for plaque detection in clinical practice. We also found that these two radioligands bound most in phenotypically vulnerable plaque phenotypes, although [$^{111}$In]In-EC0800 also has high levels of binding in phenotypically stable plaques. We found similar patterns of uptake across plaque phenotypes for the radioligands targeting SST$_2$ and CXCR4, although uptake was several factors lower than with [$^{111}$In]In-DANBIRT and [$^{111}$In]In-EC0800. However, binding of [$^{111}$In]In-DOTA-JR11 and [$^{67}$Ga]Ga-Pentixafor differed also between stable and vulnerable plaque, potentially allowing better discrimination between these plaque phenotypes. To complement the research questions raised in **Chapters 4** and **5**, we used both the SST$_2$ agonist and antagonist. Here we found that the receptor agonist [$^{111}$In]In-DOTATATE underperformed compared to [$^{111}$In]In-DOTA-JR11. Although *in vitro* uptake cannot directly be related to *in vivo* radioligand behaviour and uptake, we recommend that the radioligands directed towards the FR and LFA-1 are most beneficial to be pursued for plaque detection.

# Discussion and future outlook

## Discussion

### Imaging of inflammation to detect atherosclerosis.

Imaging of inflammation has large potential for atherosclerotic plaque detection; the plethora of reviews written on this subject confirm the interest in this imaging strategy (16,26,35-37,27-34). Inflammatory cells play a key role in the initiation, progression, and destabilization of atherosclerotic plaque (5,38) and therefore present relevant imaging targets. Imaging of inflammation has already proven its value in studies with [$^{18}$F]FDG (12,13,39-44), as this tracer was able to detect inflamed plaque despite the limitations of this tracer. Given the advantages of more specific radioligands, the clinical value can be considered even higher with currently researched radioligands.

Although different radioligands have different strengths for atherosclerosis imaging, the best radioligand is the radioligand which is readily available for patients. In this respect especially Pentixafor (targeting CXCR4) and DOTATATE (targeting SST$_2$) are relevant to highlight (see references (23,45-47)). DOTATATE is approved for clinical use in oncology by regulatory bodies (like FDA and EMA), making it more readily available for evaluation in patients suffering from other diseases. Pentixafor is currently under investigation, and has already shown promising results in patients with atherosclerosis (45,47-49).

Despite the great potential, it is important to acknowledge that atherosclerosis is a complex disease process. Other factors like neo-angiogenesis, calcification, and hypoxia also play a major role (5) and could therefore be considered as imaging targets. It is unlikely that the inflammatory status of a plaque gives a complete view of plaque vulnerability, and some plaques will have inflammatory levels below the detection threshold. It is therefore important to combine inflammatory imaging with other factors of plaque vulnerability. A number of studies review other aspects of plaque formation and composition (30,31,50-52). A number of these imaging targets are reviewed in **Chapter 2**.

### Imaging LFA-1 and SST$_2$

SST$_2$ and LFA-1 are the main targets for which preclinical *in vivo* results are documented in this thesis (**Chapters 3 & 4**). The results of [$^{111}$In]In-DOTA-JR11 and [$^{111}$In]In-DANBIRT both show highly focal radioligand uptake at plaque locations, and display specificity for plaque in competition binding assays. Imaging of SST$_2$ with DOTATATE shows major promise in a number

7

of studies (23,24,53-58). Because JR11 has a 5–10 times higher tumour uptake in oncological studies (reviewed in (25)), it has high potential to also improve SST$_2$ imaging in atherosclerosis. Despite the high promise of SST$_2$ imaging, a few uncertainties remain. *Wan et al.* showed that symptomatic carotid plaque could not be distinguished from the non-symptomatic contralateral plaque with [$^{68}$Ga]Ga-DOTATATE (24), hinting that [$^{68}$Ga]Ga-DOTATATE might be poorly suited for characterization of symptomatic carotid plaques. Moreover, in a mouse model of myocardial infarction *Thackeray et al.* showed a rapid wash-out of [$^{68}$Ga]Ga-DOTATATE from inflamed myocardium resulting in a low TBR of 0.10 ± 0.03 (59), which suggests that [$^{68}$Ga]Ga-DOTATATE is not well suited to image inflammation in the myocardium. This could indicate that [$^{68}$Ga]Ga-DOTATATE binds only shortly to SST$_2$ on macrophages. Although the results found in these studies are not in conflict with the notion that DOTATATE and SST$_2$ imaging can be used to detect plaques, they do indicate that further studies into the binding of DOTATATE in atherosclerotic tissue are required. This is in accordance with the *in vitro* study described in **Chapter 6** of this thesis, where $^{111}$In-labelled DOTATATE had the lowest uptake in any plaque type compared to $^{111}$In-labelled DOTA-JR11, DANBIRT, EC0800, or $^{67}$Ga-pentixafor. Moreover, DOTATATE showed little difference in uptake between different plaque phenotypes. How our results and those of Wan et al. and Thackeray et al. (24,59) relate to the more promising studies performed with DOTATATE (23,57,60) remains to be investigated.

A limited number of studies is available on nuclear imaging of LFA-1. Poria et al. reported high specificity of DANBIRT for murine and human LFA-1, and showed favourable kinetics of DANBIRT (61). Mota and colleagues showed increased binding of [$^{68}$Ga]Ga-DANBIRT to neutrophils following an inflammatory stimulus, and reported increased binding in aorta, mouse serum, and leukocytes in biodistribution studies in a mouse model of atherosclerosis on high fat diet (62). Moreover, they also reported on increased aortic DANBIRT uptake over time during high fat diet in ApoE$^{-/-}$ mice. Mumaw et al. used [$^{111}$In]In-DANBIRT to visualize an increase of inflammation in ferret lungs after exposure to polluted air, and found that this was in accordance with the number of neutrophils present in bronchio-alveolar lavage fluid (63). These and our own studies show the potential of DANBIRT for imaging LFA-1, and how DANBIRT might be used in other patho-physiologies as well, as LFA-1 becomes more attractive as an imaging target given the large interest in LFA-1 as a therapeutic target in a range of diseases (64-70). The affinity state of LFA-1 is strongly influenced by chemokines (as discussed in (71)), triggering a more receptive affinity state of LFA-1 around sites of inflammation. This might result in larger abundance of high affinity LFA-1 on leukocytes in inflamed areas, which is reflected by the high TBR found in **Chapter 3**.

## Comparing radioligands and relating uptake to plaque phenotypes

Most studies evaluate single radioligands, and imaging procedures in clinical practice also mostly use a single radioligand only. The differences in radioligand uptake shown in **Chapters 5 & 6** show that inflammation imaging to detect plaque can be used as an imaging method

which visualizes different aspects of plaque inflammation, thus vulnerability. While plaque detection remains an important goal, investigating how radioligand uptake is related to plaque phenotypes is important also. Table 2 shows, based on the research documented in this thesis, which of the investigated radioligands are more suited for plaque detection or plaque characterization. Moreover, comparing different radioligands in the same study is important to reliably compare how radioligands perform in terms of e.g. TBR or retention in plaque. Only a few studies compare radioligands or investigate radioligand binding more deeply (e.g. 55,73).

**Table 1** | Suitability of the radioligands discussed in this thesis in regards to plaque detection or plaque characterization.

| Radioligand | Target | Plaque detection | Plaque characterization |
|---|---|---|---|
| [$^{111}$In]In-DOTATATE | SST$_2$ | + | + |
| [$^{111}$In]In-DOTA-JR11 | SST$_2$ | ++ | ++++ |
| [$^{67}$Ga]Ga-Pentixafor | CXCR4 | ++ | ++++ |
| [$^{111}$In]In-DANBIRT | LFA-1 | ++++ | +++ |
| [$^{111}$In]In-EC0800 | FR | ++++ | +++ |

SST$_2$, somatostatin receptor subtype 2; LFA-1, leukocyte function-associated antigen-1; CXCR4, chemokine CXC motif receptor type 4; FR, folate receptor.

# Future outlook

## The search continues

A large array of radioligands targeting inflammation is assessed. Despite these efforts, the holy grail in atherosclerosis imaging, differentiation between stable and vulnerable plaque, has not been found yet. Designing and evaluating novel radioligands remains a relevant approach in this quest. However, a shift in focus away from the study of individual radioligands might be beneficial. Three avenues of research are relevant in this respect:

1. **More clinical studies.** Reviews on radioligands show that many different radioligands are evaluated in preclinical settings (30,31,50,51). Despite promising preclinical results, a limited number of studies is available of radioligands studied in patients. This is largely due to the costly and time intensive nature of patient studies, including requirements from Ethical Committees and regulatory authorities (FDA/EMA) to guarantee safety and efficacy. New approaches used by the FDA, such as requirements for exploratory investigational new drugs (eINDs), may facilitate initial stages of translational research (73). Furthermore, costs

7

and time investments may be reduced by streamlined facilities related to GMP production of the compound, toxicology studies and conducting clinical studies (74).

A better understanding how radioligands compare to each other could also facilitate earlier testing in patients as this could allow research efforts to concentrate on the most promising radioligand. Head-to head comparison of radioligands are rarely performed however, whereas a large number of inflammation targeted radioligands are explored preclinically. More direct preclinical comparison will better identify the most promising radioligands for further clinical translation. The study described in **Chapter 6** and by Rinne et al. and Borchert et al. (55,72) are good examples of studies in which radioligands are compared.

2. **Mechanistic insight into radioligand behaviour.** It is currently not known how radioligands are taken up in plaque. Plaque tissue is highly heterogenic, generally rich in lipids, and located in high blood flow environments. Many radioligands *in vivo* often only get a few passes along the plaque, in which the radioligand has to be able to penetrate the tissue. Also, they should not stick to non-target molecules and remain attached to the receptor long enough to enable visualization.

Basic knowledge on how the radioligands behave is often based on biodistribution studies. Although these avenues of research are needed to understand radioligand behaviour, new options in research are worthwhile to pursue. More fundamental research into the behaviour of radioligands can be facilitated by new *in vitro* models. For example, organ on a chip models mimic aspects of organ physiology in an *in vitro* setting. Adapting such systems to plaque biology could provide a controlled environment in which radioligand behaviour could be examined.

Combining nuclear imaging methods with other imaging modalities may further facilitate fundamental research. For example, optical imaging works by imaging bioluminescence or visualizing a fluorescently-labelled compound. Although dual labelling a ligand with a radionuclide and a fluorescent label can severely affect binding affinity, in the case of conserved binding affinity this could allow careful and real-time monitoring of how the ligands interact with plaque tissue, similar to cell tracking studies. Currently unanswered questions on how ligands enter plaque by visualizing a fluorescent label, which portion of applied ligand passes plaque tissue by counting a radionuclide attached to the ligand, or how ligands bind to cells in plaque could be answered with such methods. This could complement *in vivo* models and existing *in vitro* models.

3. **Multimodality imaging.** Early recognition of plaques (before rupture) is the ultimate goal of this research. This would significantly improve 'personalised medicine' or 'precision medicine', individually tailoring a timely start of pharmacological intervention and to stratify the risk of developing symptomatic disease. Also, assessment of coronary plaque

inflammation can aid the development and validation of new anti-atherosclerotic or anti-inflammatory therapies. Based on our research, it is most likely that nuclear imaging of (focal) inflammation in patients with atherosclerosis will consist of a hybrid scan, which combines multiple radioligands in SPECT or PET with CT or possibly MRI (current imaging approaches are discussed by Adamson et al. (4)). From this single combined scan, a clinician may be able to identify the location of the plaque, degree of calcification and deduce the plaque morphology including degree of specific inflammatory activity. Dual isotope imaging with multiple radioligand imaging with SPECT (**Chapter 5**), or PET (as discussed by Walrand et al. (75)), could facilitate this process. The individual and societal consequences of such a tool could be substantial.

7

# References

1.  GBD 2015 Mortality and Causes of Death Collaborators I. Global, regional, and national life expectancy, all-cause mortality, and cause-specific mortality for 249 causes of death , 1980–2015: a systematic analysis for the Global Burden of Disease Study 2015. Lancet. 2016;380(9859):1459–544.

2.  Finn A V, Nakano M, Narula J, Kolodgie FD, Virmani R. Concept of vulnerable/unstable plaque. Arterioscler Thromb Vasc Biol [Internet]. 2010 Jul [cited 2014 Oct 31];30(7):1282–92. Available from: http://www.ncbi.nlm.nih.gov/pubmed/20554950

3.  Carità P, Guaricci AI, Muscogiuri G, Carrabba N, Pontone G. Prognostic value and therapeutic perspectives of coronary CT angiography: A literature review. Biomed Res Int. 2018;2018.

4.  Adamson PD, Newby DE. Noninvasive imaging of the coronary arteries. Eur Heart J. 2019;40:2444–54.

5.  Libby P, Buring JE, Badimon L, Hansson GK, Deanfield J, Bittencourt MS, et al. Atherosclerosis. Nat Rev. 2019;5(56):1–18.

6.  Newby DE. Acute coronary syndromes – Triggering of acute myocardial infarction: Beyond the vulnerable plaque. Heart. 2010;96(15):1247–51.

7.  Rudd JHF, Hyafil F, Fayad ZA. Inflammation imaging in atherosclerosis. Arterioscler Thromb Vasc Biol. 2009;29(7):1009–16.

8.  Moore KJ, Tabas I. Macrophages in the Pathogenesis of Atherosclerosis. Cell [Internet]. 2011;145(3):341–55. Available from: http://dx.doi.org/10.1016/j.cell.2011.04.005

9.  Hansson GK. Inflammation, Atherosclerosis, and Coronary Artery Disease. N Engl J Med [Internet]. 2005;352(16):1685–95. Available from: http://www.ncbi.nlm.nih.gov/pubmed/15843671%0Ahttp://www.nejm.org/doi/abs/10.1056/NEJMra043430

10. Ridker PM. Clinical Application of C-Reactive Protein for Cardiovascular Disease Detection and Prevention. Circulation. 2003;107:363–9.

11. Quillard T, Libby P. Molecular imaging of atherosclerosis for improving diagnostic and therapeutic development. Circ Res [Internet]. 2012 Jul 6 [cited 2015 Jun 26];111(2):231–44. Available from: http://circres.ahajournals.org/content/111/2/231.full

12. Rudd JHF, Warburton EA, Fryer TD, Jones HA, Clark JC, Antoun N, et al. Imaging atherosclerotic plaque inflammation with [18F]-fluorodeoxyglucose positron emission tomography. Circulation. 2002;105(23):2708–11.

13. Tawakol A, Fayad Z a, Mogg R, Alon A, Klimas MT, Dansky H, et al. Intensification of statin therapy results in a rapid reduction in atherosclerotic inflammation: results of a multicenter fluorodeoxyglucose-positron emission tomography/computed tomography feasibility study. J Am Coll Cardiol [Internet]. 2013 Sep 3 [cited 2015 Jun 12];62(10):909–17. Available from: http://www.ncbi.nlm.nih.gov/pubmed/23727083

14. Figueroa AL, Subramanian SS, Cury RC, Truong QA, Gardecki JA, Tearney GJ, et al. Distribution of Inflammation Within Carotid Atherosclerotic Plaques With High-Risk Morphological Features A Comparison Between Positron Emission Tomography Activity , Plaque Morphology , and Histopathology. Circ Cardiovasc Imaging. 2012;5:69–77.

15. Buettner C, Rudd JHF, Fayad ZA. Determinants of FDG Uptake in Atherosclerosis. JACC Cardiovasc Imaging [Internet]. 2011;4(12):1302–4. Available from: http://linkinghub.elsevier.com/retrieve/pii/S1936878X11006954

16. Tarkin JM, Joshi FR, Rudd JHF. PET imaging of inflammation in atherosclerosis. Nat Rev Cardiol [Internet]. 2014;11(8):443–57. Available from: http://www.ncbi.nlm.nih.gov/pubmed/24913061

17. Benjamin EJ, Virani SS, Callaway CW, Chamberlain AM, Chang AR, Cheng S, et al. Heart disease and stroke statistics – 2018 update: A report from the American Heart Association. Vol. 137, Circulation. 2018. 67–492 p.

18. Wong MCS, Zhang DX, Wang HHX. Rapid emergence of atherosclerosis in Asia: A systematic review of coronary atherosclerotic heart disease epidemiology and implications for prevention and control strategies. Curr Opin Lipidol. 2015;26(4):257–69.

19. Libby P. Inflammation in atherosclerosis. 2002;420(December).

20. Libby P, Ridker PM, Maseri A. Clinical Cardiology : New Frontiers Inflammation and Atherosclerosis The Scientific Basis of Inflammation. 2002;

21. Ilhan F. Atherosclerosis and the role of immune cells. World J Clin Cases. 2015;3(4):345.

22. Galkina E, Ley K. Immune and inflammatory mechanisms of atherosclerosis (*). Annu Rev Immunol. 2009;27:165–97.

23. Tarkin JM, Joshi FR, Evans NR, Chowdhury MM, Figg NL, Shah AV, et al. Detection of Atherosclerotic Inflammation by 68Ga-DOTATATE PET Compared to [18F]FDG PET Imaging. J Am Coll Cardiol. 2017;69(14):1774–91.

24. Wan MYS, Endozo R, Michopoulou S, Shortman R, Rodriguez-Justo M, Menezes L, et al. PET/CT Imaging of Unstable Carotid Plaque with 68Ga-Labeled Somatostatin Receptor Ligand. J Nucl Med [Internet]. 2017;58(5):774–80. Available from: http://jnm.snmjournals.org/lookup/doi/10.2967/jnumed.116.181438

25. Fani M, Nicolas GP, Wild D. Somatostatin Receptor Antagonists for Imaging and Therapy. J Nucl Med [Internet]. 2017;58(Supplement 2):61S-66S. Available from: http://jnm.snmjournals.org/lookup/doi/10.2967/jnumed.116.186783

26. Davies JR, Rudd JHF, Weissberg PL, Narula J. Radionuclide imaging for the detection of inflammation in vulnerable plaques. J Am Coll Cardiol [Internet]. 2006 Apr 18 [cited 2015 Jun 12];47(8 Suppl):C57-68. Available from: http://www.ncbi.nlm.nih.gov/pubmed/16631511

27. Alie N, Eldib M, Fayad ZA, Mani V. Inflammation, Atherosclerosis, and Coronary Artery Disease: PET/CT for the Evaluation of Atherosclerosis and Inflammation. Clin Med Insights Cardiol [Internet]. 2014 Jan [cited 2015 May 12];8(Suppl 3):13–21. Available from: http://www.pubmedcentral.nih.gov/articlerender.fcgi?artid=4294600&tool=pmcentrez&rendertype=abstract

28. Sadeghi MM. (18)F-FDG PET and vascular inflammation: time to refine the paradigm? J Nucl Cardiol [Internet]. 2015 Apr [cited 2015 Jun 12];22(2):319–24. Available from: http://www.ncbi.nlm.nih.gov/pubmed/24925623

29. Hiari N, Rudd JHF. FDG PET imaging and cardiovascular inflammation. Curr Cardiol Rep. 2011;13(1):43–8.

30. Tavakoli S, Vashist A, Sadeghi MM. Molecular imaging of plaque vulnerability. J Nucl Cardiol. 2014;21:1112–28.

31. Langer HF, Haubner R, Pichler BJ, Gawaz M. Radionuclide imaging: a molecular key to the atherosclerotic plaque. J Am Coll Cardiol [Internet]. 2008 Jul 1 [cited 2015 Jun 18];52(1):1–12. Available from: http://www.pubmedcentral.nih.gov/articlerender.fcgi?artid=2683742&tool=pmcentrez&rendertype=abstract

32. Magnoni M, Ammirati E, Camici PG. Non-invasive molecular imaging of vulnerable atherosclerotic plaques. J Cardiol [Internet]. 2015 Apr [cited 2015 Jun 12];65:261–9. Available from: http://www.ncbi.nlm.nih.gov/pubmed/25702846

33. Joshi F, Rosenbaum D, Bordes S, Rudd JHF. Vascular imaging with positron emission tomography. J Intern Med [Internet]. 2011 Aug [cited 2015 Jun 12];270(2):99–109. Available from: http://www.ncbi.nlm.nih.gov/pubmed/21518037

34. Weber C, Noels H. Atherosclerosis: current pathogenesis and therapeutic options. Nat Med [Internet]. 2011;17(11):1410–22. Available from: http://dx.doi.org/10.1038/nm.2538

35. Sollini M, Berchiolli R, Kirienko M, Rossi A, Glaudemans AWJM, Slart R, et al. PET/MRI in Infection and Inflammation. Semin Nucl Med [Internet]. 2018;48(3):225–41. Available from: https://doi.org/10.1053/j.semnuclmed.2018.02.003

36. Krishnan S, Otaki Y, Doris M, Slipczuk L, Arnson Y, Rubeaux M, et al. Molecular Imaging of Vulnerable Coronary Plaque : A Pathophysiologic Perspective. 2019;359–65.

37. Quillard T, Libby P. Molecular imaging of atherosclerosis for improving diagnostic and therapeutic development. Circ Res [Internet]. 2012 Jul 6 [cited 2015 Jun 26];111(2):231–44. Available from: http://circres.ahajournals.org/content/111/2/231.full

38. Libby P. History of Discovery : Inflammation in Atherosclerosis. Arterioscler Thromb Vasc Biol. 2012;32(9):2045–51.

39. Mckenney-drake ML, Moghbel MC, Paydary K, Alloosh M, Houshmand S, Høilund-carlsen PF, et al. 18 F-NaF and 18 F-FDG as molecular probes in the evaluation of atherosclerosis. Eur J Nucl Med Mol Imaging [Internet]. 2018;2190–200. Available from: http://link.springer.com/10.1007/s00259-018-4078-0

40. Marnane M, Merwick A, Sheehan OC, Hannon N, Foran P, Grant T, et al. Carotid plaque inflammation on 18F-fluorodeoxyglucose positron emission tomography predicts early stroke recurrence. Ann Neurol. 2012;71(5):709–18.

7

41.  Kelly PJ, Camps-Renom P, Giannotti N, Martí-Fàbregas J, Murphy S, McNulty J, et al. Carotid Plaque Inflammation Imaged by 18 F-Fluorodeoxyglucose Positron Emission Tomography and Risk of Early Recurrent Stroke. Stroke. 2019;50(7):1766–73.

42.  Figueroa AL, Abdelbaky A, Truong QA, Corsini E, MacNabb MH, Lavender ZR, et al. Measurement of arterial activity on routine FDG PET/CT images improves prediction of risk of future CV events. JACC Cardiovasc Imaging [Internet]. 2013;6(12):1250–9. Available from: http://dx.doi.org/10.1016/j.jcmg.2013.08.006

43.  Moon SH, Cho YS, Noh TS, Choi JY, Kim BT, Lee KH. Carotid FDG uptake improves prediction of future cardiovascular events in asymptomatic individuals. JACC Cardiovasc Imaging. 2015;8(8):949–56.

44.  Wenning C, Kloth C, Kuhlmann MT, Jacobs AH, Schober O, Hermann S, et al. Serial F-18-FDG PET / CT distinguishes in fl amed from stable plaque phenotypes in shear-stress induced murine atherosclerosis. Atherosclerosis [Internet]. 2014;234(2):276–82. Available from: http://dx.doi.org/10.1016/j.atherosclerosis.2014.03.008

45.  Weiberg D, Thackeray JT, Daum G, Sohns JM, Kropf S, Wester H-J, et al. Clinical Molecular Imaging of Chemokine Receptor CXCR4 Expression in Atherosclerotic Plaque using 68 Ga-Pentixafor PET: Correlation with Cardiovascular Risk Factors and Calcified Plaque Burden. J Nucl Med [Internet]. 2018;59:266–72. Available from: http://jnm.snmjournals.org/lookup/doi/10.2967/jnumed.117.196485

46.  Derlin T, Sedding DG, Dutzmann J, Haghikia A, König T, Napp LC, et al. Imaging of chemokine receptor CXCR4 expression in culprit and nonculprit coronary atherosclerotic plaque using motion-corrected [68Ga] pentixafor PET/CT. Eur J Nucl Med Mol Imaging. 2018;45(11):1934–44.

47.  Li X, Yu W, Wollenweber T, Lu X, Wei Y, Beitzke D, et al. [68Ga]Pentixafor PET/MR imaging of chemokine receptor 4 expression in the human carotid artery. Eur J Nucl Med Mol Imaging. 2019;46:1616–25.

48.  Reiter T, Kircher M, Schirbel A, Werner RA, Kropf S, Ertl G, et al. Imaging of C-X-C Motif Chemokine Receptor CXCR4 Expression After Myocardial Infarction With [68Ga]Pentixafor-PET/CT in Correlation With Cardiac MRI. JACC Cardiovasc Imaging [Internet]. 2018; Available from: https://doi.org/10.1016/j.jcmg.2018.01.001

49.  Li X, Heber D, Leike T, Beitzke D, Lu X, Zhang X, et al. [68Ga]Pentixafor-PET/MRI for the detection of Chemokine receptor 4 expression in atherosclerotic plaques. Eur J Nucl Med Mol Imaging. 2018;45(4):558–66.

50.  Magnoni M, Ammirati E, Camici PG. Non-invasive molecular imaging of vulnerable atherosclerotic plaques. J Cardiol [Internet]. 2015;1–9. Available from: http://linkinghub.elsevier.com/retrieve/pii/S0914508715000155

51.  Meester EJ, Krenning BJ, Swart J De, Segbers M, Barrett HE. Perspectives on Small Animal Radionuclide Imaging ; Considerations and Advances in Atherosclerosis Animal Models of Atherosclerosis. 2019;6(March):1–11.

52.  Andrews JPM, Fayad ZA, Dweck MR. New methods to image unstable atherosclerotic plaques. Atherosclerosis [Internet]. 2018;272:118–28. Available from: https://doi.org/10.1016/j.atherosclerosis.2018.03.021

53.  Rominger A, Saam T, Vogl E, Ubleis C, la Fougère C, Förster S, et al. In vivo imaging of macrophage activity in the coronary arteries using 68Ga-DOTATATE PET/CT: correlation with coronary calcium burden and risk factors. J Nucl Med. 2010;51(2):193–7.

54.  Li X, Bauer W, Kreissl MC, Weirather J, Bauer E, Israel I, et al. Specific somatostatin receptor II expression in arterial plaque: 68Ga-DOTATATE autoradiographic, immunohistochemical and flow cytometric studies in apoE-deficient mice. Atherosclerosis. 2013;230(1):33–9.

55.  Rinne P, Hellberg S, Kiugel M, Virta J, Li X, Käkelä M, et al. Comparison of Somatostatin Receptor 2-Targeting PET Tracers in the Detection of Mouse Atherosclerotic Plaques. Mol Imaging Biol. 2015;18(1):99–108.

56.  Mojtahedi A, Alavi A, Thamake S, Amerinia R, Ranganathan D, Tworowska I, et al. Assessment of vulnerable atherosclerotic and fibrotic plaques in coronary arteries using 68 Ga-DOTATATE PET/CT. Am J Nucl Med Mol Imaging. 2015;5(1):65–71.

57.  Malmberg C, Ripa RS, Johnbeck CB, Knigge U, Langer SW, Mortensen J, et al. 64Cu-DOTATATE for non-invasive assessment of atherosclerosis in large arteries and its correlation with risk factors: head-to-head comparison with 68Ga-DOTATOC in 60 patients. J Nucl Med [Internet]. 2015;1–33. Available from: http://jnm.snmjournals.org/cgi/doi/10.2967/jnumed.115.161216

58.  Pedersen SF, Sandholt BV, Keller SH, Hansen AE, Clemmensen AE, Sillesen H, et al. ^{64}Cu-DOTATATE PET/MRI for Detection of Activated Macrophages in Carotid Atherosclerotic PlaquesSignificance. Arterioscler Thromb Vasc Biol [Internet]. 2015;35(7):1696–703. Available from: http://atvb.ahajournals.org/lookup/doi/10.1161/ATVBAHA.114.305067

59. Thackeray JT, Bankstahl JP, Wang Y, Korf-klingebiel M, Walte A, Wittneben A, et al. Targeting post-infarct inflammation by PET imaging: comparison of 68Ga-citrate and 68Ga-DOTATATE with 18F-FDG in a mouse model. Eur J Nucl Med Mol Imaging. 2015;42(2):317–27.

60. Li X, Samnick S, Lapa C, Israel I, Buck AK, Kreissl MC, et al. 68Ga-DOTATATE PET/CT for the detection of inflammation of large arteries: correlation with18F-FDG, calcium burden and risk factors. EJNMMI Res [Internet]. 2012;2:52. Available from: EJNMMI Research

61. Poria RB, Norenberg JP, Anderson TL, Erion J, Wagner CR, Arterburn JB, et al. Characterization of a radiolabeled small molecule targeting leukocyte function-associated antigen-1 expression in lymphoma and leukemia. Cancer Biother Radiopharm [Internet]. 2006 Oct;21(5):418–26. Available from: http://www.ncbi.nlm.nih.gov/pubmed/17105416

62. Mota R, Campen MJ, Cuellar ME, Garver WS, Hesterman J, Qutaish M, et al. In-DANBIRT In Vivo Molecular Imaging of Inflammatory Cells in Atherosclerosis. 2018;2018.

63. Mumaw CL, Levesque S, Mcgraw C, Robertson S, Lucas S, Staf JE, et al. Microglial priming through the lung – brain axis : the role of air pollution – induced circulating factors. FASEB J. 2016;30(5):1880–91.

64. Verma NK, Kelleher D. Adaptor regulation of LFA-1 signaling in T lymphocyte migration: Potential druggable targets for immunotherapies? Eur J Immunol. 2014;44(12):3484–99.

65. Phongpradist R, Chittasupho C, Okonogi S, Siahaan T, Anuchapreeda S, Ampasavate C, et al. LFA-1 on Leukemic Cells as a Target for Therapy or Drug Delivery. Curr Pharm Des. 2010;16(21):2321–30.

66. Nicolls MR, Gill RG. LFA-1 (CD11a) as a therapeutic target. Am J Transplant. 2006;6(1):27–36.

67. Walling BL, Kim M. LFA-1 in T cell migration and differentiation. Front Immunol. 2018;9(MAY).

68. Reina M, Espel E. Role of LFA-1 and ICAM-1 in cancer. Cancers (Basel). 2017;9(11):1–14.

69. Pflugfelder SC, Stern M, Zhang S, Shojaei A. LFA-1/ICAM-1 Interaction as a Therapeutic Target in Dry Eye Disease. J Ocul Pharmacol Ther. 2017;33(1):5–12.

70. Badell IR, Russell MC, Thompson PW, Turner AP, Weaver TA, Robertson JM, et al. LFA-1 - Specific therapy prolongs allograft survival in rhesus macaques. J Clin Invest. 2010;120(12):4520–31.

71. Laudanna C. Integrin activation under flow: A local affair. Nat Immunol. 2005;6(5):429–30.

72. Borchert T, Beitar L, Langer LBN, Polyak A, Wester HJ, Ross TL, et al. Dissecting the target leukocyte subpopulations of clinically relevant inflammation radiopharmaceuticals. J Nucl Cardiol. 2019;

73. Hung JC. Bringing new PET drugs to clinical practice - A regulatory perspective. Theranostics. 2013;3(11):885–93.

74. Mosessian S, Duarte-Vogel SM, Stout DB, Roos KP, Lawson GW, Jordan MC, et al. INDs for PET molecular imaging probes – Approach by an academic institution. Mol Imaging Biol. 2014;16(4):441–8.

75. Walrand S, Hesse M, Jamar F. Update on novel trends in PET / CT technology and its clinical applications. Br J Radiol. 2018;89.

76. Nguyen QD, Challapalli A, Smith G, Fortt R, Aboagye EO. Imaging apoptosis with positron emission tomography: "Bench to bedside" development of the caspase-3/7 specific radiotracer [18F]ICMT-11. Eur J Cancer [Internet]. 2012;48(4):432–40. Available from: http://dx.doi.org/10.1016/j.ejca.2011.11.033

7

# Nederlandse Samenvatting

Hart- en vaatziekten vormen de hoofdoorzaak van sterfte wereldwijd (1,17); verdere toename van hart- en vaatziekten wordt verwacht vanwege de stijging in levensduur en toename van westerse levensstijl in Aziatische en Zuid-Amerikaanse landen (18). Aderverkalking, of atherosclerose, is de voornaamste oorzaak van hartaanvallen en beroertes (6), goede diagnose en behandeling van atherosclerotische plaques is daarom van groot belang. Innovatie detectiemethodes zoals besproken in dit proefschrift zijn daarom van belang om de behandeling van de verouderende populatie te sturen. Daarnaast is onderzoek naar de toepassing van deze methoden, zoals besproken in de laatste hoofdstukken van dit proefschrift, van cruciaal belang om nieuwe technologieën zo spoedig mogelijk naar de kliniek te brengen.

Beeldvorming met behulp van radionucliden wordt al geruime tijd toegepast, en het gebruik van nucleaire beeldvormingstechnieken neemt toe. De toepassing is gestandaardiseerd en ruime kennis over scantechnieken is aanwezig. Echter, de invoering van nieuwe technieken vereist nieuwe perspectieven, nieuwe benaderingen, en veelal nieuwe expertise. In **Hoofdstuk 2** behandelen we een aantal belangrijke overwegingen bij de beeldvorming van atherosclerose in kleine dieren. Bij nieuwe state-of-the-art beeldvormingsmethoden die de hoogst haalbare gevoeligheid en nauwkeurigheid nastreven, is het van belang om bij elk aspect van de beeldvorming de hoogste standaard na te streven. Ten eerste bespraken we de noodzaak en het potentieel van nieuwe beeldvormingsmethoden in atherosclerose. Vervolgens refereren we aar verdere bronnen over diermodellen van atherosclerose en bespreken we de verschillen tussen atherosclerose in muis en mens met betrekking tot plaque samenstelling en locatie, en verschillen tussen immuuncellen. We behandelen technische overwegingen zoals kwantificatie en beeldreconstructie en beschrijven mogelijkheden in hybride beeldvorming en verschillen tussen klinische en preklinische PET en SPECT. We bespreken ook welke eigenschappen van belang zijn bij de ontwikkeling van nieuwe radioliganden. Ten slotte geven we onze visie op de toekomst van preklinische beeldvorming.

In **Hoofdstukken 3** en **4** rapporteren we over twee nieuwe beeldvormingsmethoden voor plaque detectie. In **Hoofdstuk 3** beschrijven we het onderzoek naar het nieuwe radioligand [111In]In-DANBIRT, dat bindt aan Leukocyte Function associated Antigen-1 (LFA-1). Dit is een zeer aantrekkelijk doelwit voor beeldvorming, omdat het aanwezig is op alle witte bloedcellen. Terwijl veel studies radioliganden onderzoeken die gericht zijn op macrofagen, kan beeldvorming van LFA-1 een completer beeld geven van de mate van ontsteking in plaque. Dit is van belang omdat naast macrofagen veel andere ontstekingscellen zoals neutrofielen, dendritische cellen, en monocyten een rol spelen in het ontstaan en de destabilisatie van plaques (19-22). In deze studie vonden we dat [111In]In-DANBIRT succesvol gebruikt kan worden om *in vivo* plaque te detecteren in atherosclerotische muizen met een hoge target to background ratio (TBR) en hoge nauwkeurigheid. Door middel van immuunhistochemie van macrofagen vonden we ook dat binding van [111In]In-DANBIRT en expressie van LFA-1 co-lokaliseerde met gebieden van ontsteking. Dit resultaat vonden we zowel in menselijk weefsel als in weefsel van muizen, we

concludeerden dat [^{111}In]In-DANBIRT veel potentie heeft voor *in vivo* detectie van plaque in humane studies.

**Hoofdstuk 4** beschrijft onze studie naar [^{111}In]In-DOTA-JR11, een radioligand dat bindt aan Somatostatine Receptor subtype 2 ($SST_2$). $SST_2$ komt sterk tot expressie op macrofagen en kan daarom gebruikt worden als doelwit voor de detectie van ontsteking in plaques. In eerdere beeldvormingsstudies in patiënten met $SST_2$ als doelwit detecteerden onderzoekers plaque *in vivo* in de kransslagaders (23) en halsslagaders (24) met het radioligand [^{68}Ga]Ga-[DOTA,Tyr[3]]-octreotate (DOTATATE). DOTA-JR11 is echter een andere type radioligand dan DOTATATE. Recent onderzoek (zie (25) voor een overzicht) toonde aan dat DOTA-JR11 een vijf tot tien keer hogere opname heeft dan DOTATATE in tumorweefsel. Vanwege deze hogere opname wilden we onderzoeken of DOTA-JR11 ook gebruikt kan worden in atherosclerose, omdat bij hogere opname minder zwaar ontstoken plaques potentieel ook gedetecteerd zouden kunnen worden. We onderzochten de haalbaarheid van plaque beeldvorming met [^{111}In]In-DOTA-JR11 *in vivo* in atherosclerotische muizen en in plaque weefsel van muizen en mensen. *In vivo* vonden we hoge opname van [^{111}In]In-DOTA-JR11, hetgeen in *ex vivo* en *in vitro* experimenten bevestigd werd. Vanwege de eerdere successen van atherosclerose beeldvorming met $SST_2$-bindende radioliganden zijn patiëntenstudies met DOTA-JR11 of met een directe vergelijking van DOTA-JR11 en DOTATATE nu wenselijk.

Nucleaire beeldvorming wordt voornamelijk uitgevoerd met één radioligand per beeld-vormingsprocedure. Het gebruik van meerdere radioliganden kan verschillende aspecten van ziekte in beeld brengen en daarmee meer informatie geven over welke plaque wel of niet behandeling behoeft. In **Hoofdstuk 5** beschrijven we ons onderzoek dat een eerste stap in deze richting zette. In dit onderzoek verkenden we een beeldvormingsprotocol dat beide visualisatie-doelwitten besproken in **Hoofdstuk 3** en **4** combineert. Zowel beeldvorming van LFA-1 als $SST_2$ heeft veel potentie om atherosclerose te visualiseren in de kliniek. Een (S)PE(C) T/CT-protocol dat onderscheid kan maken tussen stabiele plaque via CT, ontstoken plaque via LFA-1 beeldvorming en plaque-kwetsbaarheid door CT, LFA-1- en $SST_2$-beeldvorming te combineren zou zeer waardevol zijn. Ten eerste vonden we dat dit protocol haalbaar is in humaan plaqueweefsel *in vitro*. We vonden ook dat [^{111}In]In-DANBIRT bindt aan alle types plaque, met hogere binding aan onstabiele plaques. Verder observeerden we dat, terwijl visualisatie van $SST_2$ mogelijk was met [^{99m}Tc]Tc-[$N_4$,Asp[0],Tyr[3]]-octreotate ([^{99m}Tc]Tc-Demotate 2), er geen significante verschillen in opname waren tussen verschillende soorten plaques. Tenslotte vonden we dat radioligand-opname co-lokaliseerde met immuunhistochemie voor LFA-1 en $SST_2$. Deze resultaten wijzen erop dat beeldvorming met meerdere radioliganden mogelijk is in atherosclerose en dat [^{111}In]In-DANBIRT gebruikt kan worden om onderscheid te maken tussen verschillende plaque types, terwijl dit niet kon met het radioligand dat $SST_2$ visualiseerde in deze experimenten. Op basis van deze data is [^{111}In]In-DANBIRT aantrekkelijk voor zowel detectie van plaque als om onderscheid te maken tussen plaque-types.

Naast plaquedetectie is onderscheid tussen verschillende plaque-types een belangrijk doel in de cardiologie. In **Hoofdstuk 6** beschrijven we de studie waarin we onderzochten of dit mogelijk is met een aantal veelbelovende radioliganden. We onderzochten [$^{111}$In]In-DOTATATE en [$^{111}$In]In-DOTA-JR11 voor beeldvorming van SST$_2$, [$^{111}$In]In-DANBIRT voor LFA-1, [$^{67}$Ga]Ga-Pentixafor voor chemokine CXC motif receptor type 4 (CXCR4), en [$^{111}$In]In-EC0800 voor de Folate Receptor (FR). We gebruikten *in vitro* autoradiografie en immuunhistochemie om de aanwezigheid van deze beeldvormingsdoelwitten en de binding van de radioliganden daaraan te onderzoeken in verschillen plaque-types. [$^{111}$In]In-DANBIRT en [$^{111}$In]In-EC0800 hadden de hoogste binding in alle plaque-types en zijn daarmee potentieel het meest bruikbaar voor plaquedetectie in de kliniek. We vonden ook dat deze radioliganden de hoogste binding hadden in kwetsbare plaques, [$^{111}$In]In-EC0800 had echter ook hoge binding in stabiele plaques. [$^{111}$In]In-DOTATATE, [$^{111}$In]In-DOTA-JR11, en [$^{67}$Ga]Ga-Pentixafor hadden vergelijkbare patronen van binding, al was de mate van binding lager dan van de andere radioliganden. Echter, binding van [$^{111}$In]In-DOTA-JR11 en [$^{67}$Ga]Ga-Pentixafor verschilde ook tussen stabiele en kwetsbare plaques, wat potentieel het onderscheid tussen deze plaquetypes mogelijk maakt. Om de onderzoeksvraag in **Hoofdstuk 4** en **5** aan te vullen onderzochten we beide radioliganden besproken in **Hoofdstuk 4**. We vonden een veel hogere mate van binding van [$^{111}$In]In-DOTA-JR11 ten opzichte van [$^{111}$In]In-DOTATATE. De resultaten van radioliganden met SST$_2$ als doelwit verschilde met de resultaten voor dit doelwit in **Hoofdstuk 5**, wat suggereert dat de verschillen tussen deze radioliganden en de experimentele procedures verder onderzocht moeten worden.

Ondanks dat *in vitro* binding niet direct *in vivo* opname voorspelt, verwachten we dat plaquedetectie de meeste kans van slagen heeft door gebruik van radioliganden die LFA-1 en FR als doelwit hebben. Onderscheid tussen plaquetypes kan het best gedaan worden met radioliganden met CXCR4 of SST$_2$ als doelwit. Het gebruik van meerdere radioliganden kan daarom van belang zijn voor goede diagnose van atherosclerose.

# Referenties

1.  GBD 2015 Mortality and Causes of Death Collaborators I. Global, regional, and national life expectancy, all-cause mortality, and cause-specific mortality for 249 causes of death , 1980 – 2015: a systematic analysis for the Global Burden of Disease Study 2015. Lancet. 2016;380(9859):1459–544.

2.  Finn A V, Nakano M, Narula J, Kolodgie FD, Virmani R. Concept of vulnerable/unstable plaque. Arterioscler Thromb Vasc Biol [Internet]. 2010 Jul [cited 2014 Oct 31];30(7):1282–92. Available from: http://www.ncbi.nlm.nih.gov/pubmed/20554950

3.  Carità P, Guaricci AI, Muscogiuri G, Carrabba N, Pontone G. Prognostic value and therapeutic perspectives of coronary CT angiography: A literature review. Biomed Res Int. 2018;2018.

4.  Adamson PD, Newby DE. Noninvasive imaging of the coronary arteries. Eur Heart J. 2019;40:2444–54.

5.  Libby P, Buring JE, Badimon L, Hansson GK, Deanfield J, Bittencourt MS, et al. Atherosclerosis. Nat Rev. 2019;5(56):1–18.

6.  Newby DE. Acute coronary syndromes – Triggering of acute myocardial infarction: Beyond the vulnerable plaque. Heart. 2010;96(15):1247–51.

7.  Rudd JHF, Hyafil F, Fayad ZA. Inflammation imaging in atherosclerosis. Arterioscler Thromb Vasc Biol. 2009;29(7):1009–16.

8.  Moore KJ, Tabas I. Macrophages in the Pathogenesis of Atherosclerosis. Cell [Internet]. 2011;145(3):341–55. Available from: http://dx.doi.org/10.1016/j.cell.2011.04.005

9.  Hansson GK. Inflammation, Atherosclerosis, and Coronary Artery Disease. N Engl J Med [Internet]. 2005;352(16):1685–95. Available from: http://www.ncbi.nlm.nih.gov/pubmed/15843671%0Ahttp://www.nejm.org/doi/abs/10.1056/NEJMra043430

10. Ridker PM. Clinical Application of C-Reactive Protein for Cardiovascular Disease Detection and Prevention. Circulation. 2003;107:363–9.

11. Quillard T, Libby P. Molecular imaging of atherosclerosis for improving diagnostic and therapeutic development. Circ Res [Internet]. 2012 Jul 6 [cited 2015 Jun 26];111(2):231–44. Available from: http://circres.ahajournals.org/content/111/2/231.full

12. Rudd JHF, Warburton EA, Fryer TD, Jones HA, Clark JC, Antoun N, et al. Imaging atherosclerotic plaque inflammation with [18F]-fluorodeoxyglucose positron emission tomography. Circulation. 2002;105(23):2708–11.

13. Tawakol A, Fayad Z a, Mogg R, Alon A, Klimas MT, Dansky H, et al. Intensification of statin therapy results in a rapid reduction in atherosclerotic inflammation: results of a multicenter fluorodeoxyglucose-positron emission tomography/computed tomography feasibility study. J Am Coll Cardiol [Internet]. 2013 Sep 3 [cited 2015 Jun 12];62(10):909–17. Available from: http://www.ncbi.nlm.nih.gov/pubmed/23727083

14. Figueroa AL, Subramanian SS, Cury RC, Truong QA, Gardecki JA, Tearney GJ, et al. Distribution of Inflammation Within Carotid Atherosclerotic Plaques With High-Risk Morphological Features A Comparison Between Positron Emission Tomography Activity , Plaque Morphology , and Histopathology. Circ Cardiovasc Imaging. 2012;5:69–77.

15. Buettner C, Rudd JHF, Fayad ZA. Determinants of FDG Uptake in Atherosclerosis. JACC Cardiovasc Imaging [Internet]. 2011;4(12):1302–4. Available from: http://linkinghub.elsevier.com/retrieve/pii/S1936878X11006954

16. Tarkin JM, Joshi FR, Rudd JHF. PET imaging of inflammation in atherosclerosis. Nat Rev Cardiol [Internet]. 2014;11(8):443–57. Available from: http://www.ncbi.nlm.nih.gov/pubmed/24913061

17. Benjamin EJ, Virani SS, Callaway CW, Chamberlain AM, Chang AR, Cheng S, et al. Heart disease and stroke statistics – 2018 update: A report from the American Heart Association. Vol. 137, Circulation. 2018. 67–492 p.

18. Wong MCS, Zhang DX, Wang HHX. Rapid emergence of atherosclerosis in Asia: A systematic review of coronary atherosclerotic heart disease epidemiology and implications for prevention and control strategies. Curr Opin Lipidol. 2015;26(4):257–69.

19. Libby P. Inflammation in atherosclerosis. 2002;420(December).

20. Libby P, Ridker PM, Maseri A. Clinical Cardiology : New Frontiers Inflammation and Atherosclerosis The Scientific Basis of Inflammation. 2002; Circulation. 2002;105:1135-1143.

21. Ilhan F. Atherosclerosis and the role of immune cells. World J Clin Cases. 2015;3(4):345.

22. Galkina E, Ley K. Immune and inflammatory mechanisms of atherosclerosis (*). Annu Rev Immunol. 2009;27:165–97.

23. Tarkin JM, Joshi FR, Evans NR, Chowdhury MM, Figg NL, Shah AV, et al. Detection of Atherosclerotic Inflammation by 68Ga-DOTATATE PET Compared to [18F]FDG PET Imaging. J Am Coll Cardiol. 2017;69(14):1774–91.

24. Wan MYS, Endozo R, Michopoulou S, Shortman R, Rodriguez-Justo M, Menezes L, et al. PET/CT Imaging of Unstable Carotid Plaque with 68Ga-Labeled Somatostatin Receptor Ligand. J Nucl Med [Internet]. 2017;58(5):774–80. Available from: http://jnm.snmjournals.org/lookup/doi/10.2967/jnumed.116.181438

25. Fani M, Nicolas GP, Wild D. Somatostatin Receptor Antagonists for Imaging and Therapy. J Nucl Med [Internet]. 2017;58(Supplement 2):61S-66S. Available from: http://jnm.snmjournals.org/lookup/doi/10.2967/jnumed.116.186783

26. Davies JR, Rudd JHF, Weissberg PL, Narula J. Radionuclide imaging for the detection of inflammation in vulnerable plaques. J Am Coll Cardiol [Internet]. 2006 Apr 18 [cited 2015 Jun 12];47(8 Suppl):C57-68. Available from: http://www.ncbi.nlm.nih.gov/pubmed/16631511

27. Alie N, Eldib M, Fayad ZA, Mani V. Inflammation, Atherosclerosis, and Coronary Artery Disease: PET/CT for the Evaluation of Atherosclerosis and Inflammation. Clin Med Insights Cardiol [Internet]. 2014 Jan [cited 2015 May 12];8(Suppl 3):13–21. Available from: http://www.pubmedcentral.nih.gov/articlerender.fcgi?artid=4294600&tool=pmcentrez&rendertype=abstract

28. Sadeghi MM. (18)F-FDG PET and vascular inflammation: time to refine the paradigm? J Nucl Cardiol [Internet]. 2015 Apr [cited 2015 Jun 12];22(2):319–24. Available from: http://www.ncbi.nlm.nih.gov/pubmed/24925623

29. Hiari N, Rudd JHF. FDG PET imaging and cardiovascular inflammation. Curr Cardiol Rep. 2011;13(1):43–8.

30. Tavakoli S, Vashist A, Sadeghi MM. Molecular imaging of plaque vulnerability. J Nucl Cardiol. 2014;21:1112–28.

31. Langer HF, Haubner R, Pichler BJ, Gawaz M. Radionuclide imaging: a molecular key to the atherosclerotic plaque. J Am Coll Cardiol [Internet]. 2008 Jul 1 [cited 2015 Jun 18];52(1):1–12. Available from: http://www.pubmedcentral.nih.gov/articlerender.fcgi?artid=2683742&tool=pmcentrez&rendertype=abstract

32. Magnoni M, Ammirati E, Camici PG. Non-invasive molecular imaging of vulnerable atherosclerotic plaques. J Cardiol [Internet]. 2015 Apr [cited 2015 Jun 12];65:261–9. Available from: http://www.ncbi.nlm.nih.gov/pubmed/25702846

33. Joshi F, Rosenbaum D, Bordes S, Rudd JHF. Vascular imaging with positron emission tomography. J Intern Med [Internet]. 2011 Aug [cited 2015 Jun 12];270(2):99–109. Available from: http://www.ncbi.nlm.nih.gov/pubmed/21518037

34. Weber C, Noels H. Atherosclerosis: current pathogenesis and therapeutic options. Nat Med [Internet]. 2011;17(11):1410–22. Available from: http://dx.doi.org/10.1038/nm.2538

35. Sollini M, Berchiolli R, Kirienko M, Rossi A, Glaudemans AWJM, Slart R, et al. PET/MRI in Infection and Inflammation. Semin Nucl Med [Internet]. 2018;48(3):225–41. Available from: https://doi.org/10.1053/j.semnuclmed.2018.02.003

36. Krishnan S, Otaki Y, Doris M, Slipczuk L, Arnson Y, Rubeaux M, et al. Molecular Imaging of Vulnerable Coronary Plaque : A Pathophysiologic Perspective. 2019;359–65.

37. Quillard T, Libby P. Molecular imaging of atherosclerosis for improving diagnostic and therapeutic development. Circ Res [Internet]. 2012 Jul 6 [cited 2015 Jun 26];111(2):231–44. Available from: http://circres.ahajournals.org/content/111/2/231.full

38. Libby P. History of Discovery : Inflammation in Atherosclerosis. Arterioscler Thromb Vasc Biol. 2012;32(9):2045–51.

39. Mckenney-drake ML, Moghbel MC, Paydary K, Alloosh M, Houshmand S, Høilund-carlsen PF, et al. 18 F-NaF and 18 F-FDG as molecular probes in the evaluation of atherosclerosis. Eur J Nucl Med Mol Imaging [Internet]. 2018;2190–200. Available from: http://link.springer.com/10.1007/s00259-018-4078-0

40. Marnane M, Merwick A, Sheehan OC, Hannon N, Foran P, Grant T, et al. Carotid plaque inflammation on 18F-fluorodeoxyglucose positron emission tomography predicts early stroke recurrence. Ann Neurol. 2012;71(5):709–18.

41. Kelly PJ, Camps-Renom P, Giannotti N, Martí-Fàbregas J, Murphy S, McNulty J, et al. Carotid Plaque Inflammation Imaged by 18 F-Fluorodeoxyglucose Positron Emission Tomography and Risk of Early Recurrent Stroke. Stroke. 2019;50(7):1766–73.

42. Figueroa AL, Abdelbaky A, Truong QA, Corsini E, MacNabb MH, Lavender ZR, et al. Measurement of arterial activity on routine FDG PET/CT images improves prediction of risk of future CV events. JACC Cardiovasc Imaging [Internet]. 2013;6(12):1250–9. Available from: http://dx.doi.org/10.1016/j.jcmg.2013.08.006

43. Moon SH, Cho YS, Noh TS, Choi JY, Kim BT, Lee KH. Carotid FDG uptake improves prediction of future cardiovascular events in asymptomatic individuals. JACC Cardiovasc Imaging. 2015;8(8):949–56.

44. Wenning C, Kloth C, Kuhlmann MT, Jacobs AH, Schober O, Hermann S, et al. Serial F-18-FDG PET / CT distinguishes in fl amed from stable plaque phenotypes in shear-stress induced murine atherosclerosis. Atherosclerosis [Internet]. 2014;234(2):276–82. Available from: http://dx.doi.org/10.1016/j.atherosclerosis.2014.03.008

45. Weiberg D, Thackeray JT, Daum G, Sohns JM, Kropf S, Wester H-J, et al. Clinical Molecular Imaging of Chemokine Receptor CXCR4 Expression in Atherosclerotic Plaque using 68 Ga-Pentixafor PET: Correlation with Cardiovascular Risk Factors and Calcified Plaque Burden. J Nucl Med [Internet]. 2018;59:266–72. Available from: http://jnm.snmjournals.org/lookup/doi/10.2967/jnumed.117.196485

46. Derlin T, Sedding DG, Dutzmann J, Haghikia A, König T, Napp LC, et al. Imaging of chemokine receptor CXCR4 expression in culprit and nonculprit coronary atherosclerotic plaque using motion-corrected [68Ga] pentixafor PET/CT. Eur J Nucl Med Mol Imaging. 2018;45(11):1934–44.

47. Li X, Yu W, Wollenweber T, Lu X, Wei Y, Beitzke D, et al. [68Ga]Pentixafor PET/MR imaging of chemokine receptor 4 expression in the human carotid artery. Eur J Nucl Med Mol Imaging. 2019;46:1616–25.

48. Reiter T, Kircher M, Schirbel A, Werner RA, Kropf S, Ertl G, et al. Imaging of C-X-C Motif Chemokine Receptor CXCR4 Expression After Myocardial Infarction With [68Ga]Pentixafor-PET/CT in Correlation With Cardiac MRI. JACC Cardiovasc Imaging [Internet]. 2018; Available from: https://doi.org/10.1016/j.jcmg.2018.01.001

49. Li X, Heber D, Leike T, Beitzke D, Lu X, Zhang X, et al. [68Ga]Pentixafor-PET/MRI for the detection of Chemokine receptor 4 expression in atherosclerotic plaques. Eur J Nucl Med Mol Imaging. 2018;45(4):558–66.

50. Magnoni M, Ammirati E, Camici PG. Non-invasive molecular imaging of vulnerable atherosclerotic plaques. J Cardiol [Internet]. 2015;1–9. Available from: http://linkinghub.elsevier.com/retrieve/pii/S0914508715000155

51. Meester EJ, Krenning BJ, Swart J De, Segbers M, Barrett HE. Perspectives on Small Animal Radionuclide Imaging; Considerations and Advances in Atherosclerosis Animal Models of Atherosclerosis. 2019;6(March):1–11.

52. Andrews JPM, Fayad ZA, Dweck MR. New methods to image unstable atherosclerotic plaques. Atherosclerosis [Internet]. 2018;272:118–28. Available from: https://doi.org/10.1016/j.atherosclerosis.2018.03.021

53. Rominger A, Saam T, Vogl E, Ubleis C, la Fougère C, Förster S, et al. In vivo imaging of macrophage activity in the coronary arteries using 68Ga-DOTATATE PET/CT: correlation with coronary calcium burden and risk factors. J Nucl Med. 2010;51(2):193–7.

54. Li X, Bauer W, Kreissl MC, Weirather J, Bauer E, Israel I, et al. Specific somatostatin receptor II expression in arterial plaque: 68Ga-DOTATATE autoradiographic, immunohistochemical and flow cytometric studies in apoE-deficient mice. Atherosclerosis. 2013;230(1):33–9.

55. Rinne P, Hellberg S, Kiugel M, Virta J, Li X, Käkelä M, et al. Comparison of Somatostatin Receptor 2-Targeting PET Tracers in the Detection of Mouse Atherosclerotic Plaques. Mol Imaging Biol. 2015;18(1):99–108.

56. Mojtahedi A, Alavi A, Thamake S, Amerinia R, Ranganathan D, Tworowska I, et al. Assessment of vulnerable atherosclerotic and fibrotic plaques in coronary arteries using 68 Ga-DOTATATE PET/CT. Am J Nucl Med Mol Imaging. 2015;5(1):65–71.

57. Malmberg C, Ripa RS, Johnbeck CB, Knigge U, Langer SW, Mortensen J, et al. 64Cu-DOTATATE for non-invasive assessment of atherosclerosis in large arteries and its correlation with risk factors: head-to-head comparison with 68Ga-DOTATOC in 60 patients. J Nucl Med [Internet]. 2015;1–33. Available from: http://jnm.snmjournals.org/cgi/doi/10.2967/jnumed.115.161216

58. Pedersen SF, Sandholt BV, Keller SH, Hansen AE, Clemmensen AE, Sillesen H, et al. ^{64}Cu-DOTATATE PET/MRI for Detection of Activated Macrophages in Carotid Atherosclerotic PlaquesSignificance. Arterioscler Thromb Vasc Biol [Internet]. 2015;35(7):1696–703. Available from: http://atvb.ahajournals.org/lookup/doi/10.1161/ATVBAHA.114.305067

59. Thackeray JT, Bankstahl JP, Wang Y, Korf-klingebiel M, Walte A, Wittneben A, et al. Targeting post-infarct inflammation by PET imaging: comparison of 68Ga-citrate and 68Ga-DOTATATE with 18F-FDG in a mouse model. Eur J Nucl Med Mol Imaging. 2015;42(2):317–27.

60. Li X, Samnick S, Lapa C, Israel I, Buck AK, Kreissl MC, et al. 68Ga-DOTATATE PET/CT for the detection of inflammation of large arteries: correlation with18F-FDG, calcium burden and risk factors. EJNMMI Res [Internet]. 2012;2:52. Available from: EJNMMI Research

61. Poria RB, Norenberg JP, Anderson TL, Erion J, Wagner CR, Arterburn JB, et al. Characterization of a radiolabeled small molecule targeting leukocyte function-associated antigen-1 expression in lymphoma and leukemia. Cancer Biother Radiopharm [Internet]. 2006 Oct;21(5):418–26. Available from: http://www.ncbi.nlm.nih.gov/pubmed/17105416

62. Mota R, Campen MJ, Cuellar ME, Garver WS, Hesterman J, Qutaish M, et al. In-DANBIRT In Vivo Molecular Imaging of Inflammatory Cells in Atherosclerosis. 2018;2018.

63. Mumaw CL, Levesque S, Mcgraw C, Robertson S, Lucas S, Staf JE, et al. Microglial priming through the lung – brain axis : the role of air pollution – induced circulating factors. FASEB J. 2016;30(5):1880–91.

64. Verma NK, Kelleher D. Adaptor regulation of LFA-1 signaling in T lymphocyte migration: Potential druggable targets for immunotherapies? Eur J Immunol. 2014;44(12):3484–99.

65. Phongpradist R, Chittasupho C, Okonogi S, Siahaan T, Anuchapreeda S, Ampasavate C, et al. LFA-1 on Leukemic Cells as a Target for Therapy or Drug Delivery. Curr Pharm Des. 2010;16(21):2321–30.

66. Nicolls MR, Gill RG. LFA-1 (CD11a) as a therapeutic target. Am J Transplant. 2006;6(1):27–36.

67. Walling BL, Kim M. LFA-1 in T cell migration and differentiation. Front Immunol. 2018;9(MAY).

68. Reina M, Espel E. Role of LFA-1 and ICAM-1 in cancer. Cancers (Basel). 2017;9(11):1–14.

69. Pflugfelder SC, Stern M, Zhang S, Shojaei A. LFA-1/ICAM-1 Interaction as a Therapeutic Target in Dry Eye Disease. J Ocul Pharmacol Ther. 2017;33(1):5–12.

70. Badell IR, Russell MC, Thompson PW, Turner AP, Weaver TA, Robertson JM, et al. LFA-1 – Specific therapy prolongs allograft survival in rhesus macaques. J Clin Invest. 2010;120(12):4520–31.

71. Laudanna C. Integrin activation under flow: A local affair. Nat Immunol. 2005;6(5):429–30.

72. Borchert T, Beitar L, Langer LBN, Polyak A, Wester HJ, Ross TL, et al. Dissecting the target leukocyte subpopulations of clinically relevant inflammation radiopharmaceuticals. J Nucl Cardiol. 2019;

73. Hung JC. Bringing new PET drugs to clinical practice – A regulatory perspective. Theranostics. 2013;3(11):885–93.

74. Mosessian S, Duarte-Vogel SM, Stout DB, Roos KP, Lawson GW, Jordan MC, et al. INDs for PET molecular imaging probes – Approach by an academic institution. Mol Imaging Biol. 2014;16(4):441–8.

75. Walrand S, Hesse M, Jamar F. Update on novel trends in PET / CT technology and its clinical applications. Br J Radiol. 2018;89.

76. Nguyen QD, Challapalli A, Smith G, Fortt R, Aboagye EO. Imaging apoptosis with positron emission tomography: "Bench to bedside" development of the caspase-3/7 specific radiotracer [18F]ICMT-11. Eur J Cancer [Internet]. 2012;48(4):432–40. Available from: http://dx.doi.org/10.1016/j.ejca.2011.11.033

# Acknowledgements

First and foremost, I want to thank my main 'opperhoofd' my promotor, Marion de Jong. Marion, not only were you a great help throughout my PhD at those times when I needed help the most, you were also a great source of inspiration to me. You always made me feel empowered after a meeting, and you were inspiring as a group leader. You set a beautiful example of what a great scientist should be like, both in your profession and your person. I feel lucky that I could learn from you.

Of course, I also thank my triumvirate of chieftains: Kim, Boudewijn, and Monique. From each of you I was able to learn different things, and each of you conducted science in your own way. I will for sure remember this throughout my further career. Thank you for making this PhD-project possible.

I am also grateful to the leaders of the departments I was able to work in: Ton van der Steen, Fred Verzijlbergen, and Gabriel Krestin. The leadership you provided allowed strong research groups to flourish, groups in which I was able to perform research on a high level. Thank you.

Importantly, I want to thank my collaborators. Thomas van Wolleghem, Gulce Kaplan, Ruoyu Xing, Erik de Blois, Marcel Segbers, Jeffrey Norenberg, Hilary Barrett, and Jan de Swart. I believe you are all great scientists and it was a joy to work with you. I especially like to thank Hilary, your arrival and presence in the EMC made our 'team' of nuclear cardiology double in size :) providing a much-needed sparring partner and immensely speeding up my project. Also, to Marcel I like to express my special thanks. You are very knowledgeable, and fully contributed to each project you worked on.

I also thank all of my colleagues. Colleagues from Biomedical Engineering, Nuclear Medicine, Radiology, MILabs, and all the other colleagues I was fortunate enough to meet through committees, courses, congresses and chance encounters. Although I thoroughly enjoyed the science in my project, you guys made my time memorable, thank you.

I also like to dedicate a line to my girlfriend, Pinar. Thank you for your help. I still think you're weird.

Finally, and most importantly, I would like to stress that we 'stand on the shoulders of giants' (attributed to Bernard of Chartres), not only in work but also as people. Throughout my life I had the privilege to be around people who were inspiring, people who gave great advice, and people who outright helped me at the moment I needed it most, often without knowing it myself. These people helped shape my character. Without these admirable 'giants' I would

not have started this project, let alone finish it. Foremost amongst these are my parents; The stability, peace, and core values you provided are the main contributor to making this PhD project successful, and I can never thank you enough. If writing a thesis can be called a success, I dedicate it fully to them and the other giants. I am grateful for all I have received.

# Scientific contributions

## Journal papers

**Meester E.J.**, de Blois E., Krenning, B.J., van der Steen A.F.W., van Gaalen K., Bernsen M.R., de Jong M., van der Heiden K. Autoradiographical assessment of inflammation-targeting radioligands for atherosclerosis imaging: potential for plaque phenotype identification
*European Journal of Nuclear Medicine and Molecular Imaging, in review*

Barret H.E., **Meester E.J.**, Van Gaalen, K., Van der Heiden, K., Krenning, B.J., Beekman. FJ., de Blois, E., de Swart, J., Verhagen, H., Maina, T., Nock, B.A., Norenberg, J.P., de Jong, M., Gijsen, F., Bernsen, M.R. Imaging of Inflammatory Cellular Protagonists in Human Atherosclerosis: A Dual-Isotope SPECT Approach
*European Journal of Nuclear Medicine and Molecular Imaging,* 2020. doi: 10.1007/s00259-020-04776-0

Sari G., **Meester E.J.,** van der Zee L.C., Wouters K., van Lennep J.R., Peppelenbosch M., Boonstra A., van der Heiden K., Mulder M.M.T., Vanwolleghem T. A mouse model of humanized liver shows a human-like lipid profile, but does not form atherosclerotic plaque after western type diet.
*Biochemical and Biphysical Research Communications.* 2020. 524(2):510-515 doi:10.1016/j.bbrc.2020.01.067

**Meester E.J.**, Krenning B.J., de Blois E., de Jong M., van der Steen A.F.W., Bernsen M.R., van der Heiden K. Imaging inflammation in atherosclerotic plaques, targeting $SST_2$ with [$^{111}$In]In-DOTA-JR11 *Journal of Nuclear Cardiology*. 2020. doi: 10.1007/s12350-020-02046-y

**Meester E.J**, B. J. Krenning, J. de Swart, M. Segbers, H. E. Barrett, M. R. Bernsen, K. Van der Heiden, Marion de Jong. Perspectives on Small Animal Radionuclide Imaging in Atherosclerosis; Challenges and Advances
*Frontiers in Medicine*. 2019. 6: 39. doi: 10.3389/fmed.2019.00039

Xing R., Moerman A.M., Ridwan R.Y., van Gaalen K., **Meester E.J.**, van der Steen A.F.W., Evans P.C., Gijsen F.J.H., Van der Heiden K. The Effect of the Heart Rate Lowering Drug Ivabradine on Hemodynamics in Atherosclerotic Mice
*Nature Scientific Reports*. 2018. 8(1): 14014. doi: 10.1038/s41598-018-32458-3.

**Meester E.J.**, B. J. Krenning, R. H. de Blois, J. P. Norenberg, M. de Jong, M. R. Bernsen, K. Van der Heiden. Imaging of Atherosclerosis, Targeting LFA-1 on Inflammatory Cells with 111In-DANBIRT *Journal of Nuclear Cardiology*. 2018. 26(5): 1697-1704. doi: 10.1007/s12350-018-1244-5.

## Conference presentations

- NKRV Workshop*, Utrecht, The Netherlands,* 28/06/2019 (Invited talk)
- MoMaDc lunch*, Rotterdam, The Netherlands* 04/04/2019 (Invited talk)
- EMIM*, Glasgow, Great Britain,* 21/03/2019 (Poster presentation)
- MolMed day*, Rotterdam, The Netherlands,* 14/03/2019 (Pitch)
- NKRV Workshop*, Rotterdam, The Netherlands,* 25/01/19 (Pitch and poster presentation, won second presentation prize)
- EANM*, Dusseldorf, Germany,* 13/10/2018 (E-poster presentation)
- MILabs meeting*, Utrecht, The Netherlands,* 13/10/2018 (Oral presentation)
- Translational Cardiovascular Research Meeting*, Utrecht, The Netherlands,* 29/06/18 (Oral presentation)
- COEUR day*, Rotterdam, The Netherlands,* 05/04/2018 (Oral presentation)
- MolMed day*, Rotterdam, The Netherlands,* 15/03/2018 (Oral presentation, won presentation prize)
- MILabs meeting*, Utrecht, The Netherlands,* 17/11/2017 (Oral presentation)
- EANM*, Vienna, Austria,* 25/05/2017 (Oral presentation)
- COEUR day*, Rotterdam, The Netherlands,* 19/04/2017 (Oral presentation, won presentation prize)
- Shear Stress Symposium*, Rotterdam, The Netherlands,* 04-05/04/2017 (Poster presentation)
- Famelab*,The Netherlands, Rotterdam* 16/03/2017*, Delft* 03/04/2019
- MolMed day*, Rotterdam, The Netherlands,* 21/03/2017 (Poster presentation)
- Imaging Infections and Inflammation*, Rome, Italy,* 13/04/2016 (Poster presentation)
- COEUR day*, Rotterdam, The Netherlands,* 13/04/2016
- Papendal Course*, Arnhem, The Netherlands,* 15/10/2015 (Oral presentation)
- Papendal Course*, Arnhem, The Netherlands,* 14/10/2015 (Poster presentation)

# Biography

Eric Jan Meester was born on June 10th, 1990 in Delft, The Netherlands. He completed high school (HAVO, 2007. VWO, 2009) at Stanislas College Delft.

After high school, he studied Biology at Leiden University from 2009 to 2012. He participated in Honours College during his bachelor, obtained his high school teaching certificate, and completed multiple research projects. One project was partly performed in Caen, France, under supervision of Professor Hans Metz, where he investigated coastal species diversity in tide pools. A second project was performed with Professor Hans Witte, Dr. Hans Slabbekoorn, and Dr. Niels Bouton. In this project he investigated the effect on anthropogenic noise on fish behaviour, physiology, and morphology.

After his bachelor studies, Eric performed his Master studies in Biology at the same university from 2012 to 2014. During his masters he was elected to join the Leiden Leadership Programme, a prestigious Honours programme for excellent students. During this programme he performed a project on policy development in the Leiden University Medical Center (LUMC). During his master, he conducted two research projects. His first project, under supervision of Professor Peter Klinkhamer and Dr. Martina Stang at the department of plant phytochemistry and physiology, was partly located in Alicante, Spain. He investigated the interaction of floral shape and nectar composition in relation to flower visitation by pollinators. His second research project was conducted at the LUMC under supervision of Professor Michael Richardson and Professor Robert Klinkhamer. This project focussed on the embryological development of the crocodile cardiac ventricular septum.

Eric started his PhD research in 2015 at the Erasmus MC in Rotterdam at the departments of Cardiology: Biomedical Engineering and Radiology & Nuclear Medicine. In collaboration with Professor Marion de Jong, Dr. Kim van der Heiden, Dr. Boudewijn Krenning, and Dr. Monique Bernsen he performed the research projects documented in this thesis. During this period, he received 3 prizes for scientific presentations, obtained 2 travel grants, and gave 2 invited talks. Moreover, he co-founded the Dutch young Molecular Imaging Community (DyMIC).

After his PhD studies, Eric pursued a postdoctoral position at the Erasmus MC in 2019, department of Radiology & Nuclear Medicine, in collaboration with Dr. Simone Dalm.

# PhD portfolio

| | |
|---|---|
| Name PhD student: | Eric Meester |
| Erasmus MC Departments: | Cardiology, Biomedical Engineering |
| | Radiology & Nuclear Medicine |
| Promotor: | Marion de Jong |
| Supervisor: | Kim van der Heiden |

| Courses | Year | ECTS |
|---|---|---|
| 5a course | 2015 | 1 |
| 5b course | 2015 | 1 |
| Pubmed course: systematic literature retrieval 1 | 2015 | 0.5 |
| Pubmed course: systematic literature retrieval 2 | 2015 | 0.5 |
| Cardiovascular pharmacology course | 2015 | 0.5 |
| AMIE course | 2015 | 1.4 |
| Excel course: basics | 2016 | 0.5 |
| Excel course: advanced | 2016 | 0.5 |
| Microscopic image analysis course | 2017 | 1 |
| Presenting course | 2017 | 0.5 |
| Scientific intergrity course | 2017 | 0.4 |
| MILabs training VECTOR | 2017 | 0.3 |
| MILabs training Pmod | 2017 | 0.3 |
| Stress management course | 2017 | 2 |
| PET training | 2018 | 3 |
| Biomedical English Writing Course | 2018 | 2.5 |
| **Subtotal** | | **15.8** |

| Seminars and workshops | Year | ECTS |
|---|---|---|

| | | |
|---|---|---|
| Postdoc network workshop: Funding | 2015 | 0.2 |
| Postdoc network workshop: networking | 2017 | 0.2 |
| Postdoc network workshop | 2017 | 0.2 |
| COEUR lecture: DNA damage in CVD | 2017 | 0.1 |
| People in Science workshop | 2018 | 0.2 |
| Monocyte lunch | 2019 | 0.1 |
| Postdoc network | 2019 | 0.2 |
| **Subtotal** | | **1.2** |

| Conferences and symposia | Year | ECTS |
|---|---|---|
| Shear stress symposium | 2015 | 0.6 |
| Papendal course | 2015 | 2 |
| Translational research symposium | 2016 | 0.3 |
| Innovation for health | 2016 | 0.3 |
| MolMed day | 2016 | 0.3 |
| EMIM Utrecht | 2016 | 1 |
| COEUR day | 2016 | 0.15 |
| AMIE/OIC symposium | 2016 | 0.3 |
| Congress on imaging inflammation and infectious diseases | 2016 | 0.6 |
| MolMed day | 2017 | 0.3 |
| Shear Stress symposium | 2017 | 0.6 |
| COEUR day | 2017 | 0.15 |
| Imaging Research on the move | 2017 | 0.2 |
| PhD day EMC | 2017 | 0.15 |
| Young@heart talent day | 2017 | 0.3 |
| EANM Vienna | 2017 | 1.2 |
| Monocytes symposium | 2017 | 0.2 |
| MILabs user meeting | 2017 | 0.2 |
| **Conferences and symposia** *(Continued)* | **Year** | **ECTS** |
| Imaging Research on the move | 2017 | 0.2 |

| | | |
|---|---|---|
| Chameleon event | 2018 | 0.3 |
| Molmed day | 2018 | 0.3 |
| Translational research symposium | 2018 | 0.3 |
| PhD day EMC | 2018 | 0.15 |
| Imaging Research on the move | 2018 | 0.2 |
| MIlabs user meeting | 2018 | 0.2 |
| EANM Dusseldorf | 2018 | 1.2 |
| Young@heart talent day | 2018 | 0.3 |
| Monocyte symposium | 2018 | 0.2 |
| NKRV workshop | 2019 | 0.5 |
| MolMed day | 2019 | 0.3 |
| EMIM Glasgow | 2019 | 1 |
| COEUR symposium | 2019 | 0.1 |
| NKRV workshop | 2019 | 0.5 |
| **Subtotal** | | **15** |

| Presentations | Year | ECTS |
|---|---|---|
| 50+ talks at different congresses, workshops, groups | 2015-2019 | 5 |

| Teaching | Year | ECTS |
|---|---|---|
| Supervision of MLO student | 2018 | 0.1 |

| Other | Year | ECTS |
|---|---|---|
| exCOEURsion: Philips | 2017 | 0.3 |
| exCOEURsion: Leiden Biosciencepark | 2018 | 0.3 |

| | | |
|---|---|---|
| **Total** | | **37.8** |

Atherosclerosis is a complex and multi-factorial disease. Proper diagnosis is crucial for timely and adequate treatment, but remains difficult with current techniques. In this thesis, novel diagnostic methods developed with state of the art techniques are discussed.

**Eric J. Meester** obtained his Master of science degree in Biology. He performed his doctoral studies at the Erasmus MC in Rotterdam, the results of which are discussed in this thesis.